

**TÜRKİYE
FIRAT UNIVERSITY
THE INSTITUTE OF NATURAL AND APPLIED SCIENCES**



**MODIFICATION OF MAGNETIC NANOPARTICLES WITH
POLY(VINYL CHLORIDE) VIA CLICK CHEMISTRY**

Abdulahman TUKUR

Master's Thesis

Department of Chemistry

FEBRUARY – 2020

TÜRKİYE
FIRAT UNIVERSITY
THE INSTITUTE OF NATURAL AND APPLIED SCIENCES

Department of Chemistry

Master's Thesis

**MODIFICATION OF MAGNETIC NANOPARTICLES WITH
POLY(VINYL CHLORIDE) VIA CLICK CHEMISTRY**

Thesis Author

Abdulrahman TUKUR

Supervisor: Prof. Dr. Mehmet COŞKUN

FEBRUARY – 2020

ELAZIĞ

TÜRKİYE
FIRAT UNIVERSITY
GRADUATE SCHOOL OF NATURAL AND APPLIED SCIENCES

Chemistry Department
Program: Physical Chemistry

Master's Thesis

Title: Modification of Magnetic Nanoparticles with Poly(Vinyl Chloride) Via Click
Chemistry

Author: Abdulrahman TUKUR

First Delivery: 18.02.2020

Date of Defense: 20.03.2020

THESIS APPROVAL

This thesis was prepared according to the rules of Firat University, Graduate School of Natural and Applied Sciences. It was evaluated by the jury members who have signed the following signatures and accepted unanimously because of the defense made available to the academic audiences.

Signature

Advisor: Prof. Dr. Mehmet COŞKUN
Firat University, Faculty of Science

I Approved

Chairman: Prof. Dr. Kadir DEMIRELLI
Firat University, Faculty of Science

I Approved

Member: Prof. Dr. Esin KAYA
Mus Alparslan University, Education Faculty

I Approved

This thesis was registered at the meeting of the board of directors of the institute on

/ / 2020

Signature

Prof. Dr. Soner ÖZGEN
Director of the Institute

DECLARATION

All the information in the [Select Thesis Type from the List] title titled “The First Letter of Each Word Should Be Written Here,” in accordance with the Firat University Institute of Science thesis writing rules is correct, I am acting in accordance with scientific ethical rules in producing and presenting the information. I hereby declare that I have mentioned all the institutions/organizations and persons who have financial and moral support and that I have never used the data and information I have presented here in order to get a title.

FEBRUARY -2020

Abdulrahman TUKUR

PREFACE

Magnetic nanoparticles are used to selectively attach and modified polymer properties under the influence of an external magnetic field. In this research, a copolymer bearing on its side chain Fe_3O_4 was bonded to PVC by way of click reaction via "grafting to" approach.

I would like to express my sincere gratitude to my research supervisor Prof. Dr. Mehmet COŞKUN for the continuous support of my study and research, for his patience, motivation, enthusiasm, and immense knowledge. Besides my supervisor, I wish to express my deepest gratitude to Dr. Mustafa Ersin PEKDEMİR for his invaluable assistance, support, and encouragement.

I would like to pay my special regards to my dear wife, Maryam Maishanu, ISAH for her patience, prayers, and support from the moment she entered my life, and my dear son, Muhammad Amin, ABDULRAHMAN.

I am indebted to my late mother Aisha TUKUR who lost her life during my undergraduate studies whose prayers I always feel and I wish her God's mercy and my father Muhammad Tukur, IBRAHİM whose prayers keep me going throughout. And also, I thank my sister Ummu TUKUR for making this dream come true, siblings, friends, and my fellow labmates.

This thesis was supported by the project number **FF.18.18** by Firat University Scientific Research Projects Coordination Unit (FÜBAP)

Abdulrahman TUKUR

FEBRUARY -2020

TABLE OF CONTENTS

Page no

DECLARATION	i
PREFACE	ii
LIST OF FIGURES	viii
LIST OF TABLES	xiii
LIST OF SYMBOLS AND ABBREVIATIONS.....	xiv
1. INTRODUCTION.....	1
1.1. Polymerization reaction.....	2
1.1.1. Condensation polymerization	2
1.1.2. Anionic polymerization	3
1.1.3. Cationic polymerization.....	4
1.1.4. Free radical polymerization	4
1.1.5. Controlled radical polymerization	5
1.2. Poly (vinyl chloride).....	6
1.2.1. Production of PVC.....	7
1.2.2. Properties of PVC	7
1.2.3. Usage areas of PVC	7
1.3. Nucleophilic substitution reactions on PVC.....	8
1.4. Click reactions	9
1.5. Functionalization of polymers via click reactions	10
1.6. Inorganic nanoparticle	12
1.6.1. Magnetic nanoparticle.....	13
1.7. Modification of magnetic nanoparticles	14
1.8. Thermal investigation of polymers	15
1.8.1. Differential scanning calorimetry (DSC).....	15
1.8.2. Thermogravimetric Analysis (TGA).....	16
1.8.3. Differential thermal analysis (DTA).....	16
1.9. Electrical investigation of polymers	16
1.10. Electron microscopy investigation of polymers	17
1.10.1. Scanning electron microscopy (SEM)	17
1.10.2. Scanning electron microscope/energy dispersive x-ray spectrometer (SEM/EDX)	18
1.10.3. Transmission electron microscopy (TEM)	18
1.11. Vibration sample magnetometry (VSM)	19

1.12. Aim and objectives	20
1.13. Literature Review	20
2. MATERIALS AND METHOD.....	23
2.1. Materials	23
2.2. Instrumentation.....	23
2.3. Experimental.....	24
2.3.1. Purification of poly(vinyl chloride) (PVC).....	24
2.3.2. Synthesis of azide functional poly(vinyl chloride) (PVC-N ₃).....	24
2.3.3. Synthesis of propargyl α -bromoisobutyrate (POH-BIBB)	24
2.3.4. Atom transfer radical copolymerization of methylmethacrylate and Vinyltrimethoxysilane	25
2.3.5. Magnetic nanoparticle (Fe ₃ O ₄) bonding to the (MMA- <i>co</i> -VTM) copolymer.....	25
2.3.6. Click reaction of poly(MMA- <i>co</i> -VTM)- <i>g</i> -Fe ₃ O ₄ and azide poly(vinylchloride) PVC-N ₃	26
2.3.7. Synthesis of propargyl methacrylate (POHMAC).....	26
2.3.8. Free radical copolymerization of propargyl methacrylate and vinyltrimethoxysilane.....	27
2.3.9. Magnetic nanoparticle (Fe ₃ O ₄) bonding to the (POHMAC- <i>co</i> -VTM) copolymer	27
2.3.10. Click reaction of (POHMAC- <i>co</i> -VTM)- <i>g</i> -Fe ₃ O ₄ and azide poly(vinylchloride) PVC-N ₃	28
2.3.11. Synthesis of 3-azidopropyltrimethoxysilane (N ₃ PTMS)	29
2.3.12. Magnetic nanoparticle (Fe ₃ O ₄) bonding to 3-azidopropyltrimethoxysilane (N ₃ PTMS).....	29
2.3.13. Click reaction of N ₃ PTMS- <i>g</i> -Fe ₃ O ₄ and propargyl alcohol (POH)	30
2.3.14. Preparation of composite of PVC with POH-N ₃ PTMS- <i>g</i> -Fe ₃ O ₄	30
3. RESULTS	31
3.1. Poly(vinyl chloride).....	31
3.1.1. Characterization of PVC.....	31
3.1.2. Thermal Properties.....	33
3.2. PVC- <i>g</i> -poly(MMA- <i>co</i> -VTM)- <i>g</i> -Fe ₃ O ₄	36
3.2.1. Characterization	36
3.2.2. Thermal properties	39
3.2.3. Morphological structure.....	41
3.2.4. Magnetic properties	43
3.2.5. Electrical investigation	44
3.3. PVC- <i>g</i> -poly(POHMAC- <i>co</i> -VTM)- <i>g</i> -Fe ₃ O ₄	49
3.3.1. Characterization	49

3.3.2. Thermal properties	52
3.3.3. Magnetic property	55
3.3.4. Electrical investigation	56
3.4. Composite of PVC with POH-N ₃ PTMS-g-Fe ₃ O ₄	61
3.4.1. Characterization	61
3.4.2. Thermal properties	63
3.4.3. Morphological structures	67
3.4.4. . Magnetic property	70
3.4.5. Electrical Investigation	71
4. DISCUSSION	77
REFERENCES	83
CURRICULUM VITAE	86

ABSTRACT

Modification of Magnetic Nanoparticles with Poly(Vinyl Chloride) Via Click Chemistry

Abdulrahman TUKUR

Master's Thesis

FIRAT UNIVERSITY

Graduate School of Natural and Applied Sciences

Department of Chemistry

February 2020, Pages: xv + 85

A copolymer bearing on its side chain Fe_3O_4 was bonded to PVC by click reaction via "grafting to" approach. Firstly, propargyl α -bromoisobutyrate was synthesized. Next, vinyltrimethoxysilane and methylmethacrylate copolymerization were completed through Atom transfer radical polymerization. Magnetic nanoparticles (Fe_3O_4) were bonded to copolymer through its vinyltrimethoxysilane units. Finally, the propargyl end group of the copolymer carrying Fe_3O_4 on its side chain was bonded to azide PVC by click reaction. The chemical structure and morphology were characterized by FT-IR, ^1H , and ^{13}C NMR, SEM, and SEM-EDX. Thermal analysis showed a decrease in the stability of PVC azide compared to PVC and after grafting of the Fe_3O_4 bond copolymer, the stability increased. The copolymer showed magnetic saturation (M_s) of 41.5 emu/g. The dielectric constant (ϵ') and dielectric loss (ϵ'') of copolymers decreased with an increase in frequency. Propargyl methacrylate was synthesized from propargyl alcohol and methacryloyl chloride. Next, the copolymer was formed via Free radical polymerization of vinyltrimethoxysilane and methylmethacrylate. Fe_3O_4 was bonded to copolymer via its vinyltrimethoxysilane units. Lastly, the propargyl end group of the copolymer carrying Fe_3O_4 was bonded to PVC azide by click reaction. FT-IR characterization technique was used. Thermal Stability increased after grafting of Fe_3O_4 to the copolymer and decreased following click reaction. Fe_3O_4 bonded copolymer showed M_s of 33.7 emu/g. The ϵ' and ϵ'' of copolymers decreases with a frequency increase and for AC conductivity, it increases.

Keywords: Magnetic Nanoparticle, poly(vinyl chloride), click reaction, copolymer, ATRP

ÖZET

Klik Reaksiyonu Yardimiyla Manyetik Nanotaneciklerin Poli (vinil klorur)' le Modifikasyonu

Abdulrahman TUKUR

Yüksek lisans Tezi

FIRAT ÜNİVERSİTESİ

Fen Bilimleri Enstitüsü

Kimya Anabilim Dalı

Subat 2020, Sayfa: xv + 85

Yan zincirinde Fe_3O_4 nanotanecikleri bulunan kopolimer 'grafting to' kullanılarak klik reaksiyonu ile PVC' ye bağlandı. Öncelikle, propargil α -bromoisobutirat sentezlendi. Atom transfer radikal polimerizasyonu ile viniltrimetoksisilan ve metil metakrilat kopolimerizasyonu gerçekleştirildi. Daha sonra, manyetik nanotanecikler (Fe_3O_4) viniltrimetoksisilan birimleri üzerinden kopolimere bağlandı. Son olarak, yan zincirinde Fe_3O_4 taneciklerini taşıyan propargil son gruplu kopolimer klik reaksiyonu yoluyla azid grubu içeren PVC' ye bağlandı. Sentezlenen kopolimerin kimyasal yapısı ve morfolojisi FT-IR, 1H and ^{13}C NMR, SEM and SEM-EDX ile karakterize edildi. Termal analiz sonuçları, PVC' ye göre azid grubu içeren PVC' nin kararlılığının azaldığı ve Fe_3O_4 bağlandıktan sonra ise kararlılığının arttığını gösterdi. Fe_3O_4 ile modifiye edilen PVC' nin doyumluk manyetizasyonu (M_s) 41.5 emu/g olarak bulundu. Fe_3O_4 bağlı ve PVC ile modifiye edilmiş kopolimerin dielektrik sabiti (ϵ') ve dielektrik kayıp faktörünün (ϵ'') artan frekansla azaldığı görüldü. Propargil metakrilat, propargil alkol ve metakrilol klorür'den sentezlendi. Ardından, vinil trimetoksisilan metil metakrilat kopolimeri serbest radikal polimerizasyonu yoluyla elde edildi. Sonra, Fe_3O_4 nanotanecikleri viniltrimetoksisilan birimleri üzerinden kopolimere bağlandı. Son olarak, Fe_3O_4 taşıyan propargil son gruplu kopolimer klik reaksiyonu ile azitli PVC' ye bağlandı. FT-IR karakterizasyon tekniği kullanıldı. Kopolimere Fe_3O_4 bağlandıktan sonra termal kararlılık artarken, klik reaksiyonu sonrası azaldığı görüldü. Fe_3O_4 baplı kopolimerin M_s değeri 33.7 emu/g olarak bulundu. Kopolimerin ϵ' ve ϵ'' değerlerinin artan frekansla azaldığı, AC iletkenliğinin ise arttığı görüldü.

Anahtar Kelimeler: Manyetik nanotanecik, poli (vinil klorur), klik reaksiyonu, kopolimer, ATRP

LIST OF FIGURES

	Page no.
Figure 1.1. Scheme showing formation of a condensation polymer.....	2
Figure 1.2. Schematic representation of anionic polymerization.....	3
Figure 1.3. Schematic representation of cationic polymerization.....	4
Figure 1.4. Schematic representation of free radical polymerization mechanism	5
Figure 1.5. Scheme showing the ATRP mechanism as reported by Matyjaszewski <i>et al</i>	6
Figure 1.6. The ARGET-ATRP mechanism as proposed by Matyjaszewski et al.	6
Figure 1.7. Examples of nucleophile	8
Figure 1.8. Schematic representation of nucleophilic substitution reaction	8
Figure 1.9. (A) Uncatalyzed thermal (B) Copper (I) catalyzed cycloaddition reaction.....	10
Figure 1.10. Early CuAAC mechanism proposed by Sharpless and Fokin.	10
Figure 1.11. Block diagram of heat flux DSC	16
Figure 1.12. Image of SEM device.....	18
Figure 1.13. Image of VSM device.....	19
Figure 2.1. Synthesis of azide functional poly(vinyl chloride).....	24
Figure 2.2. Synthesis of propargyl α -bromoisobutyrate	24
Figure 2.3. Synthesis of Poly(MMA- <i>co</i> -VTM)	25
Figure 2.4. Synthesis of Poly(MMA- <i>co</i> -VTM)- <i>g</i> -Fe ₃ O ₄	26
Figure 2.5. Synthesis of PVC- <i>g</i> -poly(MMA- <i>co</i> -VTM)- <i>g</i> -Fe ₃ O ₄	26
Figure 2.6. Synthesis of propargyl methacrylate	27
Figure 2.7. Synthesis of Poly(POHMAC- <i>co</i> -VTM).....	27
Figure 2.8. Synthesis of poly(POHMAC- <i>co</i> -VTM)- <i>g</i> -Fe ₃ O ₄	28
Figure 2.9. Synthesis of PVC- <i>g</i> -poly(POHMAC- <i>co</i> -VTM)- <i>g</i> -Fe ₃ O ₄	28
Figure 2.10. Synthesis of 3-azidopropyltrimethoxysilane	29
Figure 2.11. Synthesis of 3-azidopropyltrimethoxysilane- <i>g</i> -Fe ₃ O ₄	29
Figure 2.12. Synthesis of modified Fe ₃ O ₄ via click reaction	30
Figure 3.1. FT-IR spectrum of PVC	31
Figure 3.2. PVC-N ₃ FT-IR spectrum	32
Figure 3.3. ¹ H-NMR spectrum of PVC-N ₃	32
Figure 3.4. ¹³ C-APT spectra of PVC and PVC-N ₃	33
Figure 3.5. TGA curve of PVC.....	34
Figure 3.6. DSC curve of PVC	34
Figure 3.7. TGA curve of PVC-N ₃	35

Figure 3.8. DSC curve of PVC-N ₃	35
Figure 3.9. FT-IR spectrum of propargyl- α -bromoisobutyrate	36
Figure 3.10. ¹ H-NMR spectrum of propargyl- α -bromoisobutyrate (Solvent: CDCl ₃)	37
Figure 3.11. ¹³ C-APT spectrum of propargyl- α -bromoisobutyrate (Solvent: CDCl ₃)	37
Figure 3.12. FT-IR spectrum of poly(MMA- <i>co</i> -VTM)	38
Figure 3.13. TGA curve of poly(MMA- <i>co</i> -VTM).....	39
Figure 3.14. DSC curve of poly(MMA- <i>co</i> -VTM)	39
Figure 3.15. TGA curve of poly(MMA- <i>co</i> -VTM)- <i>g</i> -Fe ₃ O ₄	40
Figure 3.16. DSC curve of poly(MMA- <i>co</i> -VTM)- <i>g</i> -Fe ₃ O ₄	40
Figure 3.17. TGA curve of PVC- <i>g</i> -poly(MMA- <i>co</i> -VTM)- <i>g</i> -Fe ₃ O ₄	40
Figure 3.18. DSC curve of PVC- <i>g</i> -poly(MMA- <i>co</i> -VTM)- <i>g</i> -Fe ₃ O ₄	41
Figure 3.19. SEM image of poly(MMA- <i>co</i> -VTM)- <i>g</i> -Fe ₃ O ₄	41
Figure 3.20. SEM-EDX image poly(MMA- <i>co</i> -VTM)- <i>g</i> -Fe ₃ O ₄	42
Figure 3.21. SEM image of PVC- <i>g</i> -poly(MMA- <i>co</i> -VTM)- <i>g</i> -Fe ₃ O	42
Figure 3.22. SEM-EDX image PVC- <i>g</i> -poly(MMA- <i>co</i> -VTM)- <i>g</i> -Fe ₃ O ₄	43
Figure 3.23. VSM plot of PVC- <i>g</i> -poly(MMA- <i>co</i> -VTM)- <i>g</i> -Fe ₃ O ₄	44
Figure 3.24. Variation of dielectric constant of poly(MMA- <i>co</i> -VTM)- <i>g</i> -Fe ₃ O ₄ with frequency at room temperature	45
Figure 3.25. Variation of dielectric loss of poly(MMA- <i>co</i> -VTM)- <i>g</i> -Fe ₃ O ₄ with frequency at room temperature.....	45
Figure 3.26. Variation of AC conductivity of poly(MMA- <i>co</i> -VTM)- <i>g</i> -Fe ₃ O ₄ with frequency at room temperature	46
Figure 3.27. Variation of AC conductivity of poly(MMA- <i>co</i> -VTM)- <i>g</i> -Fe ₃ O ₄ with angular frequency at room temperature	46
Figure 3.28. Variation of dielectric constant of PVC- <i>g</i> -poly(MMA- <i>co</i> -VTM)- <i>g</i> -Fe ₃ O ₄ with frequency at room temperature	47
Figure 3.29. Variation of dielectric loss of PVC- <i>g</i> -poly(MMA- <i>co</i> -VTM)- <i>g</i> -Fe ₃ O ₄ with frequency at room temperature	47
Figure 3.30. Variation of AC conductivity of PVC- <i>g</i> -poly(MMA- <i>co</i> -VTM)- <i>g</i> -Fe ₃ O ₄ with frequency at room temperature	48
Figure 3.31. Variation of AC conductivity of PVC- <i>g</i> -poly(MMA- <i>co</i> -VTM)- <i>g</i> -Fe ₃ O ₄ with angular frequency at room temperature	48
Figure 3.32. FT-IR spectrum of Propargyl methacrylate (POHMAC)	49
Figure 3.33. FT-IR spectrum of poly(POHMAC- <i>co</i> -VTM)	50
Figure 3.34. FT-IR spectrum of poly(POHMAC- <i>co</i> -VTM)- <i>g</i> -Fe ₃ O ₄	51
Figure 3.35. FT-IR spectrum of PVC- <i>g</i> -poly(POHMAC- <i>co</i> -VTM)- <i>g</i> -Fe ₃ O ₄	51

Figure 3.36. TGA and DTG curve of poly(POHMAC- <i>co</i> -VTM)	52
Figure 3.37. DSC curve of poly(POHMAC- <i>co</i> -VTM).....	53
Figure 3.38. TGA and DTG curve of poly(POHMAC- <i>co</i> -VTM)- <i>g</i> -Fe ₃ O ₄	53
Figure 3.39. DSC curve of poly(POHMAC- <i>co</i> -VTM)- <i>g</i> -Fe ₃ O ₄	54
Figure 3.40. TGA and DTG curve of PVC- <i>g</i> -poly(POHMAC- <i>co</i> -VTM)- <i>g</i> -Fe ₃ O ₄	54
Figure 3.41. DSC curve of PVC- <i>g</i> -poly(POHMAC- <i>co</i> -VTM)- <i>g</i> -Fe ₃ O ₄	55
Figure 3.42. VSM plot of PVC- <i>g</i> -poly(POHMAC- <i>co</i> -VTM)- <i>g</i> -Fe ₃ O ₄	56
Figure 3.43. Variation of dielectric constant of poly(POHMAC- <i>co</i> -VTM) with frequency at room temperature.....	56
Figure 3.44. Variation of dielectric loss factor of poly(POHMAC- <i>co</i> -VTM) with frequency at room temperature	57
Figure 3.45. Variation of conductivity of poly(POHMAC- <i>co</i> -VTM) with frequency at room temperature.....	57
Figure 3.46. Variation of dielectric constant of poly(POHMAC- <i>co</i> -VTM)- <i>g</i> -Fe ₃ O ₄ with frequency at room temperature	58
Figure 3.47. Variation of dielectric loss factor of poly(POHMAC- <i>co</i> -VTM)- <i>g</i> -Fe ₃ O ₄ with frequency at room temperature	58
Figure 3.48. Variation of conductivity of poly(POHMAC- <i>co</i> -VTM)- <i>g</i> -Fe ₃ O ₄ with frequency at room temperature	59
Figure 3.49. Variation of dielectric constant of PVC- <i>g</i> -poly(POHMAC- <i>co</i> -VTM)- <i>g</i> -Fe ₃ O ₄ with frequency at room temperature	59
Figure 3.50. Variation of dielectric loss factor of PVC- <i>g</i> -poly(POHMAC- <i>co</i> -VTM)- <i>g</i> -Fe ₃ O ₄ with frequency at room temperature	60
Figure 3.51. Variation of conductivity of PVC- <i>g</i> -poly(POHMAC- <i>co</i> -VTM)- <i>g</i> -Fe ₃ O ₄ with frequency at room temperature	60
Figure 3.52. FT-IR spectrum of N ₃ PTMS	61
Figure 3.53. FT-IR spectrum of N ₃ PTMS- <i>g</i> -Fe ₃ O ₄	61
Figure 3.54. FT-IR spectrum of POH-N ₃ PTMS- <i>g</i> -Fe ₃ O ₄	62
Figure 3.55. TGA and DTG curve of N ₃ PTMS- <i>g</i> -Fe ₃ O ₄	63
Figure 3.56. DSC curve of N ₃ PTMS- <i>g</i> -Fe ₃ O ₄	63
Figure 3.57. TGA and DTG curve of POH-N ₃ PTMS- <i>g</i> -Fe ₃ O ₄	64
Figure 3.58. DSC curve of POH-N ₃ PTMS- <i>g</i> -Fe ₃ O ₄	64
Figure 3.59. TGA and DTG curve of PVC / 5% (by wt) POH-N ₃ PTMS- <i>g</i> -Fe ₃ O ₄ composite.....	65
Figure 3.60. DSC curve of PVC / 5% (by wt) POH-N ₃ PTMS- <i>g</i> -Fe ₃ O ₄ composite.....	65
Figure 3.61. TGA and DTG curve of PVC / 10% POH-N ₃ PTMS- <i>g</i> -Fe ₃ O ₄ composite	66
Figure 3.62. DSC curve of PVC / 10% POH-N ₃ PTMS- <i>g</i> -Fe ₃ O ₄ composite.....	66

Figure 3.63. TGA and DTG curve of PVC / 20% (by wt) POH-N ₃ PTMS-g-Fe ₃ O ₄ composite	66
Figure 3.64. DSC curve of PVC / 20% (by wt) POH-N ₃ PTMS-g-Fe ₃ O ₄ composite	67
Figure 3.65. SEM image of N ₃ PTMS-g-Fe ₃ O ₄	68
Figure 3.66. EDX image of N ₃ PTMS-g-Fe ₃ O ₄	68
Figure 3.67. SEM image of POH-N ₃ PTMS-g-Fe ₃ O ₄	68
Figure 3.68. EDX image of POH-N ₃ PTMS-g-Fe ₃ O ₄	69
Figure 3.69. SEM image of PVC / 5% (by wt) POH-N ₃ PTMS-g-Fe ₃ O ₄ composite	69
Figure 3.70. EDX image of PVC / 5% (by wt) POH-N ₃ PTMS-g-Fe ₃ O ₄ composite	69
Figure 3.71. SEM image of PVC / 20% (by wt) POH-N ₃ PTMS-g-Fe ₃ O ₄ composite	70
Figure 3.72. EDX image of PVC / 20% (by wt) POH-N ₃ PTMS-g-Fe ₃ O ₄ composite	70
Figure 3.73. VSM plot of PVC / 10% (by wt) POH-N ₃ PTMS-g-Fe ₃ O ₄ composite	71
Figure 3.74. Variation of dielectric constant of POH-N ₃ PTMS-g-Fe ₃ O ₄ with frequency	71
Figure 3.75. Variation of dielectric loss of POH-N ₃ PTMS-g-Fe ₃ O ₄ with frequency	72
Figure 3.76. Variation of conductivity of POH-N ₃ PTMS-g-Fe ₃ O ₄ with frequency	72
Figure 3.77. Variation of dielectric constant of PVC / 5% (by wt) POH-N ₃ PTMS-g-Fe ₃ O ₄ composite with frequency	73
Figure 3.78. Variation of dielectric loss of PVC / 5% (by wt) POH-N ₃ PTMS-g-Fe ₃ O ₄ composite with frequency	73
Figure 3.79. Variation of conductivity of PVC / 5% (by wt) POH-N ₃ PTMS-g-Fe ₃ O ₄ composite with frequency	73
Figure 3.80. Variation of dielectric constant of PVC / 10% (by wt) POH-N ₃ PTMS-g-Fe ₃ O ₄ composite with frequency	74
Figure 3.81. Variation of dielectric loss of PVC / 10% (by wt) POH-N ₃ PTMS-g-Fe ₃ O ₄ composite with frequency	74
Figure 3.82. Variation of conductivity of PVC / 10% (by wt) POH-N ₃ PTMS-g-Fe ₃ O ₄ composite with frequency	74
Figure 3.83. Variation of dielectric constant of PVC / 20% (by wt) POH-N ₃ PTMS-g-Fe ₃ O ₄ composite with frequency	75
Figure 3.84. Variation of dielectric loss of PVC / 20% (by wt) POH-N ₃ PTMS-g-Fe ₃ O ₄ composite with frequency	75
Figure 3.85. Variation of conductivity of PVC / 20% (by wt) POH-N ₃ PTMS-g-Fe ₃ O ₄ composite with frequency	75
Figure 3.86. Variation of dielectric constant of PVC / POH-N ₃ PTMS-g-Fe ₃ O ₄ composites with frequency	76
Figure 3.87. Variation of dielectric loss of PVC / POH-N ₃ PTMS-g-Fe ₃ O ₄ composites with frequency	76

Figure 3.88. Variation of conductivity of PVC / POH-N₃PTMS-g-Fe₃O₄ composites with frequency..... 76



LIST OF TABLES

	Page No.
Table 3.1. FT-IR spectrum evaluation of PVC	31
Table 3.2. FT-IR spectrum evaluation of PVC-N ₃	32
Table 3.3. ¹ H-NMR spectrum evaluation of PVC-N ₃	33
Table 3.4. ¹³ C-APT spectra evaluation of PVC and PVC-N ₃	33
Table 3.5. TGA and DSC evaluation of PVC	35
Table 3.6. FT-IR spectrum evaluation of propargyl- α -bromoisobutyrate	36
Table 3.7. ¹ H-NMR spectrum evaluation of propargyl- α -bromoisobutyrate.....	37
Table 3.8. ¹³ C-APT spectrum evaluation of propargyl- α -bromoisobutyrate	38
Table 3.9. FT-IR spectrum evaluation of poly(MMA- <i>co</i> -VTM)	38
Table 3.10. TGA and DSC evaluation of PVC- <i>g</i> -poly(MMA- <i>co</i> -VTM)- <i>g</i> -Fe ₃ O ₄	41
Table 3.11. FT-IR spectrum evaluation of Propargyl methacrylate (POHMAC).....	49
Table 3.12. FT-IR spectrum evaluation of poly(POHMAC- <i>co</i> -VTM).....	50
Table 3.13. FT-IR spectrum evaluation of poly(POHMAC- <i>co</i> -VTM)- <i>g</i> -Fe ₃ O ₄	51
Table 3.14. FT-IR spectrum evaluation of PVC- <i>g</i> -poly(POHMAC- <i>co</i> -VTM)- <i>g</i> -Fe ₃ O ₄	52
Table 3.15. TGA, DTG and DSC evaluation of PVC- <i>g</i> -poly(POHMAC- <i>co</i> -VTM)- <i>g</i> -Fe ₃ O ₄	55
Table 3.16. FT-IR spectrum evaluation of N ₃ PTMS	61
Table 3.17. FT-IR spectrum evaluation of N ₃ PTMS- <i>g</i> -Fe ₃ O ₄	62
Table 3.18. FT-IR spectrum evaluation of POH-N ₃ PTMS- <i>g</i> -Fe ₃ O ₄	62
Table 3.19. TGA, DTG and DSC evaluation of POH-N ₃ PTMS- <i>g</i> -Fe ₃ O ₄	64
Table 3.20. TGA, DTG and DSC evaluation of PVC / POH-N ₃ PTMS- <i>g</i> -Fe ₃ O ₄ composites	67

LIST OF SYMBOLS AND ABBREVIATIONS

Symbols

M_s	Saturation magnetization
T_g	Glass transition temperature
T_i	Initial decomposition temperature
χ_i	Initial magnetic susceptibility
ω	Angular frequency
ε'	Dielectric constant
ε''	Dielectric loss
σ_{ac}	Alternating electrical conductivity
σ_{dc}	Direct electrical conductivity

Abbreviations

POH	Propargyl alcohol
BIBB	Bromoisobutyryl bromide
VTM	Vinyltrimethoxysilane
MMA	Methylmethacrylate
NPs	Nanoparticles
MAC	Methylacryloyl chloride
TEA	Triethylamine
DCM	Dichloromethane
THF	Tetrahydrofuran
DMF	Dimethylformamide
PVC	Poly(vinyl chloride)
PVC-N ₃	PVC azide
AIBN	Azoisobutylnitrile
DSC	Differential Scanning Calorimetry
TGA	Thermogravimetric analysis
SEM	Scanning Electron Microscope
EDX	Energy Dispersive X-ray spectroscopy

VSM	Vibration sample magnetometry
h	Hour
min	Minute
mbpy	5,5'-dimethyl-2,2'-dipyridyl
N ₃ PTMS	3-azidopropyltrimethoxysilane
DTG	Derivative thermogravimetry
ATRP	Atom transfer radical polymerization



1. INTRODUCTION

The term polymer has its origin from Greek words poly meaning “many” and meros meaning “parts.” Hence, a polymer is a huge molecule built up by the recurrence of minor chemical units. Polymers form an important class of materials without which life seems very difficult. Certain polymers, such as protein, silk, and cellulose are found in nature while many others are only produced by synthetic routes such as polystyrene, nylon, and polyethylene. Also, some natural polymers can be manufactured synthetically. An essential example is a polyisoprene which is the synthetic confirmation of natural rubber (Hevea) [1]. They are around us for everyday use; rubber, plastics, adhesives, and resins. Today, polymers touch almost every aspect of modern life and their manufacture and assembly are core global industries. Chances are almost all individuals who have touched at least single polymer products such as bottles, tires, and gadgets. Polymers are used nearly in all aspects of present-day living. Shopping bags, water bottles, phones, computers, auto parts, and food blister packs all comprise polymers. Even more sophisticated technology uses polymers such as membrane for water desalination, biopolymers for tissue engineering, and carrier used in drug controlled release.

Science of polymer origin may be dated back to the middle of the 19th century. Charles Goodyear (1830s) industrialized the vulcanization process that converted the latex form of rubber (natural) to worthwhile elastomer for tyre usage. In the 1930s, United States researchers at DuPont had manufactured a new variety of polymers including exotic materials like Teflon and rubber in the synthetic form. Dow in the year 1938 had made for the first time polystyrene on a commercial scale and In England ICI, scientists produced low-density polyethylene in the year 1839. The 1960s and 70s witnessed the emergence of several advanced high-performance plastics polymers used in engineering that go head to head well with materials of traditional form such as metals for aeronautic and automobile applications. Polyimides, polycarbonate, and polysulfones are included. The other is the rigid high-temperature polymer chain polymers. In recent times, polymers with special properties such as photoconducting, electrically conducting, and liquid crystalline has acted for a range of uses [1].

At its core, Polymer science is predominantly focused on the production of attention-grabbing new and advantageous polymeric materials for new applications and developments in current polymeric materials usually through the functionalization of functional monomers. Polymers including polypropylene, polyethylene, poly(vinyl chloride), and polystyrene are manufactured on an industrialized scale. Modification studies on polymers are very important because they will provide the formation of new functional groups and generate new usage areas for functional polymers [2].

1.1. Polymerization reaction

Polymerization is a method in which somewhat small molecules, termed a monomer, combine chemically to yield a very big molecule i.e network or chainlike, termed a polymer. The molecules of monomer may be all identical, or they might symbolize two or additional diverse compounds. Typically, no less than a hundred monomer molecules must be combined to create a product that has assured unique physical properties like high tensile strength, elasticity, or the capability to form fibers that differentiate polymers from materials made up of simpler and lesser molecules. Time and again, various thousands of monomer components are integrated into a distinct polymer molecule. The steady covalent bonds formed amongst the monomers set the polymerization process different from other processes.

1.1.1. Condensation polymerization

Condensation polymerization is chemically alike as a condensation reaction that produces a small organic molecule. These polymerizations usually take place with a loss of minute by-products e.g. water and mostly join two molecules of a different type in an alternating pattern. The monomers which given the condensation polymerization have two functional groups. These functional groups should be capable of the condensation reaction. Both of the functional groups that give condensation reactions can be in dissimilar molecules as well as in the same molecules [3]. Examples of condensation monomers are hexamethylene diamine, adipic acid, ethylene glycol, terephthalic acid, ethylene diamine, bisphenol A, terephthaloyl chloride, 1,4-butanediol, and 2,6-dimethyl phenol, etc.

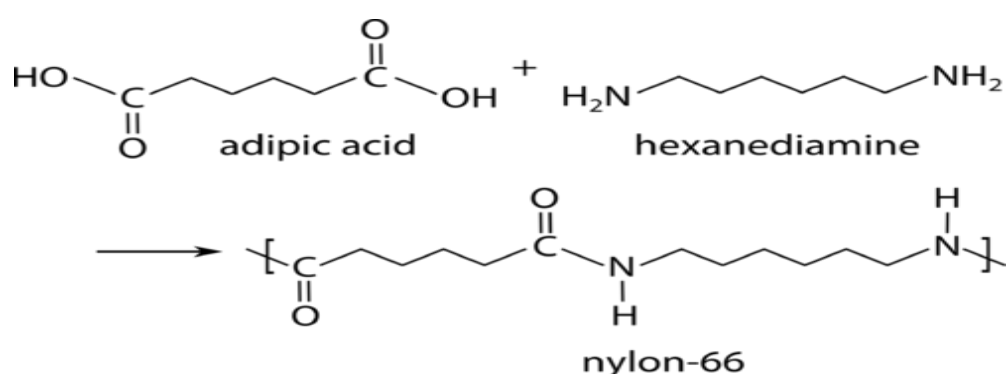


Figure 1.1. Scheme showing formation of a condensation polymer

The condensation polymerization monomers are not the same compared to those of addition polymerization. The key two characteristics for condensation polymerization polymers are;

- i. No double bonds in the monomers rather functional groups e.g. amine and alcohol.

- ii. Every monomer unit has at least binary functionality, which means two reactive sites.

Nylon-66 is an example of a polymer formed by condensation polymerization and is a polyamide.

Condensation polymers are formed extra slowly than addition counterparts, heat is required and the molecular weight generally is lower. On a chain, end functional groups stay active to facilitate the combination of groups with short chains into extensive chains at the end stages of polymerization. The presence of polar functional groups on the chains, repeatedly add to chain-chain attractions [3].

1.1.2. Anionic polymerization

Anionic polymerization is a method of addition polymerization that covers the polymerization of monomers (vinyl) with strongly electronegative groups. Entirely, the strong electronegative substituent (monomers), in the presence of carbanions polymerize freely. Certain substituents which are electron-withdrawing that stabilize the negative charge via delocalization of charge and Therefore, allow anionic polymerization consist of cyanide and carboxylic acid e.t.c. Thus, monomers such as styrenes, acrylates, epoxides, and dienes freely go through anionic polymerization. The initiators (electron donors) are strong anions or electron transfer agents. The electron transfer from an initiator to the monomer (vinyl) front-runners to the creation of a carbanion known as anion radicals [4]. Nucleophiles or Lewis bases are alkali group metals like lithium or sodium which are typical donors of an electron. Additional examples of strong nucleophilic initiators OH⁻, CN⁻, organometallic compounds like alkyl and Grignard reagents.

The kinetics of an anionic polymerization comprises of initiation and propagation. Let XMe be an organometallic compound that initiates polymerization and Mn a monomer, then the distinct steps can be shown as below [5].

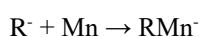
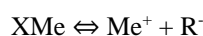
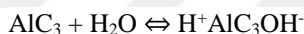


Figure 1.2. Schematic representation of anionic polymerization

In controlled systems, contaminants like H₂O or OH terminates the reaction called carbanion quenching which is present or deliberately added. The polymerization only terminates when the monomers are thoroughly consumed. Aimed at this point, this polymerization is often termed anionic “living” polymerization [5].

1.1.3. Cationic polymerization

Cationic polymerization is a method of chain-growth polymerization whereby an initiator (cationic) transfers a charge to a monomer (vinyl) therefore making it reactive. The formed monomer which is a reactive formed polymer by reacting with other monomers. A lot of vinyl monomers in the presence of a very minute quantity of catalyst of the kind used in Friedel-Crafts reactions freely undergo polymerization [4]. Catalysts of effective important are AlBr₃, AlCl₃, and BF₃ e.t.c. The aforesaid catalysts are all Lewis acids examples with strong electron-acceptor capability. The presence of co-catalyst is required in other to achieve the effectiveness of the catalyst which are Lewis bases e.g. H₂O and OH.



Monomers such as styrene, vinyl alkyl ethers, alpha-methyl styrene polymerize in the presence of the aforementioned catalyst [5]. Let X represent the catalyst, co-catalyst by YH, and the monomer by M, then the kinetics can be shown as follows.

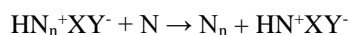
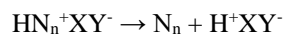
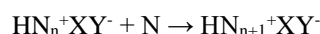
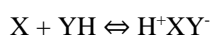


Figure 1.3. Schematic representation of cationic polymerization

1.1.4. Free radical polymerization

Free radical polymerization (FRP) is a class of chain-growth polymerization. FRP is among the techniques of polymer production in which the sequential monomer addition leads to polymer growth. The double bond of the monomer breaks changing it to propagating radical (active) [6]. Apart from its various benefits and extensive range of usage, the chain growth which is rapid and

the presence of the fast irreversible termination inflicts some restrictions. Likewise, the formation of copolymers (blocks) and complex polymer structures through FRP is unfeasible [7]. FRP proceed via four distinct stages:

Initiation: the polymerization is initiated by the formation of a reactive site.

Propagation: after the initiation step, units of monomers were added to the active polymer chain. Regeneration of the reactive site occurs after monomer addition.

Transfer: transfer of an active site to a free molecule such as a monomer or polymer occurs here. It results in a new molecule that is capable of undergoing propagation and a terminated molecule.

Termination: extinction of active site frontrunners to terminated (inert) macromolecules. It takes place via either combination or disproportion. The FRP mechanism is demonstrated schematically below.

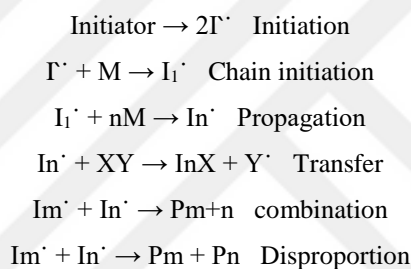


Figure 1.4. Schematic representation of free radical polymerization mechanism

1.1.5. Controlled radical polymerization

Controlled radical polymerization (CRP) depends on absolutely pure reactions so that no impurities can cause termination. CRP stops only when all the monomer is used. The reaction continues in the presence of an additional monomer. Copolymers (block) are produced using this method. This polymerization can be terminated and start again at any time. This innovative technology facilitates the synthesise of tailored polymers with composition control and macromolecular structure [8]. Currently, NMP, RAFT, and ATRP are the three most effective methods of CRP.

ATRP was first virtually at once in 1995 revealed by Sawamoto et al. and Matyjaszewski et al. Ruthenium-mediated polymerization was revealed by Sawamoto while the more common copper-catalyzed form of ATRP was detailed by Matyjaszewski [9]. One of the fastest rising areas of chemistry is ATRP and the process makes available control of diverse monomers polymerization under dissimilar conditions of the reaction and with ATRP also, it is feasible to synthesise polymers with an array of structures. The general mechanism of ATRP is shown in Figure 1.5.

of the most made polymers on functionalization studies. Many functionalization studies were carried out on PVC. The most basic reaction that PVC undergoes is the nucleophilic substitution reaction of the chlorine atom. Other-initiated research effort targeting the enhancement of several properties of PVC for producing innovative materials for particular uses includes grafting, copolymerization, and blending of vinyl chloride monomer [12].

1.2.1. Production of PVC

PVC is formed by vinyl chloride monomer (VCM) polymerization. The core polymerization techniques are suspension, bulk, and emulsion. Almost 80% of polymerization comprises the suspension. First, the resource VCM is pressurized and liquefied and then fed into the polymerization vessel which contains H₂O and suspending agents. then, the initiator is served into the vessel, and PVC is manufactured under pressure at 40-60 °C. The importance of H₂O is to control the heat given off during the process. PVC is produced in the form of particles of small size that grow and when preferred size is reached, the reaction terminates and vinyl chloride (unreacted) is distilled off for re-use. Finally, The PVC is dried and a white powder called PVC resin is formed.

1.2.2. Properties of PVC

- i. Electrical Properties: good material used for insulation because of its dielectric strength
- ii. Durability: resistant to shock, weathering, corrosion, and abrasion
- iii. Mechanical Properties: lightweight, tough and resistant to abrasion
- iv. Chemical Resistance: resistant to all chemicals of inorganic origin. It has precise resistance counter to dilute acids, alkalis, and hydrocarbons which are aliphatic.
- v. Flame Retardancy: self-extinguishing products due to the high contents of chlorine.

1.2.3. Usage areas of PVC

- i. Construction: frames, pipes for water, roofing, insulation for cables, greenhouses, and lining for roof and windows.
- ii. Domestic: Curtain supports, drawer sides, lamination, cases for audio and videotapes, wall covering, and cloth made of up leather.
- iii. Transport: seatbacks, under and window seal, insulation for wires, and decorative trim
- iv. Electrical: pipes for insulation, electrical boxes, switches and socket, plug housing, terminals for batteries, insulation for cable and wire, cable jacket
- v. Others: credit cards, traffic signs, inflatables, sports equipment, toys for children, and garden hoses.

1.3. Nucleophilic substitution reactions on PVC

A nucleophile is a molecule that is attracted strongly to a positive charge area in another molecule. Nucleophiles are either wholly anion or else have a partial negative charge someplace on a molecule [13].

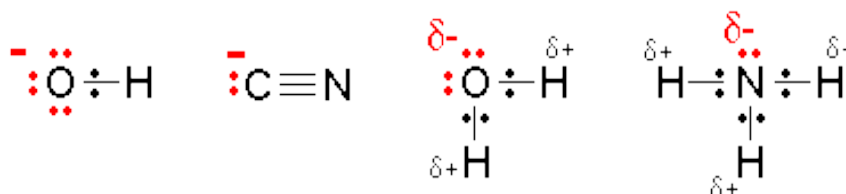


Figure 1.7. Examples of nucleophile

Each of the nucleophiles carries a single lone pair of electrons at least either on an atom with a complete negative charge or on an atom which is highly electronegative with a partial negative charge.

Nucleophilic substitution reaction is a vital type of reaction where a nucleophile which is electron-rich selectively attacks the positive or partially positive charge of an atom or a group of atoms to substitute a leaving group. Subsequently, a new bond forms between the electrophile (AY) carbon which is partially positive, and the nucleophile (X), and bond breaks between the partially positive carbon of the electrophile and the partially negative leaving group (Y) [3, 13].

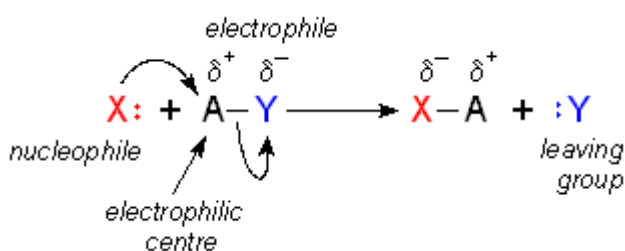


Figure 1.8. Schematic representation of nucleophilic substitution reaction

Quite a lot of chemical reactions were useful for instance degradation, substitution, and elimination. Undoubtedly, the utmost studied is nucleophilic substitution. On the other hand, once the nucleophile basicity goes beyond its nucleophilic power, the HCl removal takes place through substitution. Nucleophilic substitution in PVC of chlorine by a sequence of functional groups has been well-thought-out by various writers as a suitable technique for properties improvement, in precise the stability (thermal) via the replacement of chlorines which can easily be changed [14, 15]. In the chemical PVC modification, the broadly used nucleophilic reagents are the azide and

dithiocarbamate groups. while the azide anion is moderately strong in protic solvents, even stronger in dipolar aprotic solvents. It obtains high degrees of conversion by reacting easily with PVC in dipolar solvents, even though at these modification levels a clear elimination is achieved at the same time. The PVC azide group has been extra changed into various derivatives and is significant in terms of modification and functionalization [16]. Cl substitution in PVC by I⁻, SCN⁻, OH⁻ and N₃⁻ was conducted by Kameda et al. (2009) in a DMF or ethylene glycol solvent. The polymer-modified by substituting Cl in PVC with I shows the conductive property, SCN⁻ substituted PVC demonstrates antibacterial effect, and the modification with N₃⁻ lead to more polymer class with functionality due to the N₃ group reactivity. In the case of phthalimide anion, an ion-exchange resin is projected.

He et al. (2012) documented greatly efficient PVC dechlorination at atmospheric pressure with 1-butyl-3-methylimidazoliumhydroxyde at 180 °C. Navarro et al. (2008) took in aromatic thiols alteration such as 4-fluorothiophenol, 4-chlorothiophenol, 3,4-difluoro thiophenol, pentachlorothiophenol, and pentafluorothiophenol with PVC using cyclohexane as a solvent. Many chemical modifications of PVC were presented by Moulay (2010) centered on the last decade's information, along with related uses. Additionally, nucleophilic reactions have also been reported with various thiol compounds [11, 17-20].

1.4. Click reactions

From the time it was introduced, click chemistry has attracted a considerable extent of attentiveness. The title click chemistry was designated by Sharpless *et al.* (2001) and was defined as “a reaction that is flexible, varied in range, great in yield, side products are minutes that are without difficulty removed by non-chromatographic technique, is stereospecific but not certainly enantioselective, the conditions of the reaction are simple, is not easily affected by H₂O or oxygen, uses reagents which are simply obtainable, no solvent is necessary or easily removed solvent or benign similar to H₂O, isolation of the product is easy, a thermodynamic driving force is extraordinary(>20 kcal/mol) and completion is fast” [21].

Cu-I-catalyzed azide/alkyne cycloaddition (CuAAC) is almost all in click reaction that justifies the aforementioned conditions. The non-catalyzed azide/alkyne reaction has been identified from the time when (1893) when A. Michael give an account of the earliest reaction of diethyl acetylene dicarboxylate and phenyl azide to give 1,2,3-triazoles. The reaction is called Huisgen reaction. The reaction products are 1,4 and 1,5-disubstitution mixture while the CuAAC reaction of terminal alkynes, the formation of the 1,4-disubstituted triazoles is choosy as below with a diversity of Cu-I catalysts or Cu-I catalysts precursors [22].

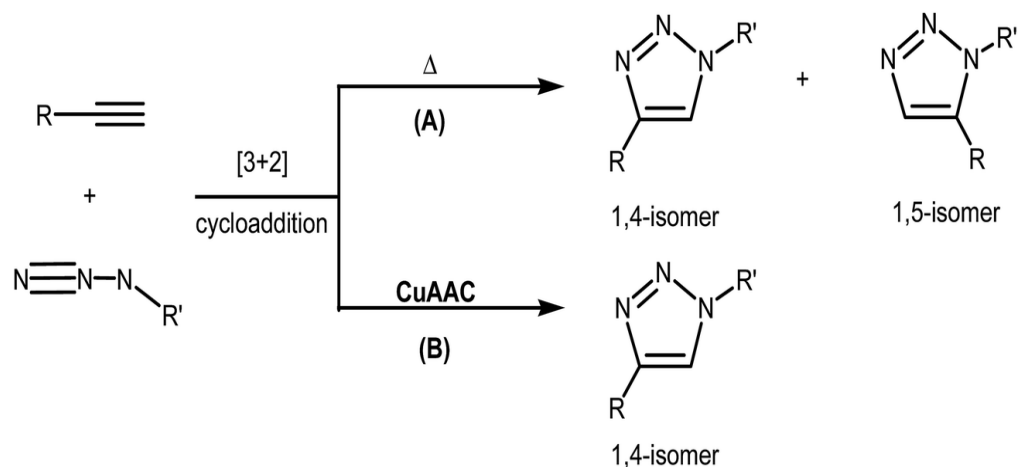


Figure 1.9. (A) Uncatalyzed thermal (B) Copper (I) catalyzed cycloaddition reaction

Sharpless and Fokin presented a premature mechanism as shown in Figure 1.11 that has aided on the use of CuAAC azides reaction utilizing terminal alkynes as a worthy idea in their seminar report.

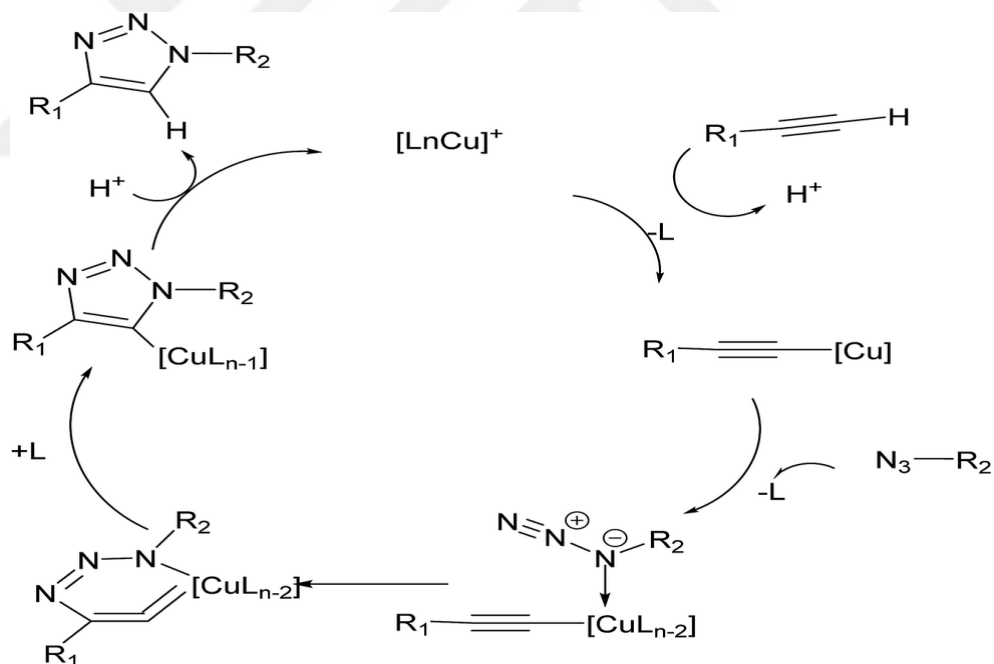


Figure 1.10. Early CuAAC mechanism proposed by Sharpless and Fokin [23, 24].

1.5. Functionalization of polymers via click reactions

In recent decades, polymerization chemistry has progressed remarkably. Similarly, post-polymerization advanced by permitting chemists with interest in polymer to influence the strength of organic synthesis for the cohort of gradually more molecules which are functional and

complex. A reactive precursor of polymer functionalization over and over again proves useful over functional monomers that undergo direct polymerization. Post-polymerization modification additionally suggests a method for polymers synthesis with pendant sets that would else go through side reactions with respect to polymerization conditions or that would ascertain interesting for characterization or processing. In the understanding of these points deliberated, post-polymerization modification is matured enough to the degree that it and direct polymerization should be a well-thought-out and in the same way sustainable method for functional polymers preparation [2].

Lutz et al. (2005) described the initial polystyrenes end-functionalization using ATRP. The CuAAC of many functional acetylenes with azido-PS permitted the measurable emergence of end-functionalized polystyrene with a carboxylic acid or a vinyl group. The copolymers formed were cast-off in a 1,3-dipolar cycloaddition (second click reaction) with poly (ethylene oxide) methyl ether 4-pentynoate, come about the emergence of brush-like polymer material with hydrophilic PEO side chains with a reasonable grafting density [25, 26]. Haddleton et al. (2005) described the other technique for ATRP- generated macromolecules clicking by polymerization with an azide functionalized initiator. This early information headed to the prompt spread of further techniques recounting the amalgamation of ATRP and CuAAC to aid the creation of functional telechelic, networks, and bio nanoparticles. CuAAC has furthermore been successfully joined with extra controlled polymerization ways and means comprising RAFT and NMP [26, 27]. Fleischmann et al. (2008) established a unique, fine, and clear random terpolymer produced using NMP [28].

Also, Gondi et al. (2007) label styrene polymerization and azide functional N,N-dimethylacrylamide used as agents of chain transfer agents to mediate RAFT [26]. Li et al. (2007) by way of RAFT polymerization polymerized 2-azidoethyl methacrylate (AzMA) and post-functionalization of polyAzMA was performed successfully through CuAAC with phenylacetylene by way of insignificant difference in the Mw distribution [29]. The tactic of merging RAFT with click reaction can be useful to make a varied variety of polymeric functional materials, mainly once the pendant moiety possibly will affect the polymerization reaction [26]. It is also important to note that, there are binding of other polymers by grafting reactions [30, 31].

1.6. Functionalization of PVC via click reactions

One of the most important types of reactions made on PVC is the “click” reaction. It is possible with this reaction type to assign a varied range of functional groups to PVC. For the click reactions on the PVC, the nucleophilic substitution reaction with the azide ion is carried out first, and then, azide on PVC is linked by an addition reaction to the acetylene derivative compound to

give 1,2,3-triazine ring. The catalyst used for such reactions type is copper (I)-bipyridine complex.

In 2008, Kiskan et al. reported the formation of benzoxazines from azide functionalized PVC and propargylbenzoxazine [12]. Attachment of propargyl ether monoethyl phthalate type of plasticizer to PVC azide lead formation of modified PVC in which the T_g of the PVC modified was inferior to that of the unmodified PVC showed that the plasticization effect was positive [21, 32].

Cationic polymers of bacterial type bearing alkyne groups were well manufactured and grafted onto azide functionalized surfaces of PVC, the acquired cationic surfaces demonstrated improved polarity and hydrophilicity relating to PVC and azide PVC and the great bactericidal effectiveness of the cationic surfaces synthesized against *E. coli* and *S. epidermidis* were shown by the live and dead test [30].

Polysaccharides, as well as polyethylene glycol bearing alkyne groups, were well synthesized and grafted onto surfaces of PVC azide. The acquired surfaces demonstrated improved polarity and hydrophilicity relating to PVC and azide PVC. Similar to PEG, Methyl Cellulose, and Hydroxyethyl Cellulose grafted onto PVC with azide surfaces unveiled an increase bacteria repellent outcome against *E. coli* [30].

1.6. Inorganic nanoparticle

Size is the central describing feature of all nanomaterials. It is a simple idea to comprehend, it is extra challenging to relate for the reason that there are no natural, physical or chemical limits that outline the “nanoscale.” By resolution, 1-100 nm is the range in terms of size utmost frequently used in orientation to nanomaterials but there is no bright spot that demarks the nanoscale from a chemical or biological view [33]. Among the various nanomaterials, inorganic nanoparticles are exceptionally important in modern technologies. They can be without problems and economically produced and mass-produced and for this motive, they can be extra freely unified into uses.

Nanoparticles may perhaps be made from materials by various physical and chemical means, with the particles in their elemental masterpiece, size, form, physical and chemical properties [34]. The physical approach involves vapor deposition and depends based on dividing the main precursor constituents into minor nanoparticles. The chemical method by and large consists of the reduction of metal ions into atomic form in the existence of stabilizing agents tailed by a controlled atoms collection [35]. The chemical approach of nanoparticle synthesis has ascertained to be further current than the usage of physical ways and means.

At the nanoscale dimension, the riches of the materials may alter considerably to diverge thoroughly from their main precursors. The decrease in material size leads to a shoot up in the

proportion of surface atoms which leads to a shoot up in reactivity which shapes them very much reactive catalysts with the atomic surface, the axes for basic catalytic activity [36]. As a result, nanoparticles have distinctive electronic, magnetic, mechanical, and optical material goods that ascend plainly in line for their size which is in the nanometer-scale. For these distinctive assets, NPs can be engaged in uses in different fields such as catalysis, treatment of wastewater, drug delivery, textiles, tissue engineering, cancer treatment, and MRI.

1.6.1. Magnetic nanoparticle

Magnetic NPs have lots of exceptional magnetic properties, for instance, superparamagnetic, high magnetic susceptibility and coercivity, etc. Magnetic nanoparticles are of countless importance for scholars from a wide-ranging discipline such as polymer modification, catalysis, and bioapplications [37].

Synthesis of magnetic nanoparticle: In the most recent decades, considerable work has been advanced to the production of MNPs and a lot of documents have recounts well-organized production ways to creates precise shape, steady, monodispersed and biocompatible MNPs. Some of the methods are;

Co-Precipitation: The supreme straight process for the production of MNPs is by way of co-precipitation. It comprises of reacting ferric and ferrous ions in a 1:2 molar ratio in a greatly basic solution at either elevated or room temperature. The MNPs shape and size entirely size and shape of the MNPs be determined by the salt type used sulfates, the ions ratio, the pH point, the temperature of the reaction, media ionic strength, and other parameters e.g. stirring rate. This process would desperately modify the chemical and physical possessions of the nanosized MNPs [38].

Microemulsion: The microemulsion is a thermodynamically unchanging isotropic dispersion of two immiscible parts (H_2O and oil) underneath the existing surfactant. At the interface between the water and oil, the surfactant particle may produce a single layer with the hydrophilic upper groups liquefied in the aqueous part while the lower hydrophobic of the surfactant particles in the oil part. As per the binary systems (oil/surfactant or water/surfactant), self-convene different types of structures can be found extending from cylindrical to spherical micelles to lamellar phases and also bicontinuous microemulsion, which possibly will harmonize with principally aqueous or oil parts [39].

Thermal decomposition: An organic solution segment decomposition method has remained commonly cast-off in MNPs production and disintegration of $Fe(cup)_3$, $Fe(acac)_3$ or $Fe(CO)_5$ tailed by oxidation can steer to excellence monodispersed MNPs which typically entails a relatively complex temperature and dense procedure. Even though the thermal disintegration

technique has a lot of merits for bringing into being very much monodispersed units with tapered size dissemination, the demerit is that the consequential NPs liquefied only in non-polar solvent generally [38]. Other methods of magnetic nanoparticle synthesis are Hydrothermal synthesis and Sonochemical synthesis [40-42].

Properties of magnetic nanoparticles

Magnetic property: The magnetic nanoparticle's properties rest on the process of synthesis and chemical configuration. Mainly, 1 to 100 nm is the range in terms of the size of Fe_3O_4 and can exhibit superparamagnetism which is initiated by thermal effects that the thermal fluctuations are an adequate amount to unexpectedly demagnetize an earlier saturated assemblage and as a result, these particles have zero coercivity and have no hysteresis. In this situation, a magnetic field (external) is in a position to magnetize the nanoparticles with far greater magnetic susceptibility [43]. As soon as the field is wiped off, Fe_3O_4 show certainly not magnetization. These effects can be worthwhile for targeted drug delivery and controlled therapy.

Magnetocaloric effect: MCE is defined as the ability of various magnetic materials to become active the minute they are positioned in a magnetic field and become inactive as soon as they are detached from a magnetic field. The activity is in terms of heat. Fe_3O_4 offers a favorable substitute to typical bulk materials for the reason that, their particle dimension-reliant on superparamagnetic structures. Furthermore, the great surface area in magnetic nanoparticles has the prospective to make available enhanced heat give-and-take with the immediate environs [43].

Physical property: Magnetic effects are initiated by activities of particles that have at the very same time electric charges and mass. They are electrons, protons, positive and negative ions, and holes. A magnetic dipole is created by a spinning electron charged particle called magneton. Magnetons are allied with sets in ferromagnetic materials [44].

1.7. Modification of magnetic nanoparticles

In recent times, polymers functionalized iron oxide NPs are being paid extra considerable thoughtfulness, due to the benefits of coating (polymers) will raise repellant forces to stabilize the van der Waals and the magnetic and attractive forces pro tem on the NPs. To add to it, the coating of polymers on the NPs (iron oxide) surface comes with a great perspective in the implementation of numerous fields. Besides, polymer functionalized iron oxide NPs have been comprehensively studied owing to importance in their distinctive chemical or physical properties [38].

Presently, two main key evolving ways to produce polymers functionalized MNPs are; first is for the intention of increasing a variety of usage. e.g a polymerization by microemulsion to produce a poly(ethylene glycol) modified with Fe_3O_4 with a magnetic core and polymer with hydrophilic shell was described in 2004 by Gupta et al. [38]. The size average of the modified

Fe₃O₄ exists to be round 40-50nm and size distribution which is narrow. The other is to develop a monodisperse Fe₃O₄ with controlled composition and a well-defined shape [45]. In 2004, Zhang et al. defined a process for the synthesis of Fe₃O₄ using templates of polymer microgels [38]. Through ATRP surface-initiated carried out in solvents which is polar, several polymers coated with Fe₃O₄ were well advanced [46, 47]. ATRP can be cast-off in polymers synthesis with Mw distribution which is narrow, copolymers like random, graft and block, and as a final point to recognize adjusting the thickness of the functionalized polymer Fe₃O₄ polymeric size and shell. Sun et al. (2007) have described Fe₃O₄/PS synthesis through ATRP (surface-initiated). Initially, initiators were bond covalently onto Fe₃O₄ surface, which was the integration of ligand exchange reaction and condensation of triethoxysilane with an ATRP site of initiation, 2-Bromo-2-methyl-N-(3-(triethoxysilyl)propyl) propanamide. Then and there, the shell of PS was grafted from the sites of initiation on to Fe₃O₄ surface via ATRP [38].

1.8. Thermal investigation of polymers

Thermal investigation of polymers integrates those methods in which a number of a physical parameter of the system is set on and documented as a function of temperature (T). Measurements centered on dynamic relationships between temperature and mass, volume, the heat of reaction. Some of the thermal methods of analysis are;

1.8.1. Differential scanning calorimetry (DSC)

DSC is a thermoanalytical process in which the change in the amount of heat required to increase the temperature of a sample and reference are studied. Equally, the sample and reference are held in reserve at narrowly the equivalent temperature throughout the investigation. DSC is a system used for assessing the energy needed to form a practically zero temperature variance between a material and an inert material that act as a reference. DSC can be used to study the T_g , melting and boiling temperature, crystallization temperature and time, percentage crystallinity, thermal stability, reaction kinetics, and purity e.t.c [48].

DSC equipment is consists of a measurement compartment and a computer. In the compartment, two pans are heated. The sample under study is contained within the sample pan and a subsequent pan which is used as a reference is normally empty. The computer is set up to observe the temperature and control the rate of change of the pan temperature. About 10 °C/min is the usual heating rate. The outcome is a scheme of the variation in heat (q) against temperature (T).

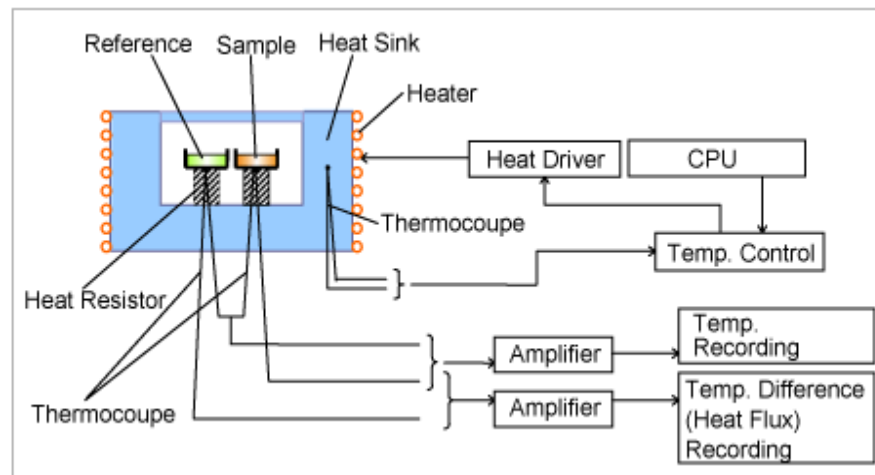


Figure 1.11. Block diagram of heat flux DSC

1.8.2. Thermogravimetric Analysis (TGA)

TGA is a technique in which the weight of a material in an environment heated or cooled at a well-ordered rate is note down for temperature or time. A large number of chemical substances consistently decompose upon heating and the underlying principle of TGA is the idea of heating a sample to observe weight changes. It consists of a sample/sample holder, sensors to ascertain the property of the sample, and the temperature and also a computer for data regulation, processing, and collection [49]. The techniques of analysis generally adopted are,

- i. Dynamic TGA: it involves constant increased in temperature linear with time
- ii. Isothermal TGA: retained continuous temperature aimed at a given time for the period of which its weight is noted down.

1.8.3. Differential thermal analysis (DTA)

DTA involves the method of documenting the change in temperature amongst material and a reference material contrary to either temperature or time. Thus, a differential thermogram consists of a record of the changes in sample and reference temperature plotted as a function of time, sample temperature, reference temperature, or furnace temperature. Both reference and sample are positioned evenly in the furnace. It is regulated under a temperature program and the sample temperature and reference are altered. Through the course, a differential thermocouple is arranged to mark the temperature change between the reference and the sample [48].

1.9. Electrical investigation of polymers

Polymers have been known for quite a long as insulating materials and are a lot used to insulate electrical devices and cables. And yet, there is various polymers type that conducts

electricity. The conductivity property of these polymers is centered on the occurrence of double bonds which are conjugated alongside the polymer backbone. Conjugation single-handedly leads to little electrical conductivity. Additionally, doping the polymers with charge carriers that make holes available. New holes are formed by filling neighboring carbon atoms electrons and so on. Hence, agreeing to the movement of charge over a lengthy distance.

1.10. Electron microscopy investigation of polymers

Electron microscopes have been technologically advanced owing to the resolution limits of approximately 300 nm light microscopes enforced by the visible light wavelength. An electron microscope uses an electron beam as an alternative to visible light to illuminate the sample and create an enlarged image. Since the Broglie wavelengths of electrons are approximately 100,000 times shorter than visible light, the electron microscope can reach 0.05 nm resolution and magnification up to approximately 10,000,000x.

1.10.1. Scanning electron microscopy (SEM)

SEM uses a high-energy fixated beam of electrons to produce a range of signals at the sample's surface that is solid. The signals that arise from interactions of electron-sample disclose evidence concerning the sample comprising external morphology, chemical composition, and crystalline structure. In the majority of usage, results are poised above a designated region on the surface of the specimen, and a 2-dimensional image is made that shows spatial differences in these possessions. Areas extending from just about 1 cm to 5 microns in width can be imaged in a scanning mode using regular SEM methods (magnification varies from 20X to nearly 30,000X and range of spatial resolution from 50 to 100nm). The SEM is prone to carrying out analyses of designated point positions on the specimen [50].

The crucial constituents of all SEMs are the source of electrons, lenses for electrons, chamber for samples, detectors for electrons, and display/data output devices. The SEM is regularly cast-off to produce high-resolution images of substances (SEI) and to display spatial variation in chemical compositions [50]. The picture of the Zeis EVO MA10 scanning electron microscope (SEM) device used in this research in Firat university central laboratory is shown below.

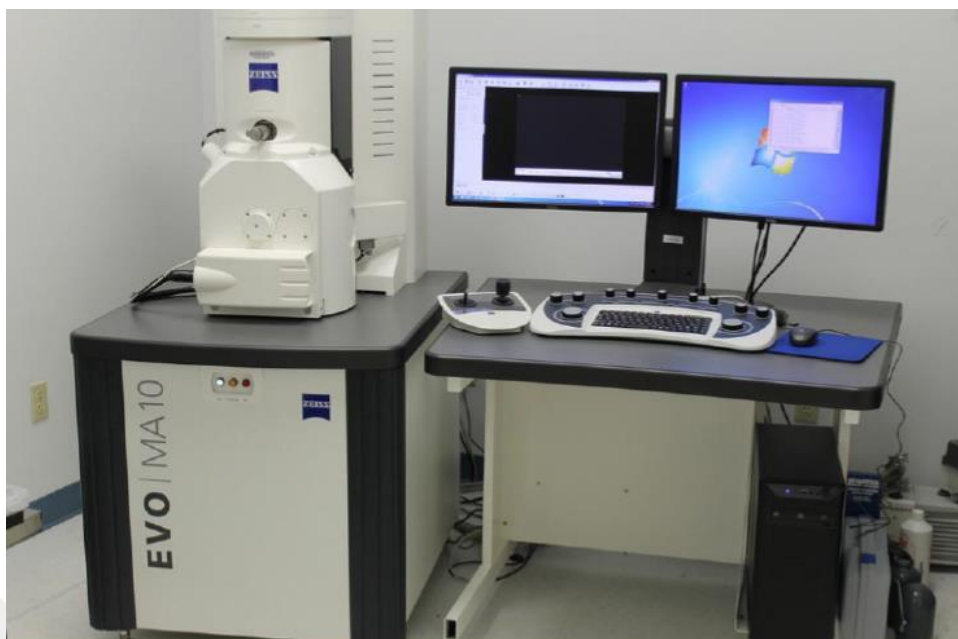


Figure 1.12. Image of SEM device.

1.10.2. Scanning electron microscope/energy dispersive x-ray spectrometer (SEM/EDX)

SEM/EDX is the finest recognized and utmost extensively used of the external analytical processes. Using primary focused scanning electron beam, images of high resolutions are made and also an outstanding depth of field. The primary electrons pass on a surface with energy (0.5-30kV) and create many secondary electrons with low energy. These secondary electron's intensity is mainly overseen by the sample surface topography. An image of the surface of the sample can, as a result, be created by calculating the intensity of the secondary electron for the position of the scanning primary electron beam [51].

1.10.3. Transmission electron microscopy (TEM)

TEM was the first electron microscope type made by Max Knoll and Ernst Ruska in 1931. It was precisely made according to the light transmission microscope blueprint, but a parallel electron beam was used instead of light. Currently, 400 kV TEM can make available resolutions lower than 0.2 nm and allow samples observation of approximately 500 nm thickness. TEM consists of basic parts which are electron gun that produces the electron current that focuses on a small, thin aligned beam of light using lens aperture and lens lenses. The beam hits the prepared sample and a portion of the electron beam is transmitted. The part which is transmitted focuses on the objective lens that creates the image. The image flow down the column via the extended intermediate and projector lenses via each lens [52].

TEM is a suitable method to examine in all kinds of carbon materials, including graphite their structural units. It also provides details about technique, topography, morphology, composition, and crystallographic features. TEM is a distinct solid tool for the qualitative and quantitative characterization of the micro and nanostructures and chemical structures of the material. On the other hand, it ought to be used as a complementary process rather than isolation when evaluating organic or carbonated samples [52].

1.11. Vibration sample magnetometry (VSM)

VSM is widely used in magnetic measurement because of its accuracy and precision. The VSM technique examines the periodic motion of a magnetic sample and the periodic magnetic field change resulting from this motion. It works according to the Faraday law, which is based on the principle that magnetic field change creates an electric field. In VSM measurements, the sample is positioned in a fixed magnetic field. When the sample placed in the device is magnetic, the applied magnetic field will want to regulate the magnetic moments. For magnetization to be large, it must be so large in the constant magnetic field. The magnetic dipoles in the sample will generate a magnetic field and when the VSM is moved by the motor, the magnetic field will vary as a function of time and induced current will occur.

The device can measure between 2K-400K. VSM device used in this research to examine the magnetic properties of Fe_3O_4 click products is given below and is a Quantum Design PPMS-9T device located in the Scientific and Technological Research Center at İnönü University.



Figure 1.13. Image of VSM device.

1.12. Aim and objectives

The foremost purpose of this research is to synthesize the magnetic poly (vinyl chloride), PVC. For this purpose, "click" reactions performed on PVC will be used. The appropriately functionalized magnetic nanoparticle will be connected through a "click" reaction to the PVC.

The objectives of the research are to:

- i. Characterize the structure of PVC, PVC-azide, and other PVC bearing compounds using FT-IR, $^1\text{H-NMR}$, and $^{13}\text{CNMR}$.
- ii. Characterize the magnetic nanoparticle-bearing compounds using FT-IR, VSM, SEM, and SEM-EDX techniques.
- iii. Investigate the thermal behaviors of all PVC-based products such as TGA, DTG, and DSC.
- iv. Investigate the electrical and dielectric properties of all PVC-based products relative to PVC.

1.13. Literature Review

For chemical modification of PVC, nucleophilic substitution reaction of the chlorine atom on the PVC chains is of paramount importance and requires strongly nucleophilic agents. This is well-thought-out by many authors as a suitable way of enhancing material goods particularly thermal stability via substitution of labile Cl atoms and mechanical properties [16]. Chemical modification of PVC by nucleophilic substitution of chlorine in PVC by I, SCN^- , phthalimide anion, and N_3^- was carried out by Kameda et al. (2009) in a solution of Nu/DMF or Nu/EG and the result is PVC Cl is substituted. Elimination was favored when PVC was evaluated in the Nu/EG solution with Nu/Cl. The substitution to dechlorination ratio was notable $\text{OH}^- > \text{SCN}^- = \text{N}_3^- > \text{phthalimide anion} > \text{I}$ in the descending sequence. A high substitution to dechlorination ratio was observed for the Nu/DMF solution in the direction $\text{SCN}^- > \text{N}_3^- > \text{I} > \text{phthalimide anion}$. The sequence was alike to those of reactivity constant of the nucleophile, $\text{I} > \text{SCN}^- > \text{N}_3^- > \text{phthalimide anion}$ in one as well as the other cases excluding for I. Substitution to dechlorination ratio was greater for I, SCN^- , N_3^- and phthalimide anion in DMF than in EG by relating the influence of EG and DMF on the substitution of Cl in PVC with Nu in solution [53].

Reinecke and Mijiangos (1995) reported that PVC chemical modification chains with thiol compounds which are bifunctional were achieved by introducing different functional groups. Up to 50% degree of substitution was achieved using para-substituted aromatic agents [54]. In 2006, Martinez synthesized PVC-g-PS via stereoselective PVC nucleophilic substitution with sodium azide as a nucleophile which shows that the very low reactivity improved the stereospecific nature of PVC substitution reaction and the grafting of styrene from PVC [16]. Nagasaki et al.

(2013) studied the modification of PVC with long alkyl chains with layered double hydroxides (DLH) as a basic catalyst by nucleophilic substitution. Apart from thiols and alcohols, PVC also reacted with amines and carboxylic acids. Thioglycolic acid derivatives in a high degree of substitution reacted with PVC. Reactivity was very low in cyclohexanone but substitution selectivity was exceptionally high while in N,N- Dimethylacetamide, reactivity was higher than cyclohexanone but elimination reaction also followed. Modification caused a lower degradation temperature [55].

PVC modification with new functional groups on the effect of reactivity of hydrogen bonds, specific volume, and stiffness was reported by Herrero et al. (2002). Bifunctional thio compounds, aliphatic and aromatic compounds were verified. The effect of functionalities on protic and nonprotic reactivity was studied. Protic functionalities prime to polymers with intensely improved T_g point signifying a significant system stiffening as a result of hydrogen bonds physical interaction and for modified PVC with substituents which are non-protic, the softening point temperature does not change to a great extent [11]. Salavagione et al. (2010) studied MWCNTs' functionalization by PVC substitution which is stereoselective. The nucleophilic substitution reaction was with potassium 4-hydroxythiophenolate [56]. Martinez and Millan (2003) studied the stereoselective PVC nucleophilic substitution with 4-Acetamidothiophenolate [16].

On PVC, click reactions were performed as reported by Kiskan et al. (2008) the formation of benzoxazines from PVC-N₃ and propargyl benzoxazine. The PVC clicked to benzoxazine formed a thermoset PVC with thermal stability which is higher than commercial PVC by going through thermally activated curing without catalyst present [12]. It was predicted that this novel polymers which are thermally curable family can be applied midway for the outline of further multipart macromolecular systems like interpenetrating networks and NPs through the collapse of the intramolecular chain [57]. Jia et al. (2017) reported the plasticization of PVC-N₃ with triethyl citrate of bio-based origin and which was through modification by chemical means for the very first time. The acquired modified PVC material showed an increase in thermal stability and decrease T_g related to PVC plasticized with dioctyl phthalate. Modified triethyl citrate PVC elongation at break and tensile strength were respectively 360.7% and 16.2 MPa meaning that the plasticization of PVC was through chemical reaction [58].

The CuAAC click reaction enables the combination of alkynes terminal group with azides by forming 1,4-disubstituted triazoles whereby copper(I) acts as the catalyst. In 2017, Asan and Ozturk synthesized poly (vinyl chloride-g-ethylene glycol) graft copolymers carried out using propargyl polyethylene glycol and azide functionalized PVC. The time that influenced the reactions and concentration were accessed as the prime parameters and it was observed that the copolymers formed were rather soft-rigid as polyethylene glycol was and PVC was rigid [21].

Akat and Ozkan (2010) successfully synthesize PVC bearing side-chain thioxanthone photoactive groups. The modification creates considerable change in PVC chemistry. Polymeric photoinitiators obtained were revealed to proficiently start FRP of mono- and multifunctional monomers through the mechanism of hydrogen abstraction devoid of the use of extra hydrogen donors such as amines [59].

Ouerghui et al. reported the extraction of heavy metals (Cd, Cu, Ni, and Pb) using the PVC triazole formed from PVC azide and alkyne compound of acyl chloride-containing different side-chain group and propargylamine. The polymers were then assessed based on their metallic ions extraction ability of the metals from the solution. The ions are extracted based on selectivity and affinity in the order $Cd^{2+} > Pb^{2+} > Cu^{2+} > Ni^{2+}$. In 2015, Yang *et al.* using click reaction covalently linked cardanol to chains of PVC. It acts as an internal plasticizer, and the PVC modified with cardanol shows decreased T_g , outstanding thermal stability, and migration which is near zero [60].

Lee et al. (2016) revealed through click grafting of hyperbranched polyglycerol vastly self-plasticized PVC for the first period. The plasticizing influence of the grafted HPG on PVC was studied by different analytical techniques. Grafted PVC free volume increased ably by HPG structure which lowers the T_g related to PVC plasticized. HPG significantly advances the elasticity of the PVC grafted at ordinary temperature by viscoelastic analysis and also upholds the system segmental motion [61]. In 2013, Paulak et al. reported the modification of PVC membranes with TEG, PEG and cysteine molecules via click chemistry which shows increased hydrophilicity of the surface by modification of the surface with PEG derivatives as demonstrated by contact angle measurement [62]. Zhu et al. (2015) reported self-healing PVC centered on microencapsulated nucleophilic thiol-click chemistry [63].

In 2016, Chung and Liu showed the forging scheme in the production of lignin grafted 5-acetylaminopentyl acrylate polymer which was synthesized by CuAAC click reaction of azide functional polymer and alkyne-modified lignin. The analysis of static tensile strength shows that 15-20 wt % lignin content composite revealed the best ideal properties such as flexibility and rubber-like structure. Owing to the high acetyl amino group's degree of hydrogen bonding, the material displayed self-healing material goods [64].

The nanocomposites of polymers with inorganic nanoparticles bear distinctive benefits. The varied functional properties of inorganic nanoparticles such as electronic, and magnetic can come into by the composite uniting with improved mechanical properties.

2. MATERIALS AND METHOD

2.1. Materials

Inorganic nanoparticle: magnetic nanoparticles (Fe_3O_4)

- Polymer: Poly(vinylchloride) (PVC)
- Monomers: Vinyltrimethoxysilane (VTM), methylmethacrylate (MMA), methacryloyl chloride (MAC)
- Initiators: α -Bromoisobutyryl bromide (BIBB) for ATRP, (AIBN) for free-radical polymerization
- Solvents: Tetrahydrofuran (THF), N,N-Dimethylformamide (DMF), Dichloromethane (DCM), Diphenyl ether, absolute ethanol, and acetonitrile
- Precipitators: Ethanol, methanol, ether, and hexane
- Other Chemicals used: copper (I) bromide (Cu(I)Br) and 5,5'-dimethyl-2,2'-bipyridyl as catalyst complex for ATRP and click reactions, propargyl alcohol (POH) for click reactions, sodium azide (NaN_3) for azidation reaction, 3-chloropropyltrimethoxysilane (CITMS), triethylamine (TEA), (TEABr), anhydrous magnesium sulphate (MgSO_4) and aluminum oxide (Al_2O_3).

2.2. Instrumentation

- Avery Berkel VA304-1AAZM13AAE electronic weighing balance was used
- Infrared spectra were recorded using Perkin Elmer spectrum one FT-IR spectrometer
- Sonication was carried out using ultrasonic sonicator FY-US-01 digital instrument
- PerkinElmer instruments Sapphire DSC was used to carry out calorimetric measurements
- PerkinElmer instruments Pyris Diamond TGA/DTA was used to carry out thermal stability studies
- Avence III Bruker 400MHz and 100MHz was used to record $^1\text{H-NMR}$ and $^{13}\text{C-NMR}$ spectra respectively
- Samples were dried using Nu Nuve EV 018 vacuum oven
- Solvents evaporation was carried out using BUCHI rotavopar R-200
- Dielectric measurements were carried out using QuadTech 7600 precision LCR meter
- VELP Scientifica ARE model magnetic stirrer is used for heating and mixing
- Other materials used are polymerization tubes, volumetric flasks, beakers, thermometer, measuring cylinder, Petri dish, pipette, dropper, funnel, pestle, and mortar.

2.3. Experimental

2.3.1. Purification of poly(vinyl chloride) (PVC)

PVC was purified as the cited literature [21] as follows; 100 mL tetrahydrofuran (THF) in a beaker was used to dissolve 10.00 g of PVC till a homogeneous solution was formed. The solution was precipitated dropwise in 1000 mL ethanol. The precipitate was filtered, stayed overnight in ethanol, and re-filtered. It was then dried at room temperature for 24 h and under vacuum for 24 h at 40 °C.

2.3.2. Synthesis of azide functional poly(vinyl chloride) (PVC-N3)

In a 100 mL N, N-Dimethylformamide (DMF) in a flask, 5.00 g of purified PVC was added followed by 6.00 g sodium azide (NaN_3) and Argon gas was injected for 15 min into the solution. The resulting solution was stirred for 24 h at 30 °C precipitated into methanol/water (1:1 by volume) and cooled for 30 min. The precipitate was filtered, stayed overnight in methanol/water mixture, filtered, and dried for 24 h at ambient temperature followed by vacuum at 40 °C for 48 h [64].

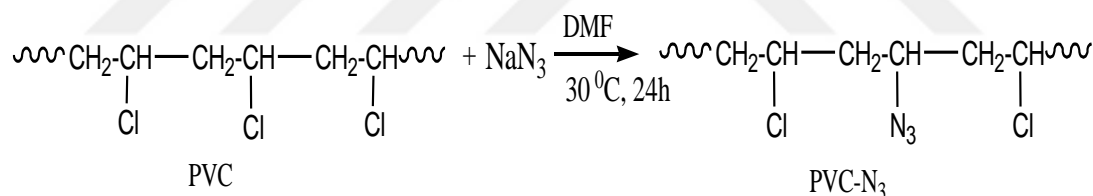


Figure 2.1. Synthesis of azide functional poly(vinyl chloride)

2.3.3. Synthesis of propargyl α -bromoisobutyrate (POH-BIBB)

0.98 g propargyl alcohol (POH) and 1.76 g TEA were added into a conical flask, followed by 20 mL dichloromethane (DCM). The solution was magnetically stirred in an ice bath until the temperature drops to 0-5 °C. 4.00 g BIBB was added dropwise, argon gas was for 15 min bubbled

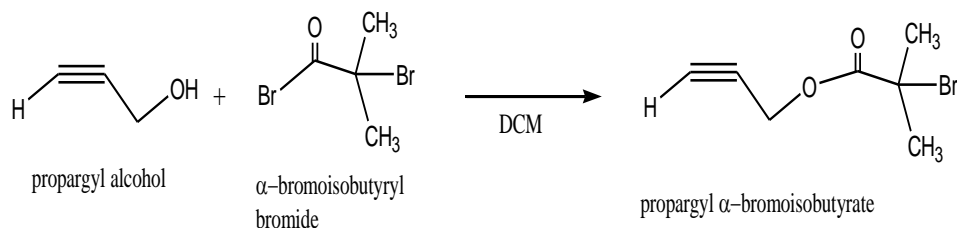


Figure 2.2. Synthesis of propargyl α -bromoisobutyrate

through, and continued overnight at ambient temperature. After completion of the reaction, the solution was filtered and evaporated. The crude mixture obtained was dissolved in DCM, poured into a separation funnel, and washed thrice with distilled water. The solvent phase was filtered, dried over anhydrous MgSO_4 , and stays overnight in the fridge. Then, filtered and evaporated leaving behind the product.

2.3.4. Atom transfer radical copolymerization of methylmethacrylate and Vinyltrimethoxysilane

Polymerization tube was charged with 0.06 g (0.4 mmol) Cu(I)Br , 0.184 g (1 mmol) 5,5'-dimethyl-2,2'-dipyridyl (mbpy), and 5 mL diphenyl ether and stirred at about 30 °C for 15 min. 3.00 g (20 mmol) vinyltrimethoxysilane (VTM), 2.00 g (20 mmol) methylmethacrylate (MMA), and 0.41 g (2 ml) POH-BIBB were dissolved in 15 mL diphenyl ether and was poured into the tube. Argon was bubbled for 15 min, the tube was firmly sealed, and continued for 24 h at 90 °C. Then, the mixture was passed from end to end of the Al_2O_3 column to get rid of the catalyst complex and precipitated in ether (cold), filtered off and dried under vacuum for 24 h at 50 °C.

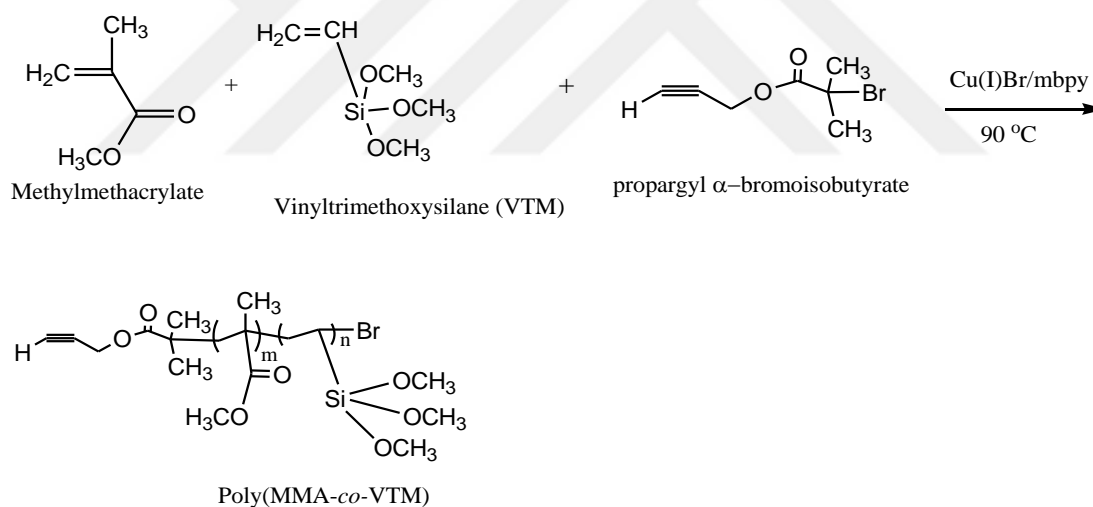


Figure 2.3. Synthesis of Poly(MMA-co-VTM)

2.3.5. Magnetic nanoparticle (Fe_3O_4) bonding to the (MMA-co-VTM) copolymer

In a 250 mL flask, 0.50 g Fe_3O_4 was sonicated in 100 mL absolute ethanol for 30 min. Copolymer (0.70 g) was added, Argon was injected for about 15 min and 6 h stirring at environs temperature then, for 48 h under reflux. Subsequently, the copolymer formed, poly (MMA-co-VTM)-g- Fe_3O_4 , was magnetically separated, washed with ethyl alcohol, and dried at ambient temperature followed by vacuum at for 24 h at 50 °C.

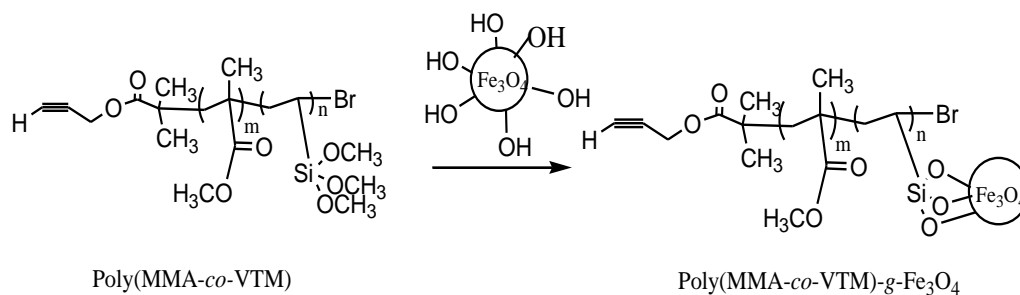


Figure 2.4. Synthesis of Poly(MMA-co-VTM)-g-Fe₃O₄

2.3.6. Click reaction of poly(MMA-co-VTM)-g-Fe₃O₄ and azide poly(vinylchloride) PVC-N₃

0.40 g of poly (MMA-co-VTM)-g-Fe₃O₄ was sonicated in 20 mL THF. 0.60 g PVC-N₃, 0.004 g (0.03 mmol) Cu(I)Br, and 0.014 g (0.075 mmol) mbpy were dissolved in 20 mL of THF and added to the sonicated mixture. Argon was passed through for about 15 min, the reaction continued for 24 h at 30-35 °C. The product was magnetically separated, washed with THF under the magnet, and dried under vacuum for 24 h at 50 °C.

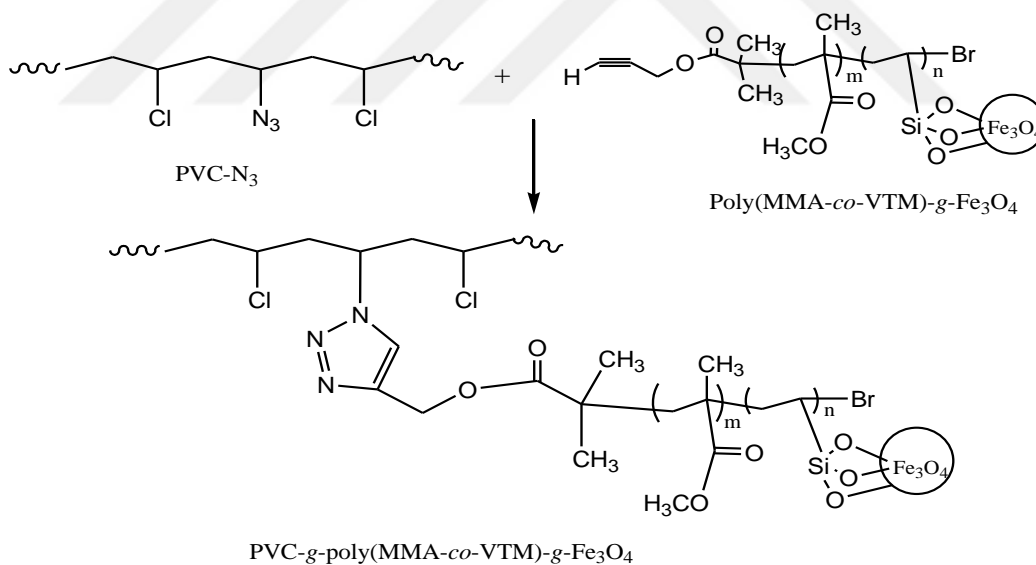


Figure 2.5. Synthesis of PVC-g-poly(MMA-co-VTM)-g-Fe₃O₄

2.3.7. Synthesis of propargyl methacrylate (POHMAC)

In a conical flask containing 10 mL dichloromethane (DCM), 0.54 g (9.57 mmol) POH was added followed by 0.97 g triethylamine (TEA). The solution was magnetically stirred in an ice bath until the temperature drops to 0-5 °C. 1.00 g MAC was added dropwise, argon gas introduced for 15 min into the mixture and the reaction continued for 24 h. After completion, the

solution was filtered, evaporated and the residue obtained was dissolved thoroughly in DCM. The solution was poured into a separation funnel, washed thrice with water and the solvent phase was filtered. Dried over anhydrous MgSO_4 overnight in a fridge and then filtered followed by solvent evaporation.

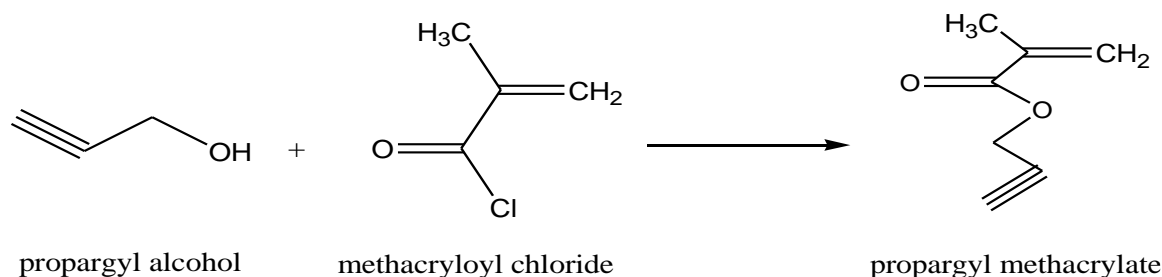


Figure 2.6. Synthesis of propargyl methacrylate

2.3.8. Free radical copolymerization of propargyl methacrylate and vinyltrimethoxysilane

In a polymerization tube, 0.60 g (4.83 mmol) POHMAC, 0.80 g (4.83 mmol) VTM and 0.016 g (0.096 mmol) azoisobutylnitrile (AIBN) were discharged followed by 5 mL THF. Argon was bubbled for 15 min and the polymerization continued at for 24 h at 70 °C. At the end of the reaction, the solution was precipitated in cold hexane, filtered and dry at ambient temperature for 48 h followed by a vacuum.

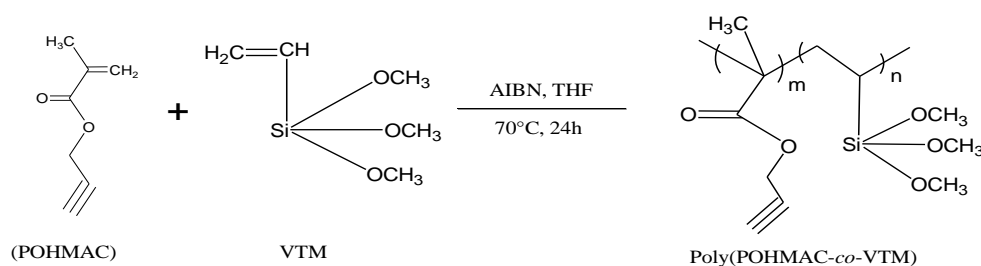


Figure 2.7. Synthesis of Poly(POHMAC-co-VTM)

2.3.9. Magnetic nanoparticle (Fe_3O_4) bonding to the (POHMAC-co-VTM) copolymer

In a flask, 0.80 g Fe_3O_4 was sonicated in 40 mL THF for 30 min. 0.80 g POHMAC-co-VTM was added, Argos was bubbled for 15 min and continued for 6 h at ambient temperature and then under reflux for 24 h. After completion, Fe_3O_4 copolymer, poly(POHMAC-co-VTM)-g-

Fe_3O_4 were magnetically separated and washed under a magnet with THF. The copolymer was dried at ambient temperature for 24 h then under vacuum at 45 °C for 24 h.

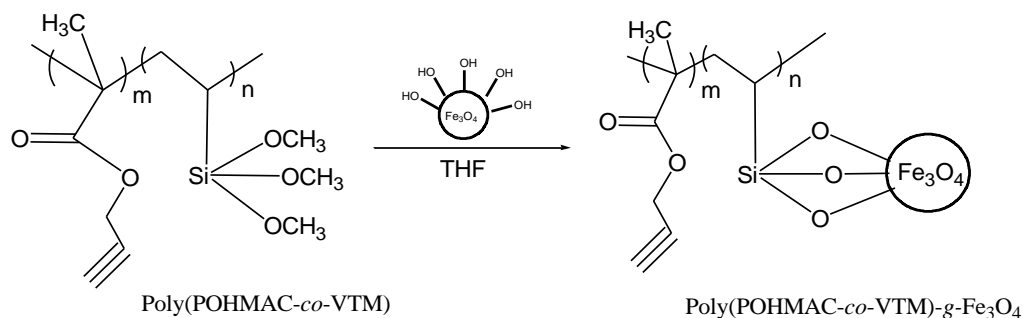


Figure 2.8. Synthesis of poly(POHMAC-*co*-VTM)-*g*- Fe_3O_4

2.3.10. Click reaction of (POHMAC-*co*-VTM)-*g*- Fe_3O_4 and azide poly(vinylchloride) PVC- N_3

0.50 g poly(POHMAC-*co*-VTM)-*g*- Fe_3O_4 was sonicated for 30 min in 20 mL DMF and 0.75 g PVC- N_3 was dissolved in 10 mL followed by 0.005 g Cu(I)Br, and 0.0175g mbpy and then added to the sonicated mixture. Argon was injected for 15 min, the reaction continued at 30-35 °C for 48 h. After completion of the reaction, the product PVC-*g*-poly(POHMAC-*co*-VTM)-*g*- Fe_3O_4 was magnetically separated, washed with DMF under magnetic, and dried at ambient temperature for 24 h then under vacuum at 45 °C for 48 h.

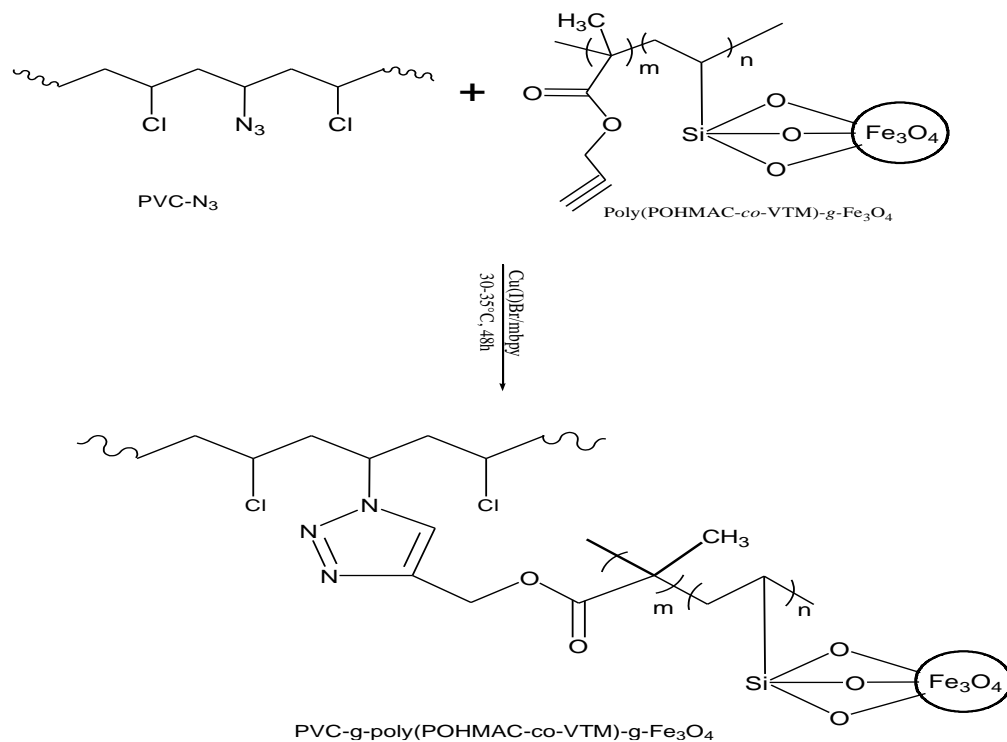


Figure 2.9. Synthesis of PVC-*g*-poly(POHMAC-*co*-VTM)-*g*- Fe_3O_4

2.3.11. Synthesis of 3-azidopropyltrimethoxysilane (N₃PTMS)

2.14 g (33.2 mmol) NaN₃, 3.30 g (16.6 mmol) 3-chloropropyltrimethoxysilane (CITMS), and 0.84 g (4 mmol) tetraethylammonium bromide (TEABr) were added into a round bottom flask with a single neck stocked with reflux condenser containing 50 mL acetonitrile, under argon atmosphere. The reaction continued under reflux for 18 h. After completion, the solvent was evaporated and the crude like mixture obtained was diluted in dry hexane and the solution was filtered. The solvent was evaporated from the subsequent filtrate. The 3-azidopropyltrimethoxysilane was formed as a colorless liquid [68].

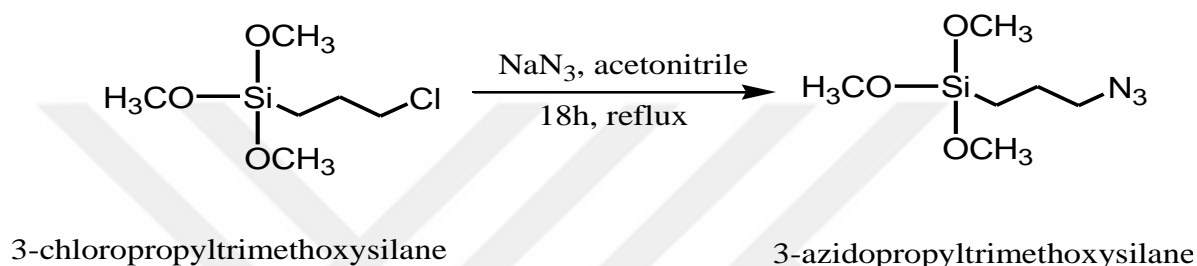


Figure 2.10. Synthesis of 3-azidopropyltrimethoxysilane

2.3.12. Magnetic nanoparticle (Fe₃O₄) bonding to 3-azidopropyltrimethoxysilane (N₃PTMS)

In a flask, 2.00 g Fe₃O₄ was homogenized in 75 mL absolute ethanol for 30 min. 2.00 g N₃PTMS was added, Argon was introduced for approximately 15 min and continued for 6 h at ambient temperature then 48 h under reflux. After completion, Fe₃O₄ bonded to N₃PTMS was separated magnetically, the product (N₃PTMS-g-Fe₃O₄) washed with alcohol, and dried at ambient temperature followed by vacuum for 24 h at 50 °C.

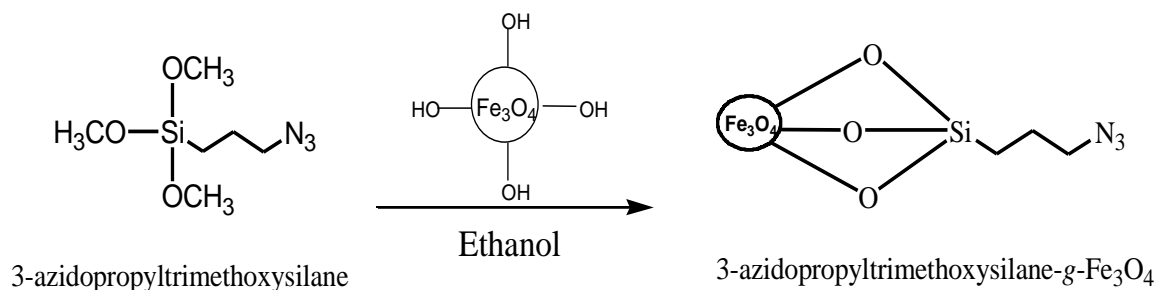


Figure 2.11. Synthesis of 3-azidopropyltrimethoxysilane-g-Fe₃O₄

2.3.13. Click reaction of N₃PTMS-g-Fe₃O₄ and propargyl alcohol (POH)

In a flask, 1.00 g N₃PTMS-g-Fe₃O₄ was homogenized in 15 mL DMF with a sonicator for 30 min. 1.33 g POH was added to the dispersed solution. 0.07 g (0.48 mmol) Cu(I)Br and 0.22 g (0.48 mmol) mbpy were dissolved in 5 mL in a flask and poured into the previous solution. Argon was injected for 15 min and continued at 30 °C for 24 h. The product was washed with DCM under magnetic and dried at ambient temperature for 24 h followed by vacuum at 50 °C for 24 h.

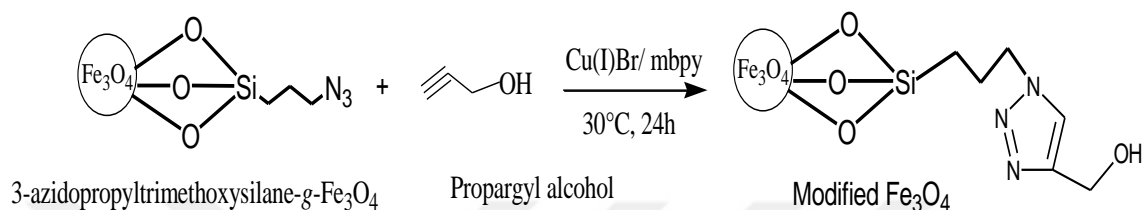


Figure 2.12 Synthesis of modified Fe₃O₄ via click reaction

2.3.14. Preparation of composite of PVC with POH-N₃PTMS-g-Fe₃O₄

Firstly, 10 mL THF was used to dissolve 0.50 g PVC. 5% (0.025 g) POH-N₃PTMS-g-Fe₃O₄ was added to the mixture and sonicated for 45 min. The resulting solution was precipitated in ethanol, filtered, dried at room temperature then vacuum at 45 °C for 24 h. The aforementioned procedure was used to prepare 10% (0.05 g) and 20% (0.10 g) composite.

3. RESULTS

3.1. Poly(vinyl chloride)

PVC was purified by dissolving in THF and precipitated in ethanol. The purified PVC undergoes azidation reaction with NaN_3 to form PVC- N_3 . The PVC and PVC- N_3 were characterized using FT-IR, $^1\text{H-NMR}$, and $^{13}\text{C-NMR}$.

3.1.1. Characterization of PVC

The IR spectrum of PVC is given in Figure 3.1 and the IR spectrum is evaluated in Table 3.1 below.

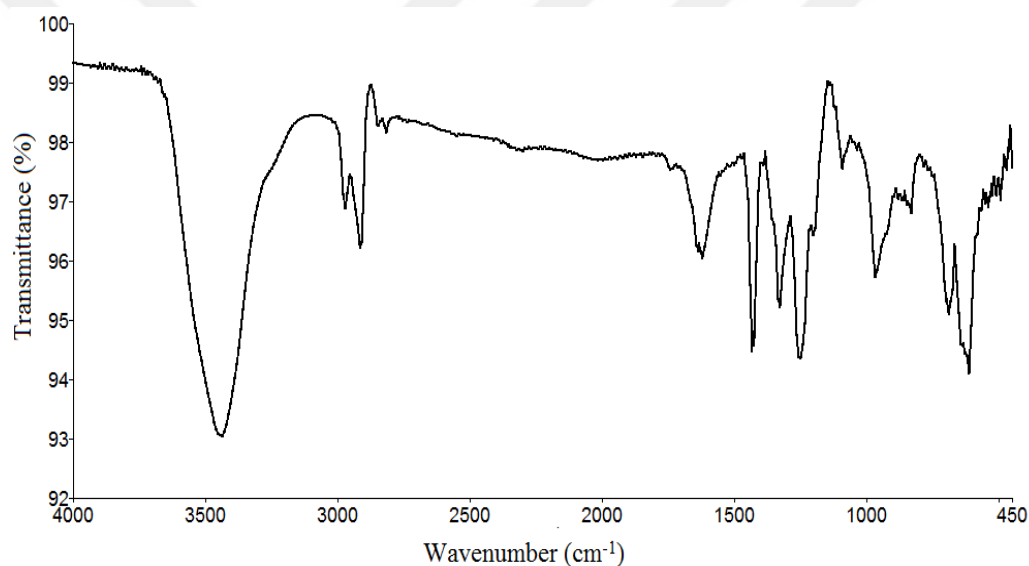


Figure 3.1. FT-IR spectrum of PVC

The IR spectrum of PVC- N_3 is given in Figure 3.2 and the IR spectrum is evaluated in Table 3.2 below.

Table 3.1. FT-IR spectrum evaluation of PVC

Wavenumber (cm^{-1})	Vibration Type
2972-2912	C-H stretching (aliphatic CH_2 , CH)
1251	CH bending on CHCl
612	C-Cl stretching

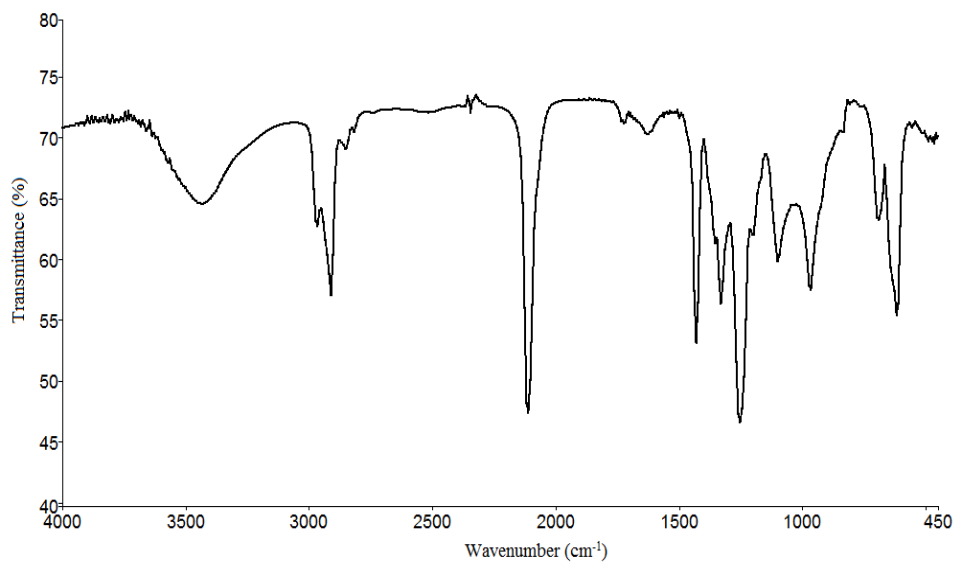


Figure 3.2. PVC-N₃ FT-IR spectrum

The ¹H-NMR spectrum of PVC-N₃ is shown in Figure 3.3 and evaluated in Table 3.3.

Table 3.2. FT-IR spectrum evaluation of PVC-N₃

Wavenumber (cm ⁻¹)	Vibration Type
2115	N ⁻ =N ⁺ =N ⁻ stretching
2969-2911	C-H stretching (aliphatic CH ₂ , CH)
1254	CH bending on CHCl
615	C-Cl stretching

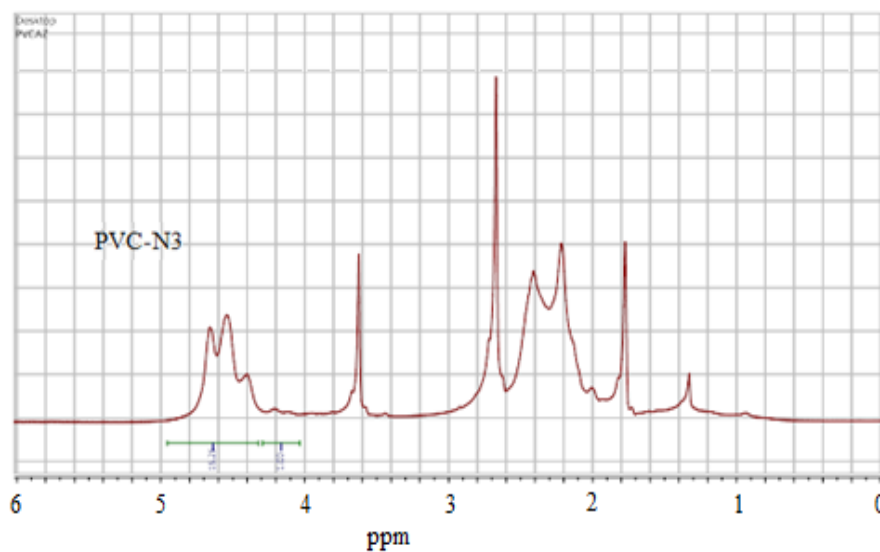
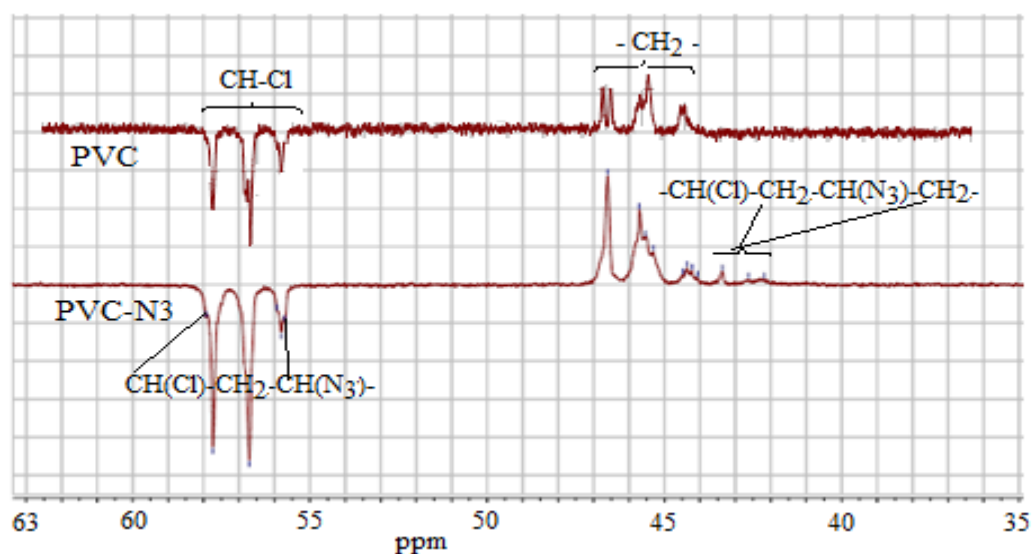


Figure 3.3. ¹H-NMR spectrum of PVC-N₃

Table 3.3. $^1\text{H-NMR}$ spectrum evaluation of PVC- N_3

Chemical Shift (ppm)	Signal Type
3.85-4.3	CHN_3-
4.3-4.8	CHCl-
2.0-2.9	CH_2-

The $^{13}\text{C-APT}$ spectra of PVC and PVC- N_3 are shown in Figure 3.4 and evaluated in Table 3.4.

**Figure 3.4.** $^{13}\text{C-APT}$ spectra of PVC and PVC- N_3 **Table 3.4.** $^{13}\text{C-APT}$ spectra evaluation of PVC and PVC- N_3

Chemical Shift (ppm)	Signal Type
55.6	$-\text{CH}(\text{Cl})-\text{CH}_2-\underline{\text{C}}\text{H}(\text{N}_3)-$
58.10	$-\underline{\text{C}}\text{H}(\text{Cl})-\text{CH}_2-\text{CH}(\text{N}_3)-$
42.19-44.03	$-\text{CH}(\text{Cl})-\underline{\text{C}}\text{H}_2-\text{CH}(\text{N}_3)-\underline{\text{C}}\text{H}_2$

3.1.2. Thermal Properties

The TGA and DSC curves of PVC were given in Figure 3.5 and 3.6 while that of PVC- N_3 were given in Figure 3.7 and 3.8 respectively. The curves were evaluated in Table 3.5.

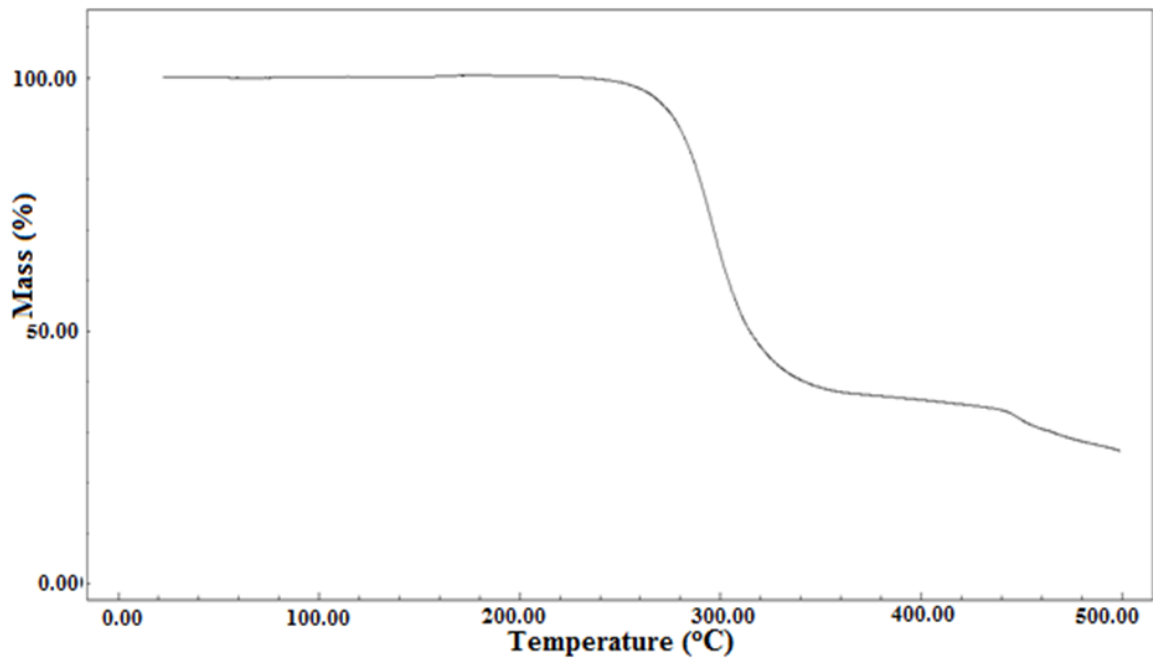


Figure 3.5. TGA curve of PVC

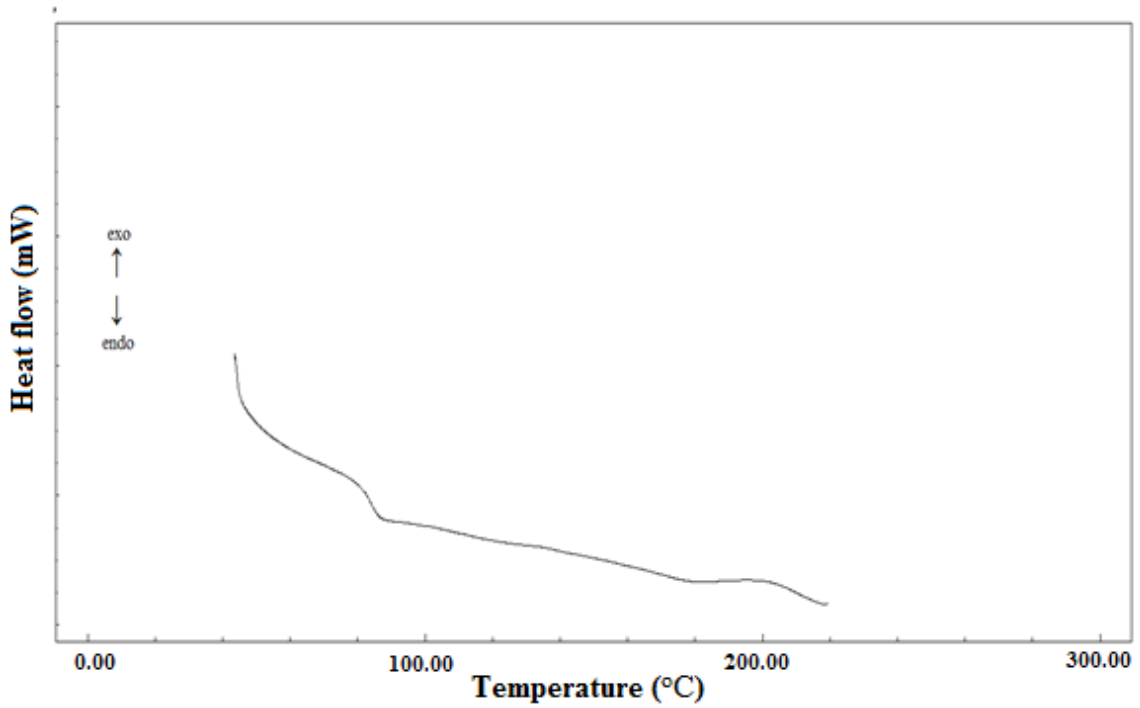


Figure 3.6. DSC curve of PVC

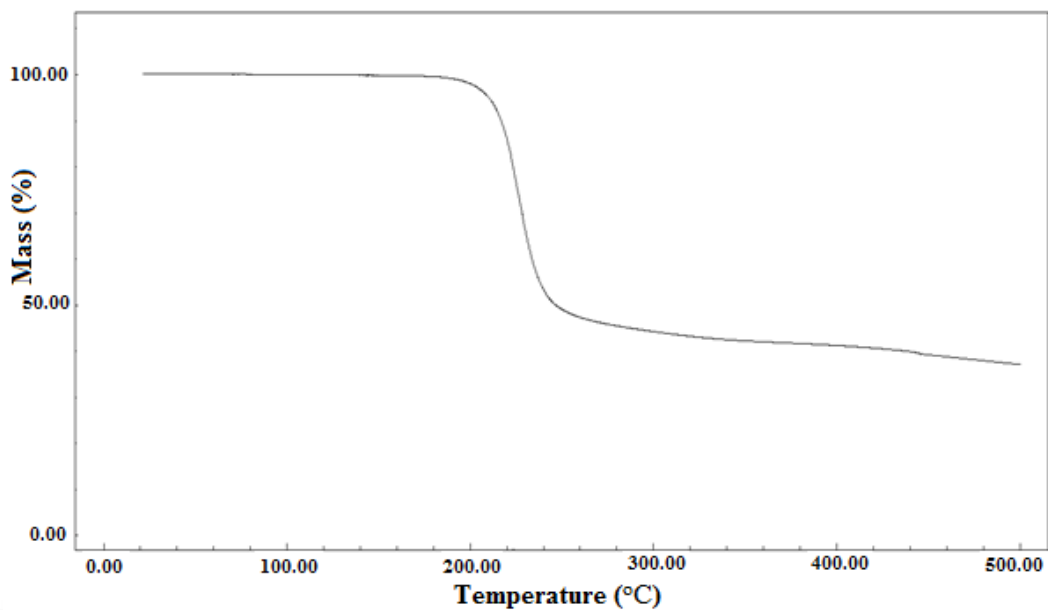


Figure 3.7. TGA curve of PVC-N₃

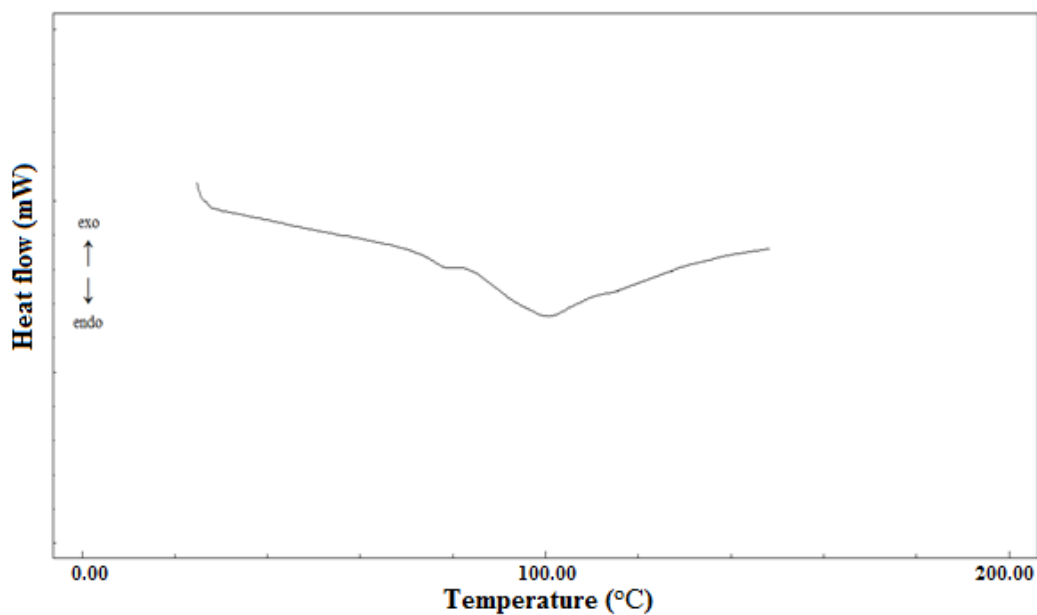


Figure 3.8. DSC curve of PVC-N₃

Table 3.5. TGA and DSC evaluation of PVC

Polymer	T_g (°C)	T_i (°C)	Weight loss (%) at 350 °C	% Residue at 500 °C
PVC	84.2	238	61.7	18.3
PVC-N ₃	75.8	180	56.7	35.0

3.2. PVC-g-poly(MMA-co-VTM)-g-Fe₃O₄

3.2.1. Characterization

The FT-IR spectrum of propargyl- α -bromoisobutyrate is given in Figure 3.9 and evaluated in Table 3.6.

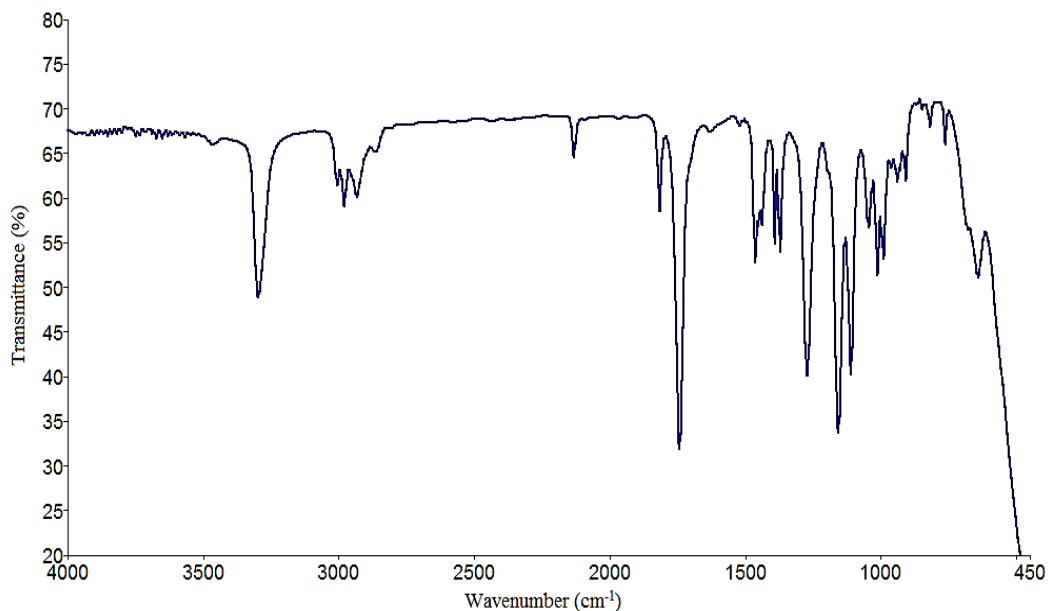


Figure 3.9. FT-IR spectrum of propargyl- α -bromoisobutyrate

Table 3.6. FT-IR spectrum evaluation of propargyl- α -bromoisobutyrate

Wavelength (cm ⁻¹)	Vibration Type
3294	\equiv C-H stretching
2928-3006	C-H stretching
2129	C \equiv C stretching
1730	Ester carbonyl stretching in MMA units
1372; 1388	geminal -CH ₃
1107; 1155	C(=O)-O- symmetric and asymmetric stretching
641	C-Br stretching

The ¹H-NMR spectrum of propargyl- α -bromoisobutyrate is given in Figure 3.10 and evaluated in Table 3.7.

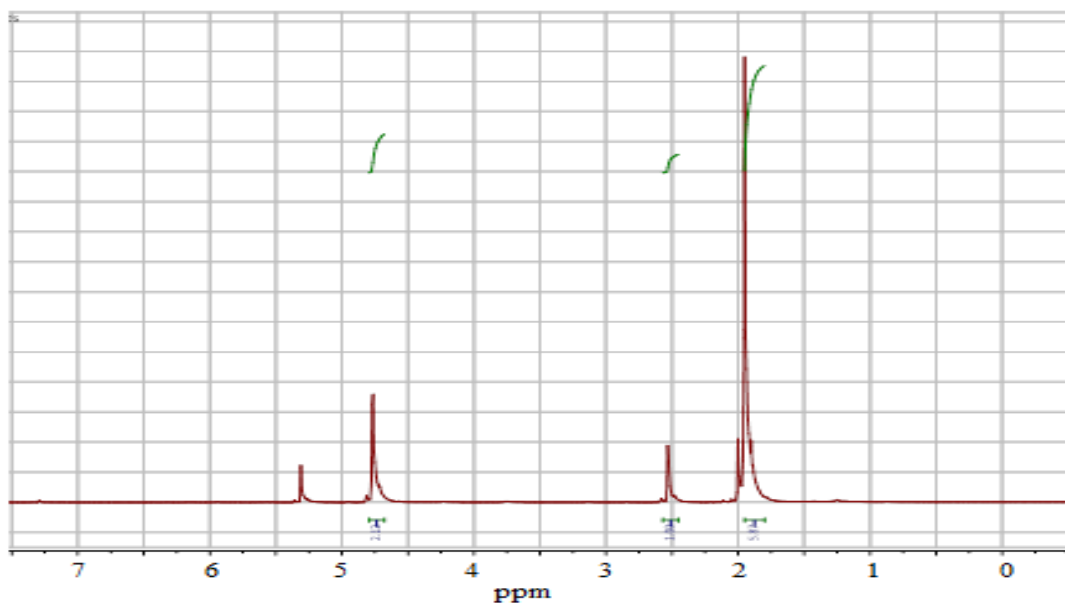


Figure 3.10. $^1\text{H-NMR}$ spectrum of propargyl- α -bromoisobutyrate (Solvent: CDCl_3)

Table 3.7. $^1\text{H-NMR}$ spectrum evaluation of propargyl- α -bromoisobutyrate

Chemical Shift (ppm)	Signal Type
4.6	$-\text{CH}_2-\text{O}-$
2.5	$\equiv\text{C-H}$
1.8	geminal CH_3
5.3	$-\text{CH}_2\text{Cl}_2$

The $^{13}\text{C-APT}$ spectrum of propargyl- α -bromoisobutyrate is given in Figure 3.11 and evaluated in Table 3.8.

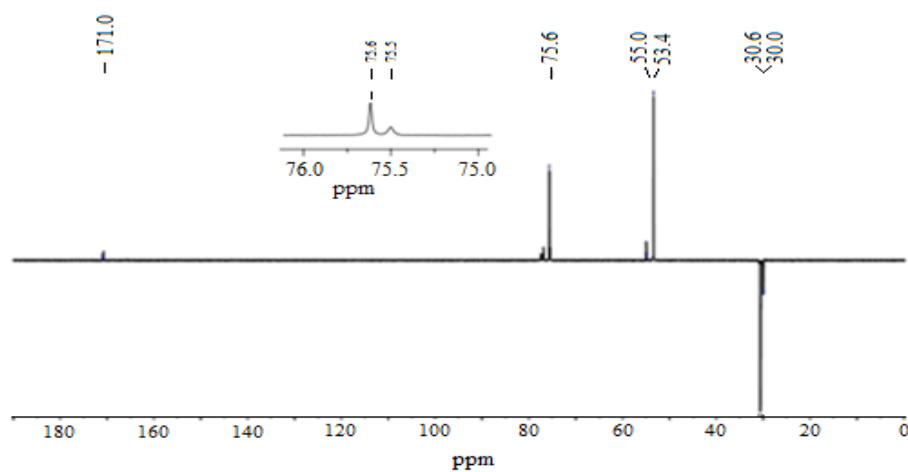
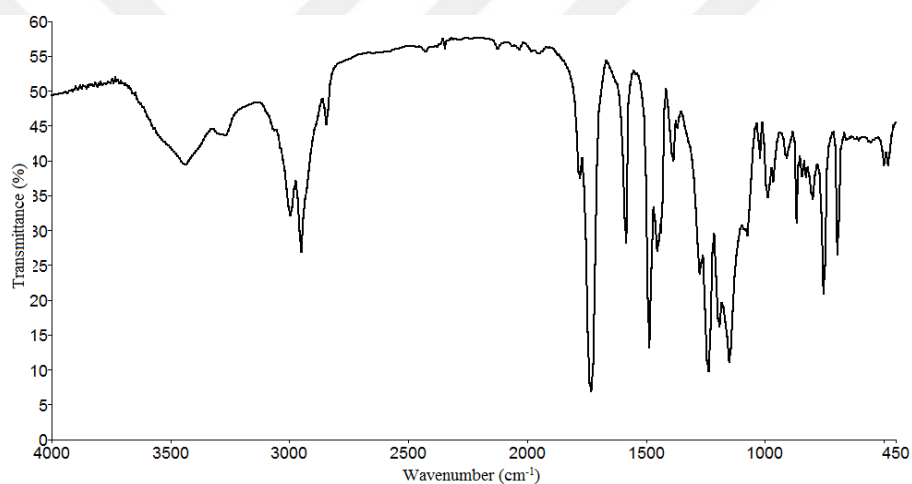


Figure 3.11. $^{13}\text{C-APT}$ spectrum of propargyl- α -bromoisobutyrate (Solvent: CDCl_3)

Table 3.8. ^{13}C -APT spectrum evaluation of propargyl- α -bromoisobutyrate

Chemical Shift (ppm)	Signal Type
171.0	C = O
75.6	CH ₂ O
75.5	C \equiv C
55.0	C-Br
53.4	CH ₂ Cl ₂
30.6	CH ₃
30	H-C \equiv

The FT-IR spectrum of poly(MMA-*co*-VTM) is given in figure 3.12 and evaluated in table 3.9.

**Figure 3.12.** FT-IR spectrum of poly(MMA-*co*-VTM)**Table 3.9.** FT-IR spectrum evaluation of poly(MMA-*co*-VTM)

Wavelength (cm ⁻¹)	Vibration Type
3268	\equiv C-H stretching
2950-2998	C-H stretching (Aliphatic -CH ₂ - and -CH ₃ groups)
2124	C \equiv C stretching
1735	Ester carbonyl stretching
1387	geminal -CH ₃
1147	C(=O)-O- stretching
1073	Si-O
692	C-Br stretching

3.2.2. Thermal properties

The TGA curves were obtained by heating the samples to 600 °C at a heating rate of 10 °C/min while for the DSC curves, the samples were heated up to 200 °C at a heating rate of 20 °C/min and both are evaluated in Table 3.10.

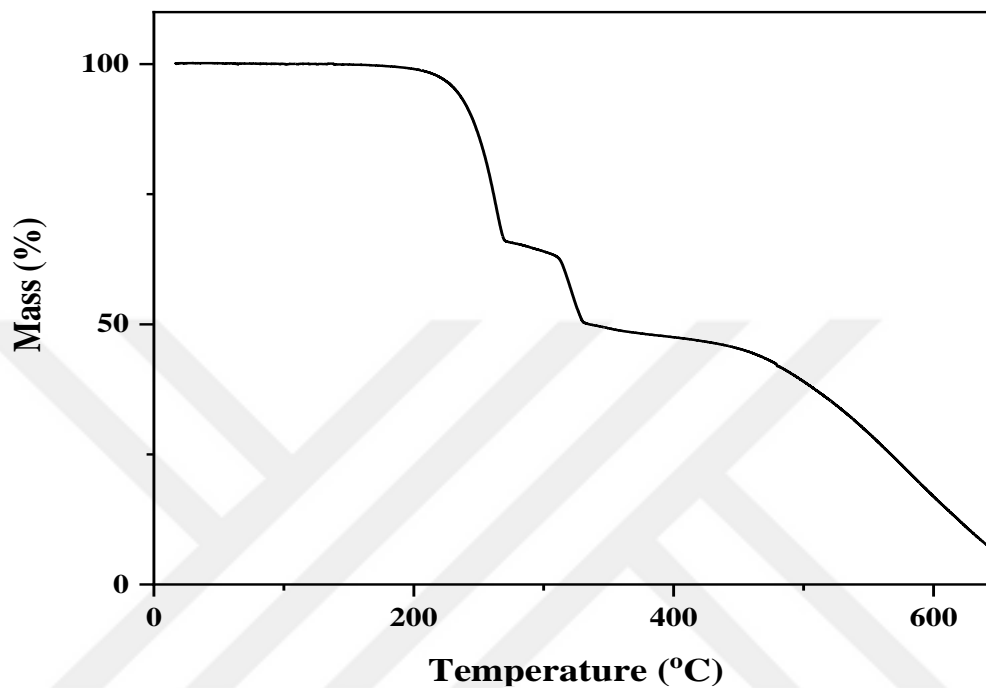


Figure 3.13. TGA curve of poly(MMA-co-VTM)

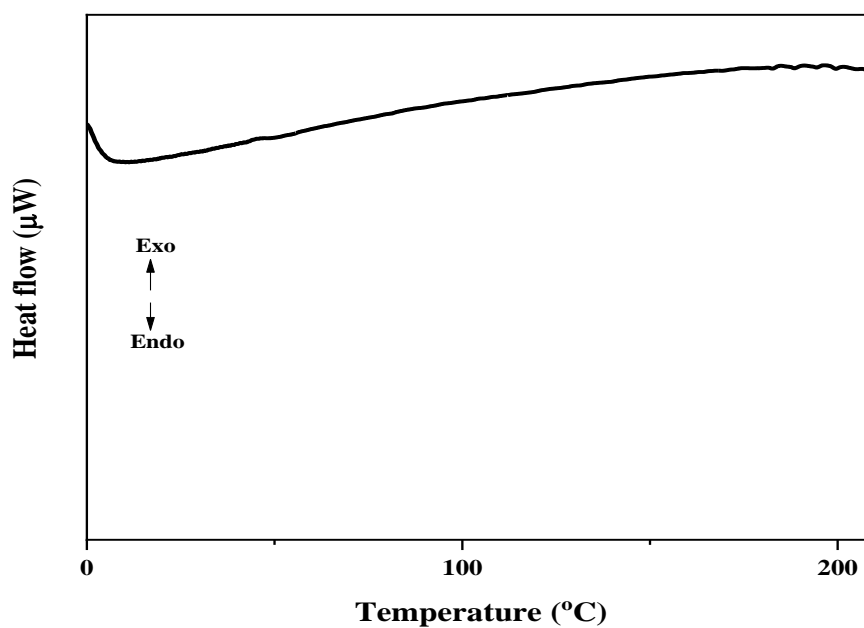


Figure 3.14. DSC curve of poly(MMA-co-VTM)

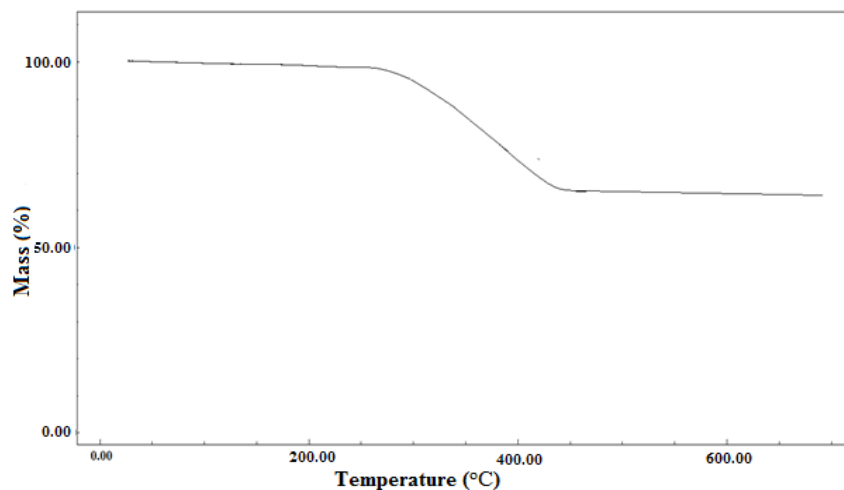


Figure 3.15. TGA curve of poly(MMA-co-VTM)-g-Fe₃O₄

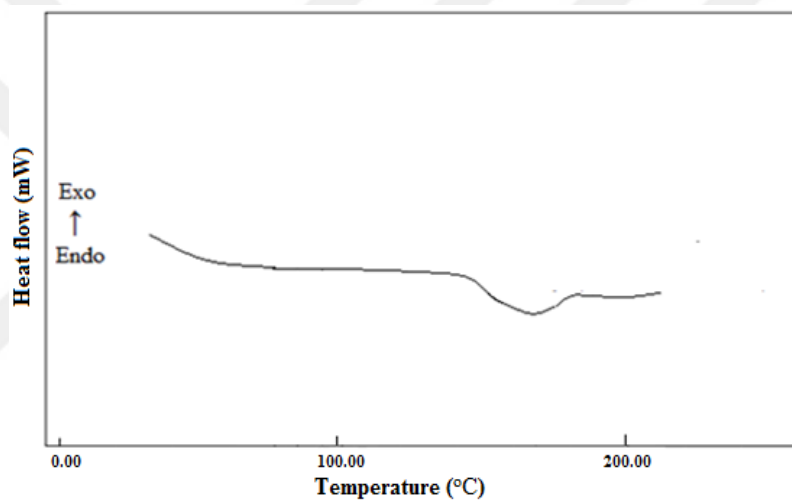


Figure 3.16. DSC curve of poly(MMA-co-VTM)-g-Fe₃O₄

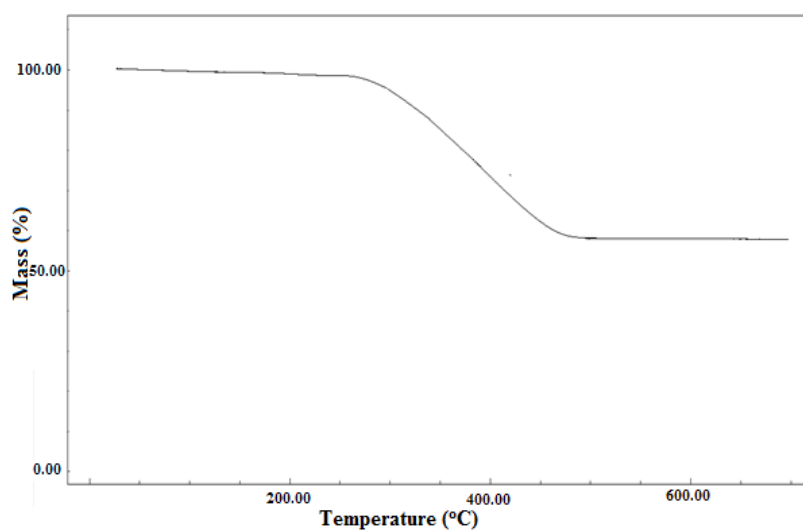


Figure 3.17. TGA curve of PVC-g-poly(MMA-co-VTM)-g-Fe₃O₄

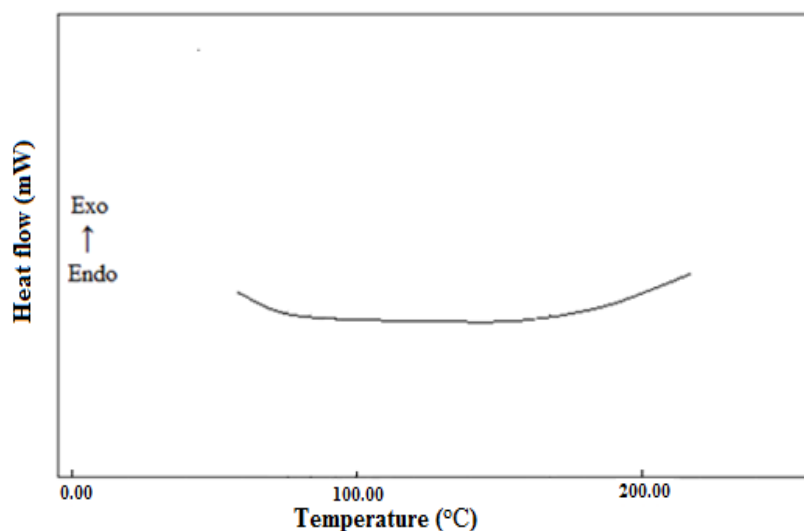


Figure 3.18. DSC curve of PVC-g-poly(MMA-co-VTM)-g-Fe₃O₄

Table 3.10. TGA and DSC evaluation of PVC-g-poly(MMA-co-VTM)-g-Fe₃O₄

Polymer	T_g	T_i	Weight loss (%)	% Residue
	(°C)	(°C)	at 350 °C	at 500 °C
Poly(MMA-co-VTM)	48.0	192	50.8	39.0
Poly(MMA-co-VTM)-g-Fe ₃ O ₄	94.0	265	15.0	65.8
PVC-g-poly(MMA-co-VTM)-g-Fe ₃ O ₄	-	265	15.0	58.3

3.2.3. Morphological structure

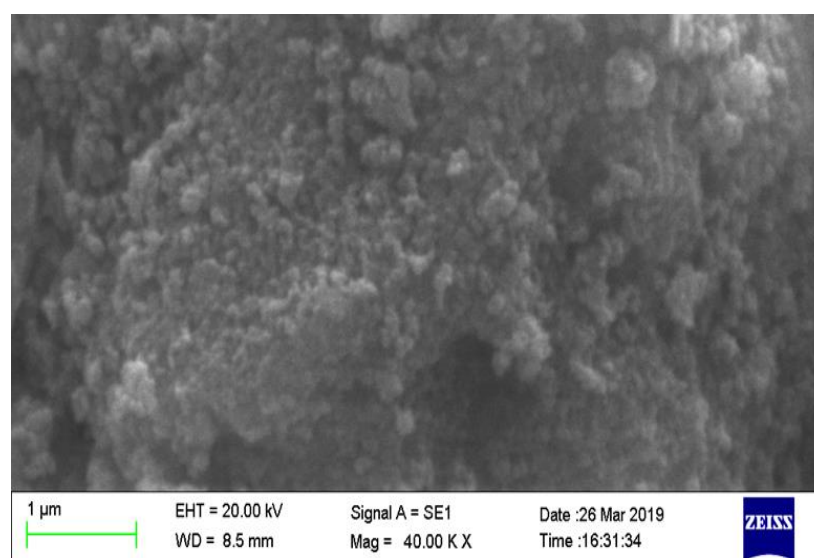


Figure 3.19. SEM image of poly(MMA-co-VTM)-g-Fe₃O₄

Figure 3.19 shows the SEM image of poly(MMA-co-VTM)-g-Fe₃O₄ and EDX analysis evaluation is given in Figure 3.20. SEM image of PVC-g-poly(MMA-co-VTM)-g-Fe₃O₄ is given in Figure 3.21 and SEM-EDX evaluation in Figure 3.22.

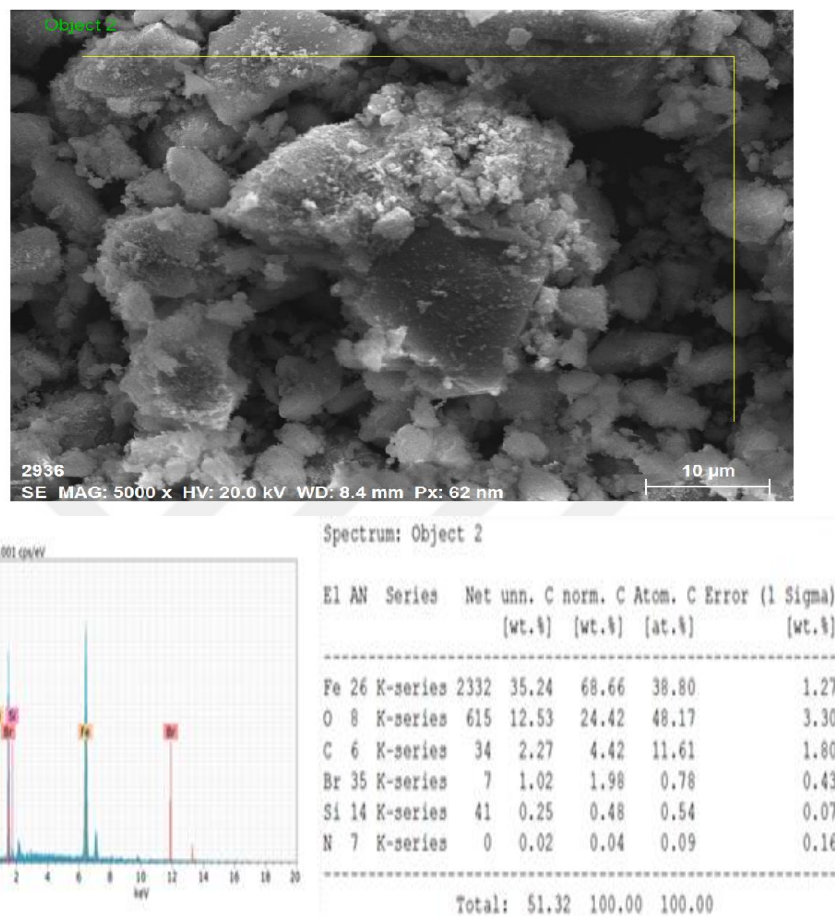


Figure 3.20. SEM-EDX image poly(MMA-co-VTM)-g-Fe₃O₄

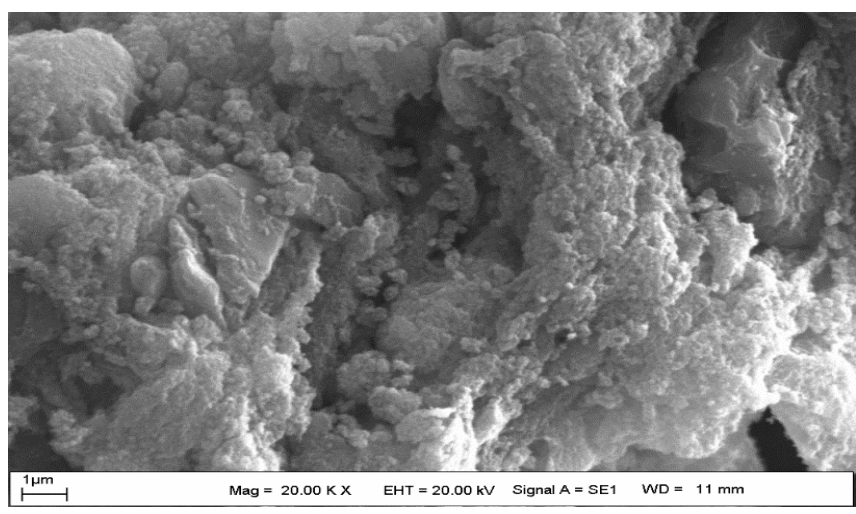
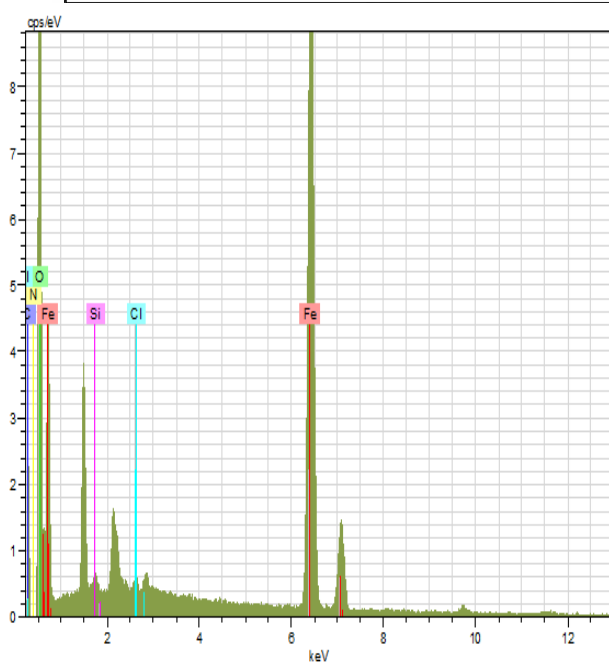
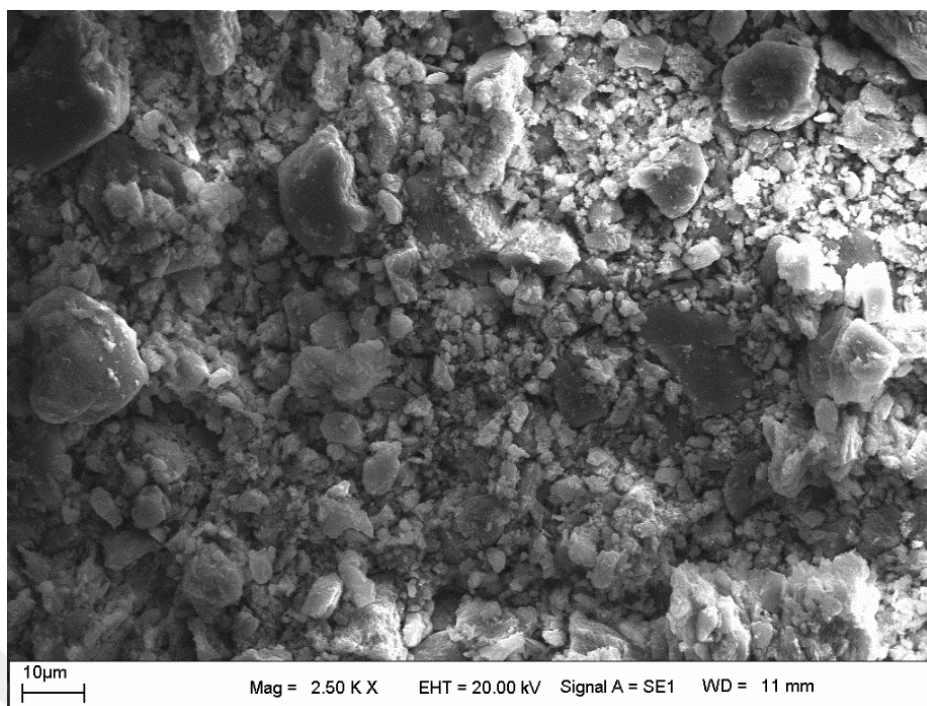


Figure 3.21. SEM image of PVC-g-poly(MMA-co-VTM)-g-Fe₃O₄



El	AN	Series	unn. [wt.-%]	C norm. [wt.-%]	C Atom. [at.-%]	C Error [%]
Fe	26	K-series	54.51	60.85	30.42	1.5
C	6	K-series	3.27	3.65	8.47	0.7
Cl	17	K-series	0.55	0.61	0.48	0.1
Si	14	K-series	0.30	0.34	0.33	0.0
N	7	K-series	0.00	0.00	0.00	0.0
O	8	K-series	30.96	34.56	60.30	3.8
Total:			89.58	100.00	100.00	

Figure 3.22. SEM-EDX image PVC-g-poly(MMA-co-VTM)-g-Fe₃O₄

3.2.4. Magnetic properties

The magnetization curve of Fe₃O₄ modified with poly(MMA-co-VTM) through click reaction with PVC azide in Figure 3.23 was obtained with VSM. The magnetization curve shows that Fe₃O₄ does not lose its magnetic property after modification.

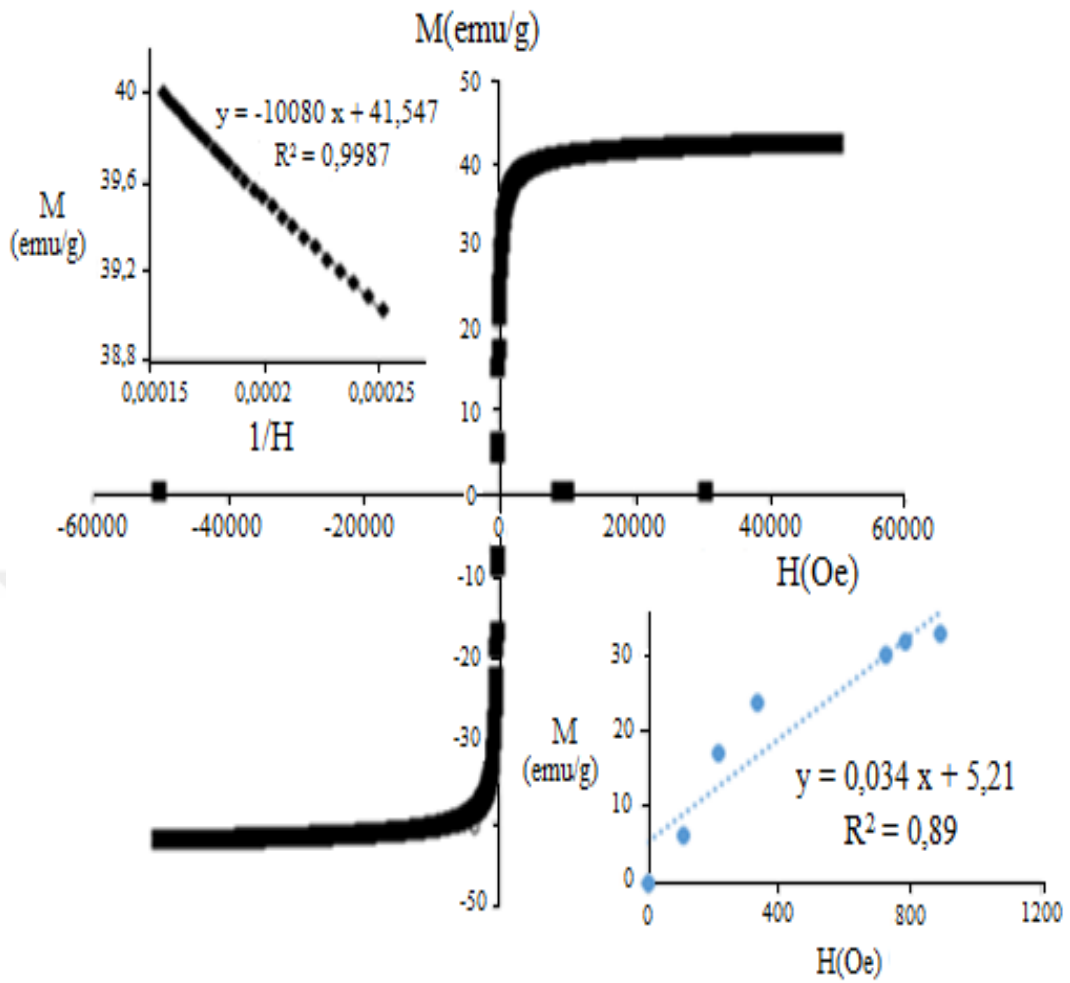


Figure 3.23. VSM plot of PVC-g-poly(MMA-co-VTM)-g-Fe₃O₄

3.2.5. Electrical investigation

Figure 3.24 – 3.31 shows the variation of dielectric constant, dielectric loss, AC conductivity with frequency at room temperature, and AC conductivity with angular frequency at room temperature of poly(MMA-co-VTM)-g-Fe₃O₄ and PVC-g-poly(MMA-co-VTM)-g-Fe₃O₄ respectively.

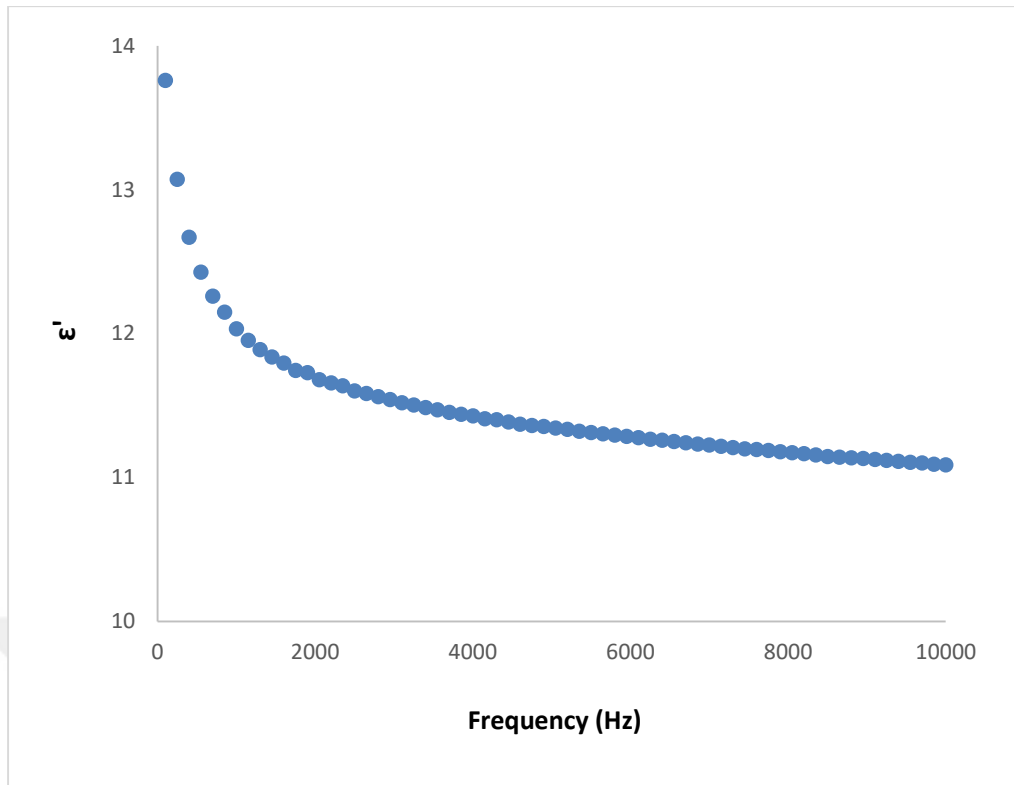


Figure 3.24. Variation of dielectric constant of poly(MMA-co-VTM)-g-Fe₃O₄ with frequency at room temperature

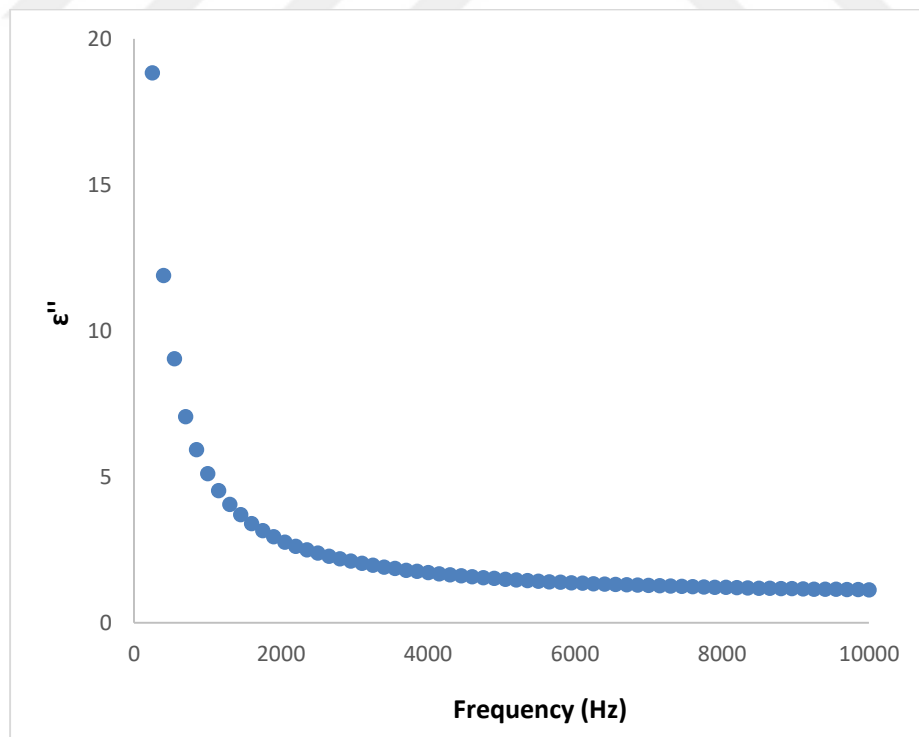


Figure 3.25. Variation of dielectric loss of poly(MMA-co-VTM)-g-Fe₃O₄ with frequency at room temperature

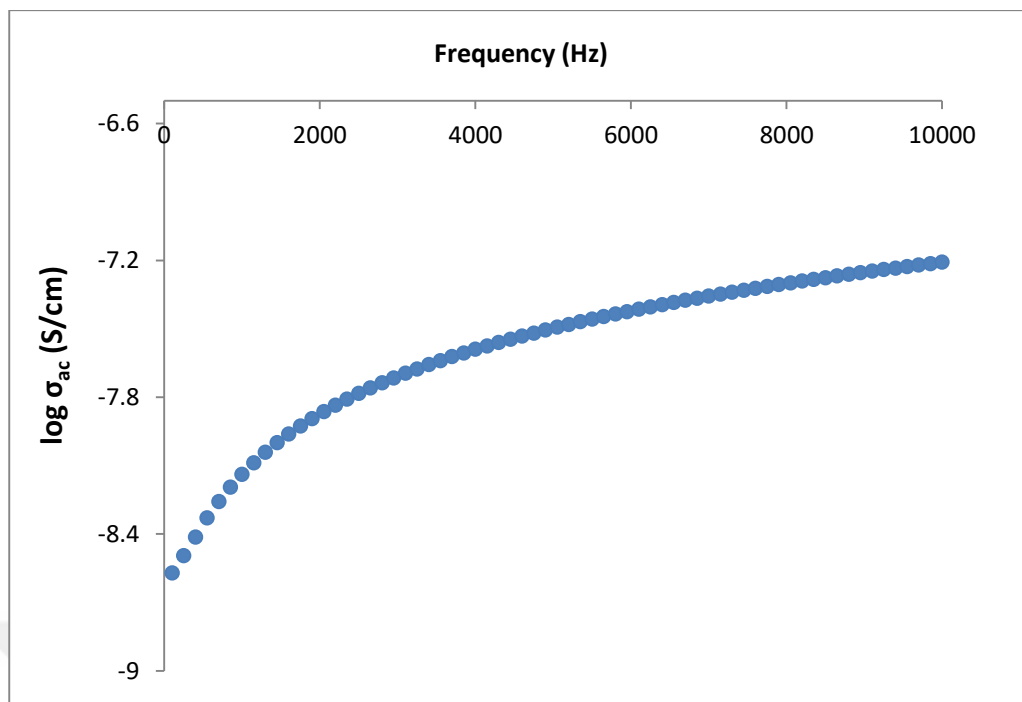


Figure 3.26. Variation of AC conductivity of poly(MMA-co-VTM)-g-Fe₃O₄ with frequency at room temperature

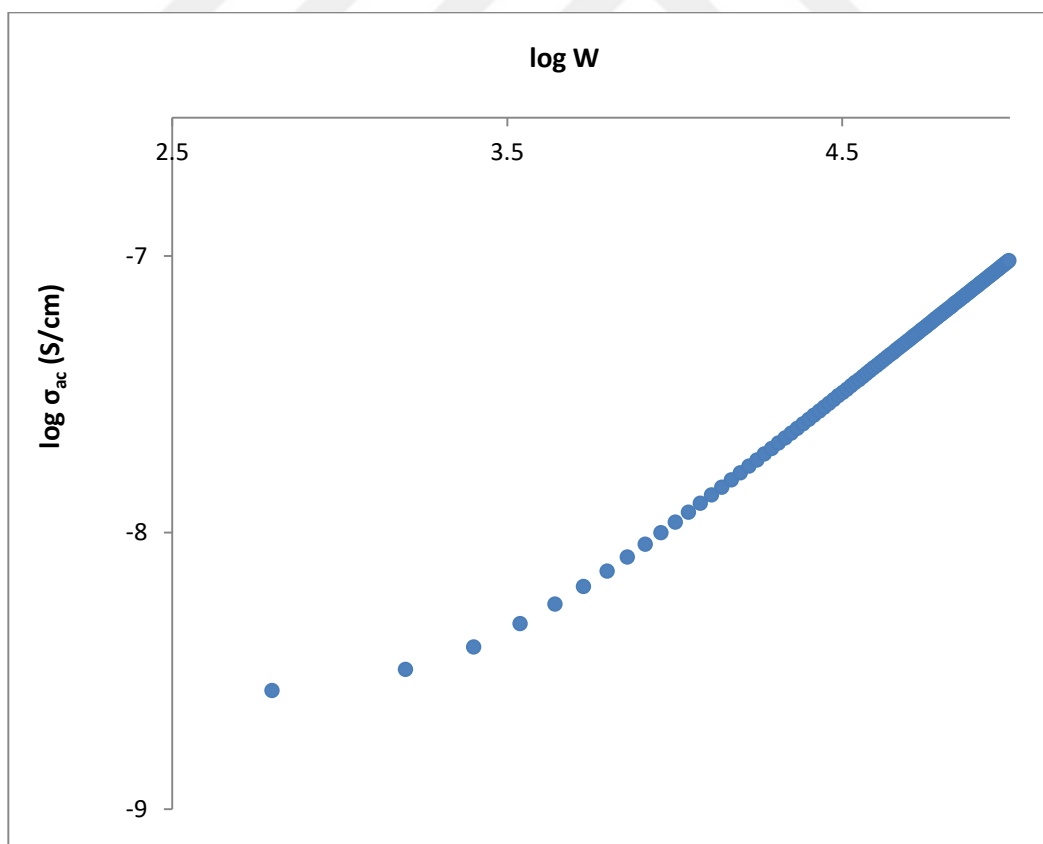


Figure 3.27. Variation of AC conductivity of poly(MMA-co-VTM)-g-Fe₃O₄ with angular frequency at room temperature

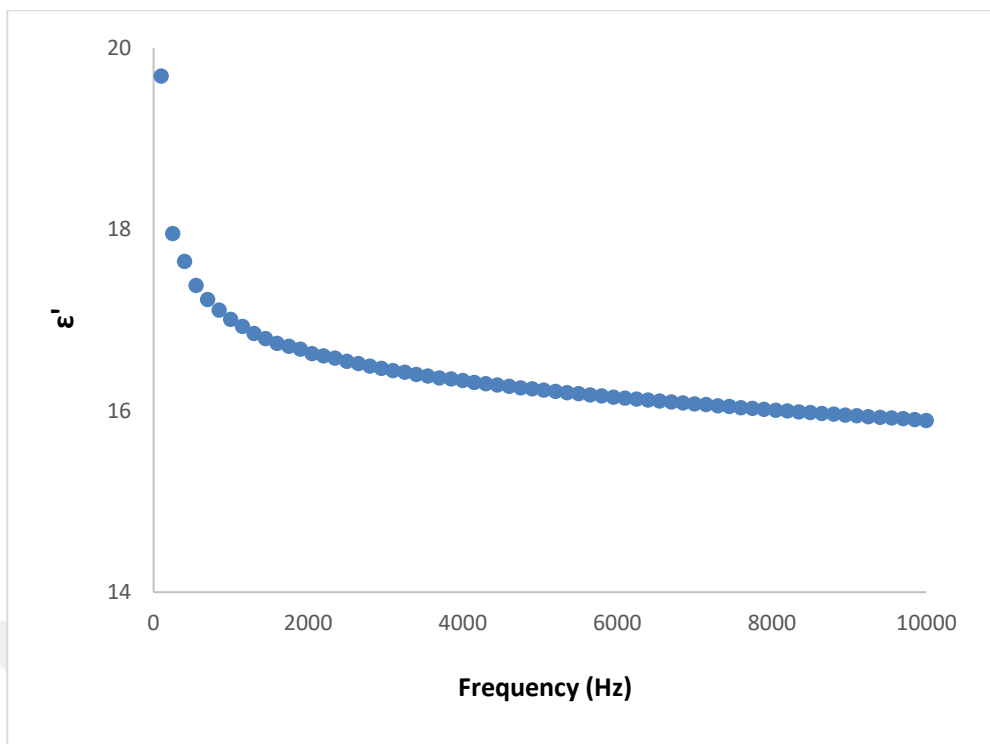


Figure 3.28. Variation of dielectric constant of PVC-g-poly(MMA-co-VTM)-g-Fe₃O₄ with frequency at room temperature

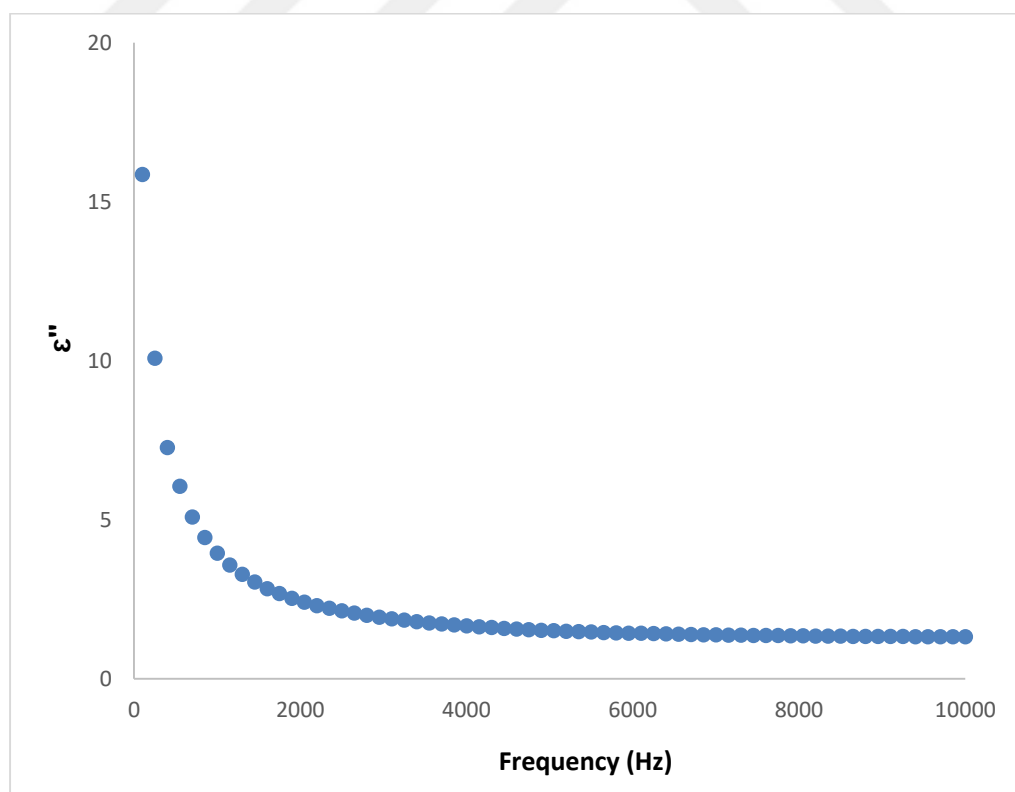


Figure 3.29. Variation of dielectric loss of PVC-g-poly(MMA-co-VTM)-g-Fe₃O₄ with frequency at room temperature

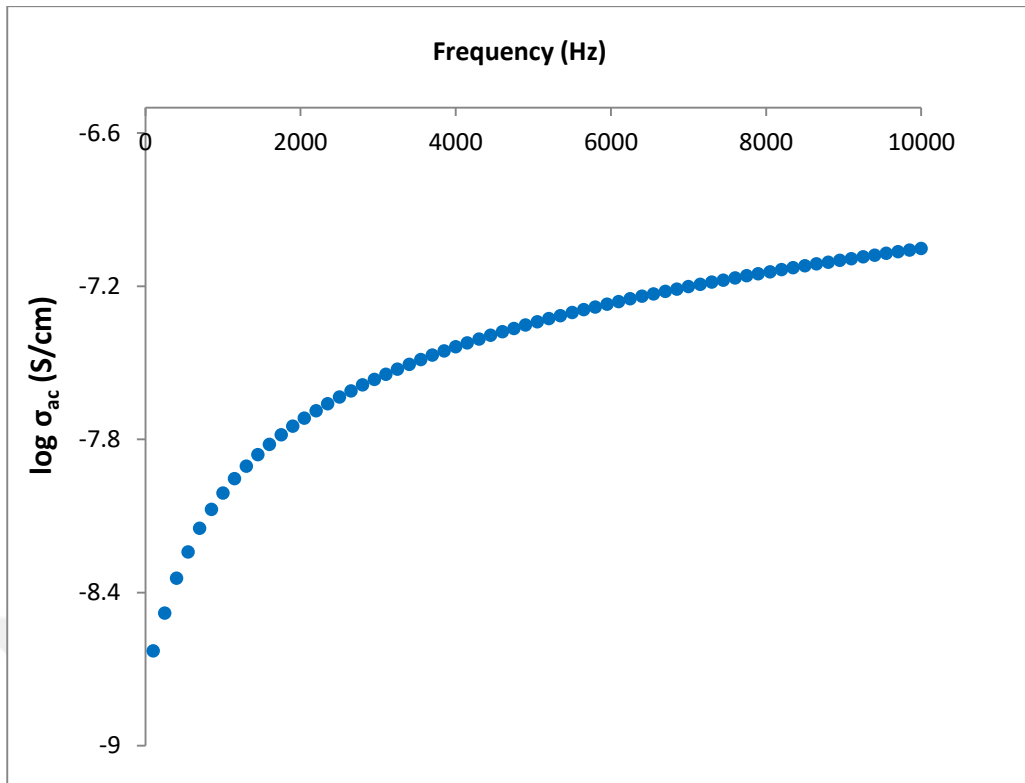


Figure 3.30. Variation of AC conductivity of PVC-g-poly(MMA-co-VTM)-g-Fe₃O₄ with frequency at room temperature

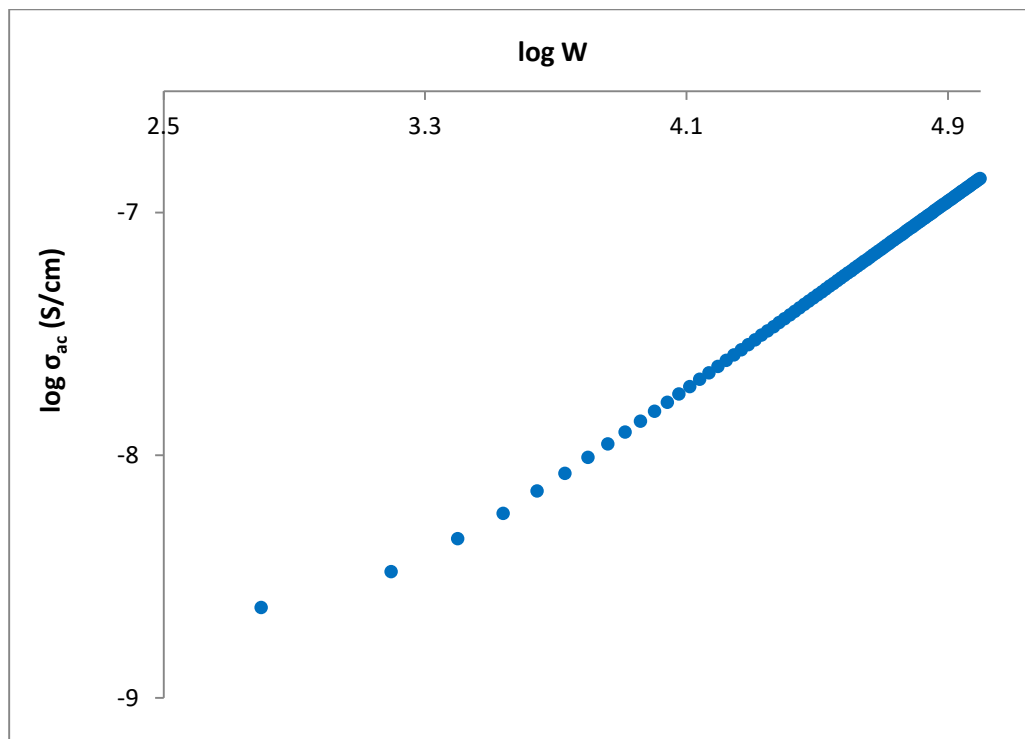


Figure 3.31. Variation of AC conductivity of PVC-g-poly(MMA-co-VTM)-g-Fe₃O₄ with angular frequency at room temperature

3.3. PVC-g-poly(POHMAC-co-VTM)-g-Fe₃O₄

3.3.1. Characterization

The FT-IR spectrum of propargyl methacrylate (POHMAC) is given in Figure 3.32 and evaluated in Table 3.11.

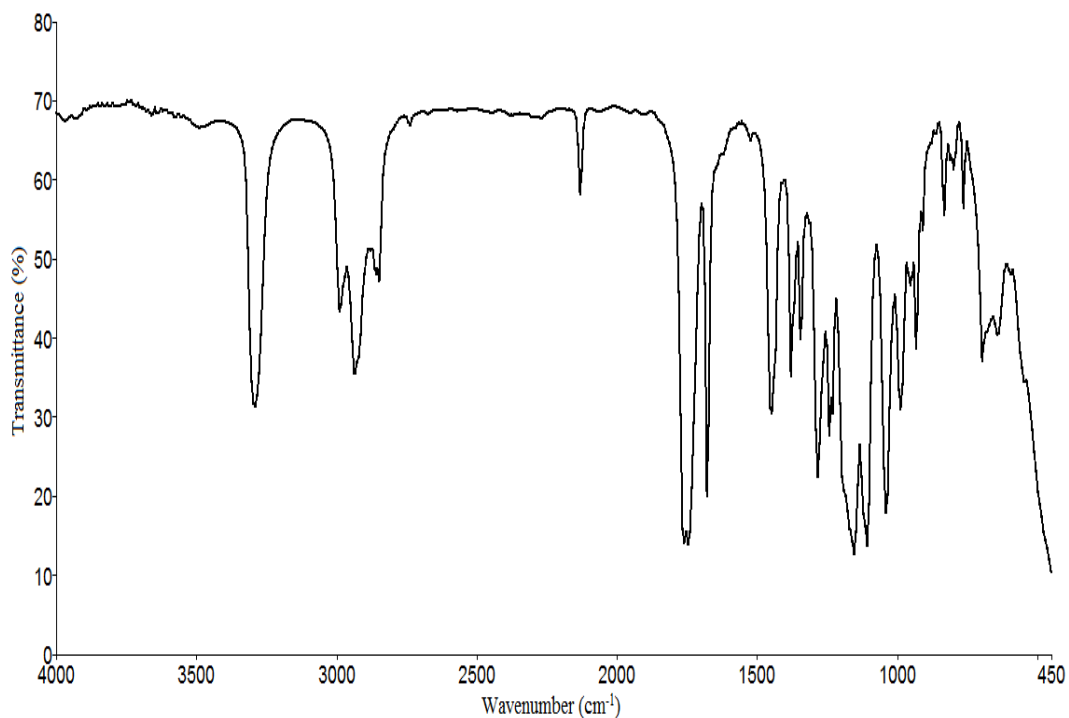


Figure 3.32. FT-IR spectrum of Propargyl methacrylate (POHMAC)

Table 3.11. FT-IR spectrum evaluation of Propargyl methacrylate (POHMAC)

Wavelength (cm ⁻¹)	Vibration Type
3293	≡C-H stretching
2935	C-H stretching (Aliphatic -CH ₂ - and -CH ₃)
2130	C≡C stretching
1740	Ester carbonyl stretching
1678	C=C
1107; 1155	C(=O)-O- symmetric and asymmetric stretching

The FT-IR spectrum of poly(POHMAC-co-VTM) is given in Figure 3.33 and evaluated in Table 3.12.

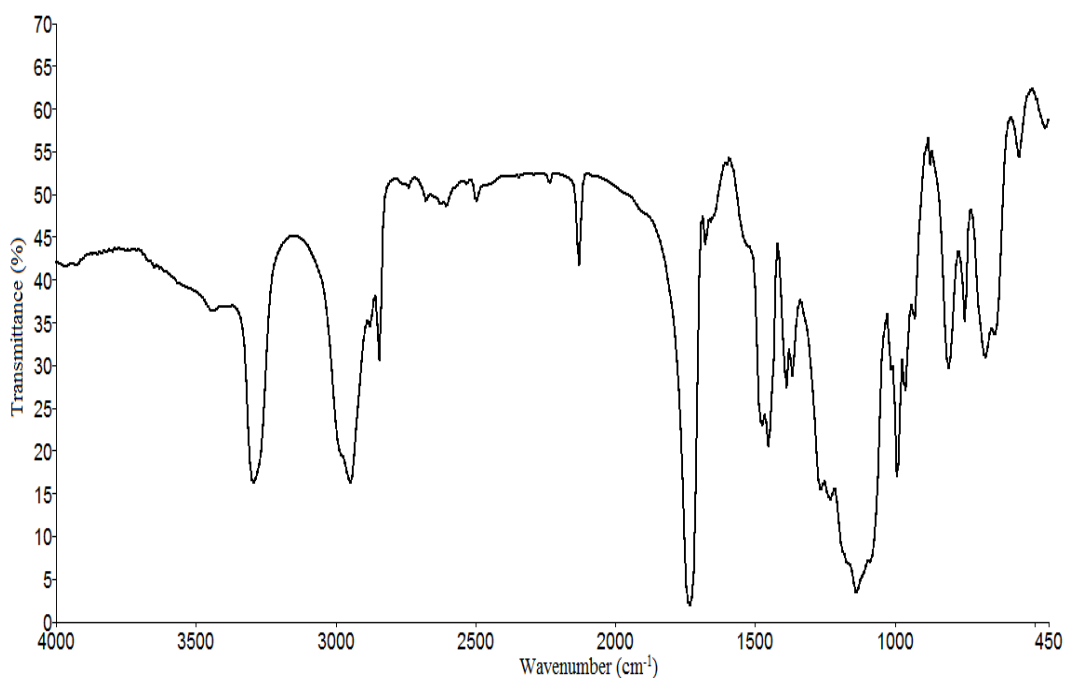


Figure 3.33. FT-IR spectrum of poly(POHMAC-*co*-VTM)

Table 3.12. FT-IR spectrum evaluation of poly(POHMAC-*co*-VTM)

Wavelength (cm ⁻¹)	Vibration Type
3294	≡C-H stretching
2946	C-H stretching (Aliphatic -CH ₂ - and -CH ₃)
2129	C≡C stretching
1745	Ester carbonyl stretching
1138	Si-O
990	C-H bending

The FT-IR spectrum of poly(POHMAC-*co*-VTM)-*g*-Fe₃O₄ is shown in Figure 3.34 and evaluated in Table 3.13.

The FT-IR spectrum of PVC-*g*-poly(POHMAC-*co*-VTM)-*g*-Fe₃O₄ is shown in Figure 3.35 and evaluated in Table 3.14.

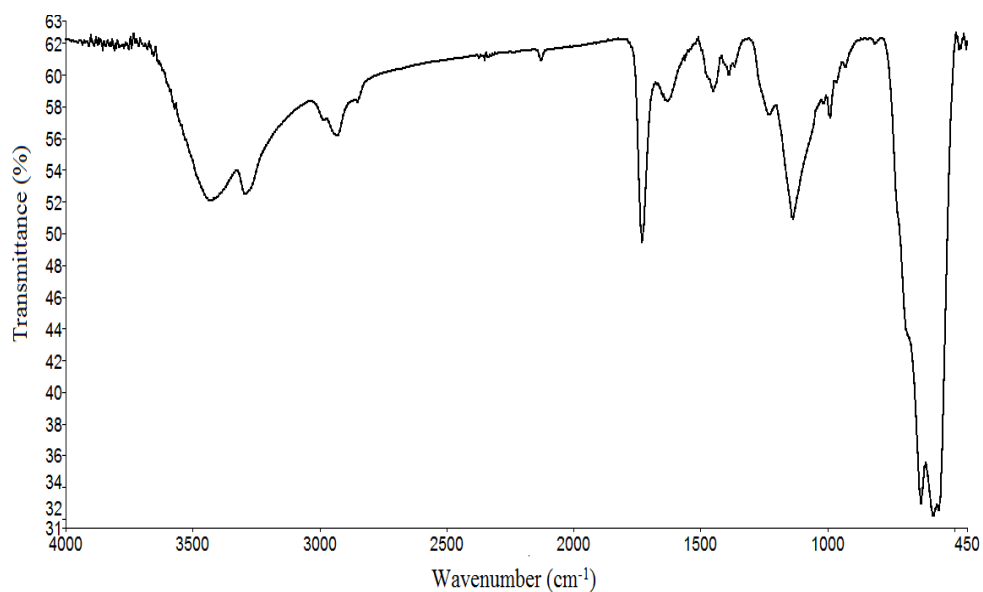


Figure 3.34. FT-IR spectrum of poly(POHMAC-*co*-VTM)-*g*-Fe₃O₄

Table 3.13. FT-IR spectrum evaluation of poly(POHMAC-*co*-VTM)-*g*-Fe₃O₄

Wavelength (cm ⁻¹)	Vibration Type
3292	≡C-H stretching
2929	aliphatic C-H stretch
2128	C≡C stretching
1745	Ester carbonyl stretching
1137	Si-O stretch
583	Fe-O stretch indicating the presence of Fe ₃ O ₄

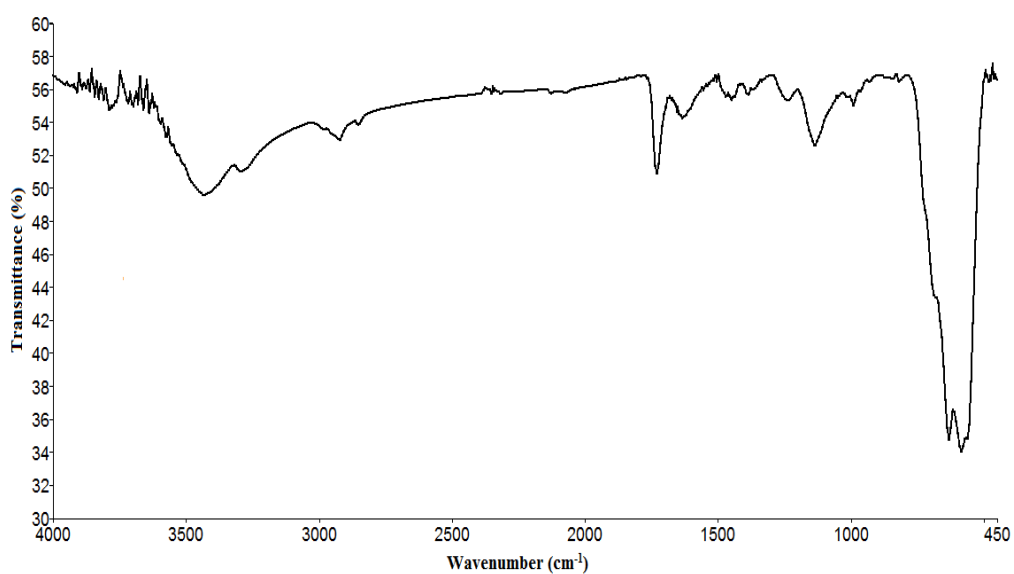


Figure 3.35. FT-IR spectrum of PVC-*g*-poly(POHMAC-*co*-VTM)-*g*-Fe₃O₄

Table 3.14. FT-IR spectrum evaluation of PVC-*g*-poly(POHMAC-*co*-VTM)-*g*-Fe₃O₄

Wavelength (cm ⁻¹)	Vibration Type
3433	C-H stretch
2921	aliphatic C-H stretch
1634	C=C in the ring
1137	Si-O stretch
584	Fe-O

3.3.2. Thermal properties

Figures 3.36 - 3.41 show the TGA and DTG curves and DSC curves of poly(POHMAC-*co*-VTM), poly(POHMAC-*co*-VTM)-*g*-Fe₃O₄ and PVC-*g*-poly(POHMAC-*co*-VTM)-*g*-Fe₃O₄ respectively. They are evaluated in Table 3.15. For the TGA, samples were heated up to 800 °C at a heating rate of 10 °C/min.

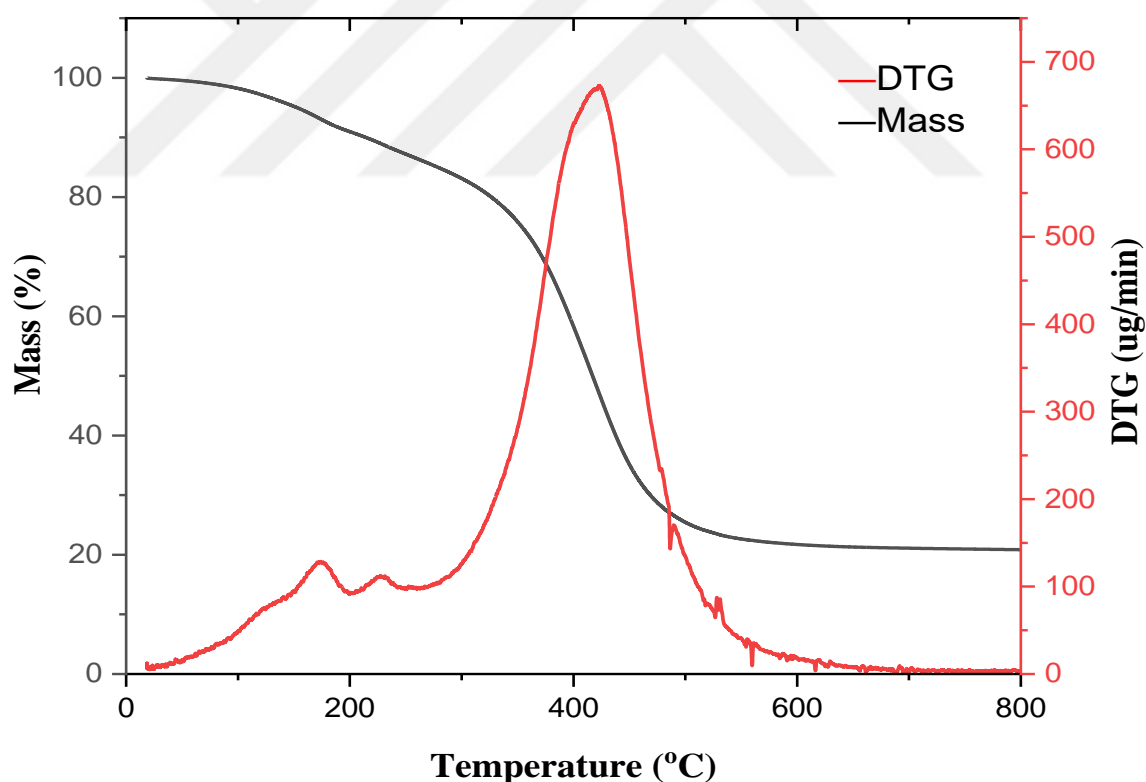


Figure 3.36. TGA and DTG curve of poly(POHMAC-*co*-VTM)

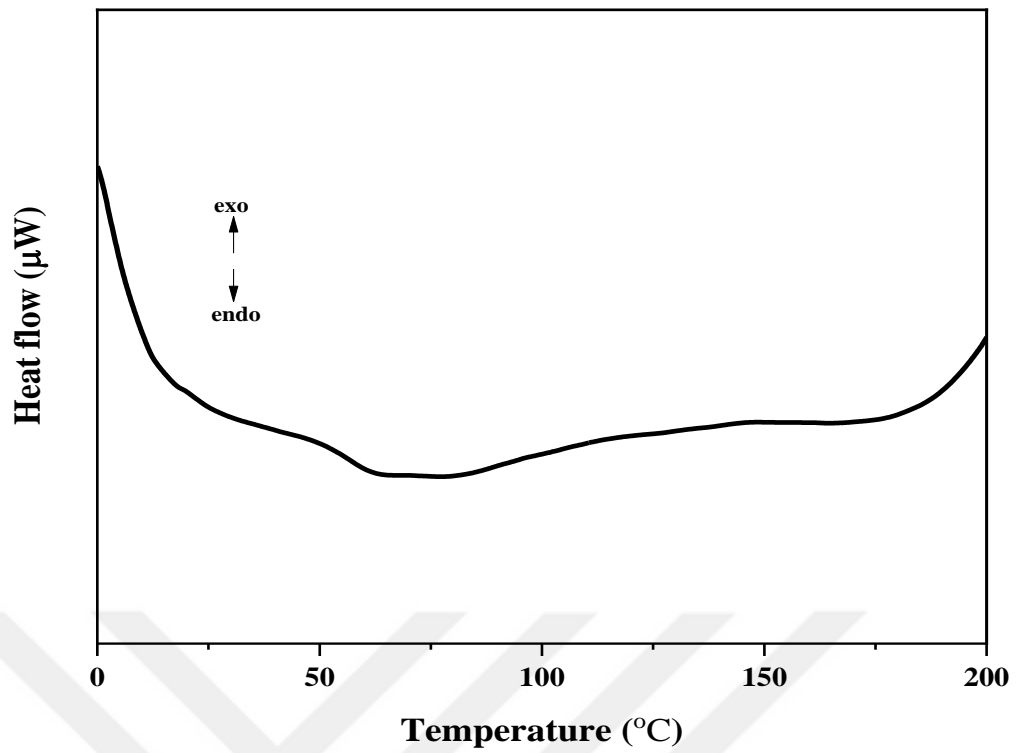


Figure 3.37. DSC curve of poly(POHMAC-co-VTM)

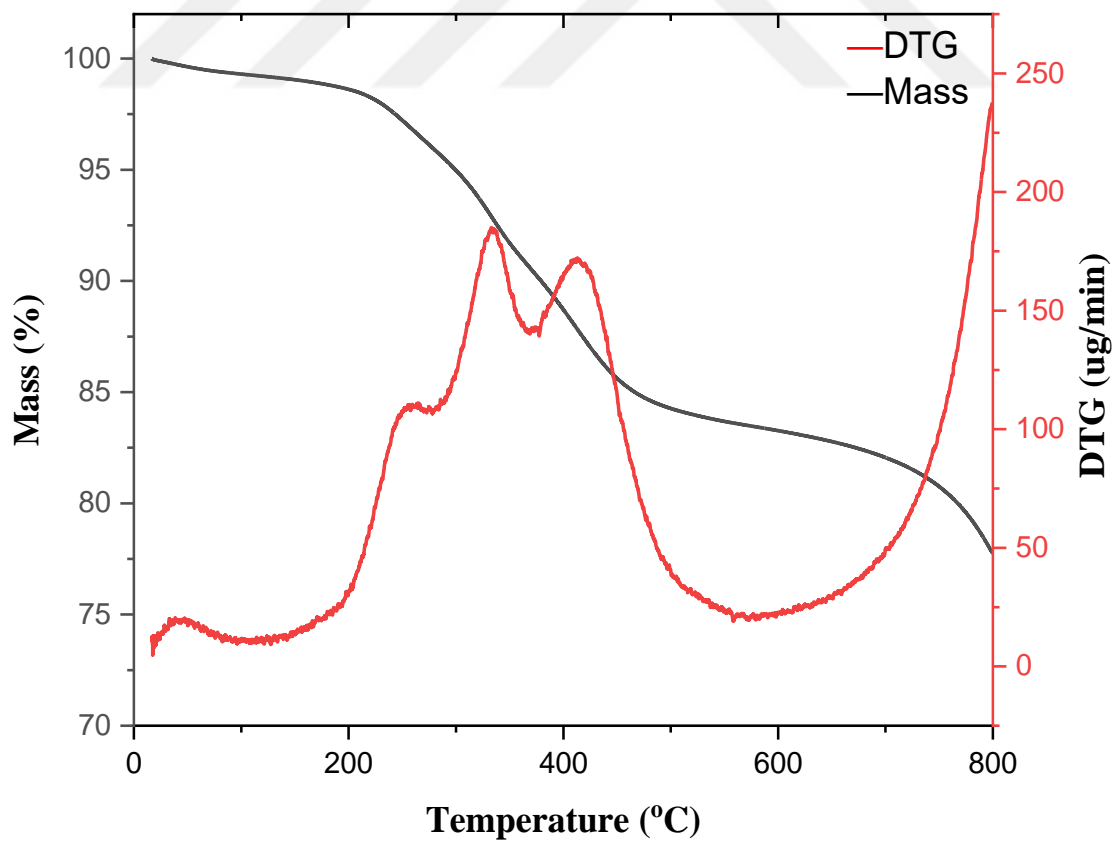


Figure 3.38. TGA and DTG curve of poly(POHMAC-co-VTM)-g-Fe₃O₄

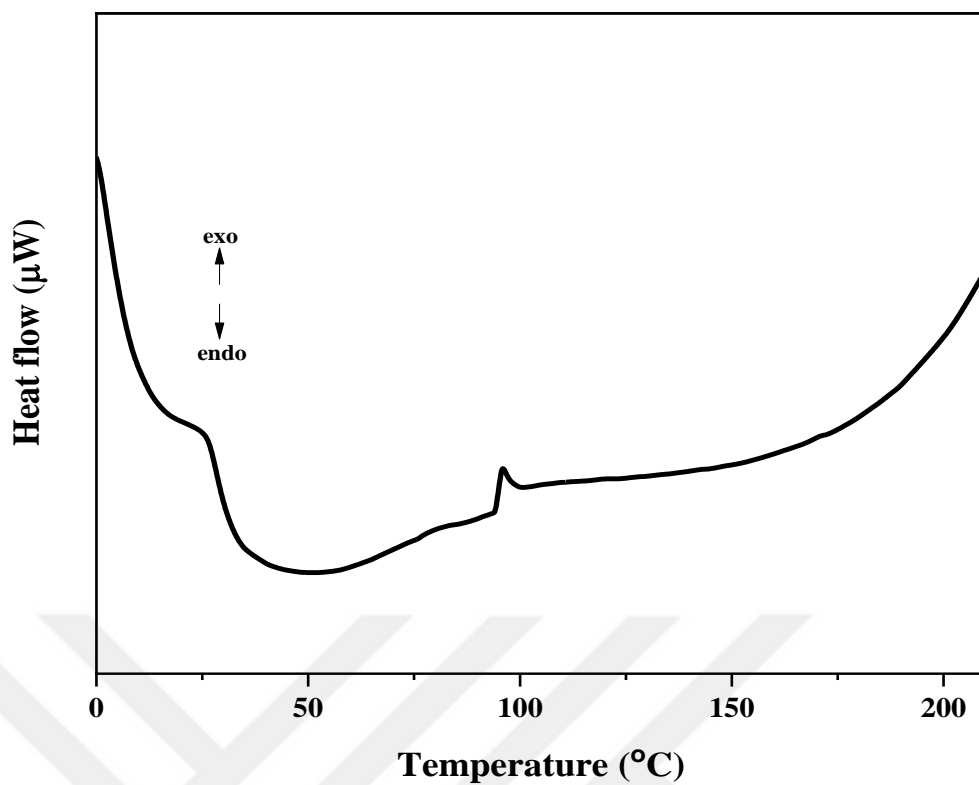


Figure 3.39. DSC curve of poly(POHMAC-co-VTM)-g-Fe₃O₄

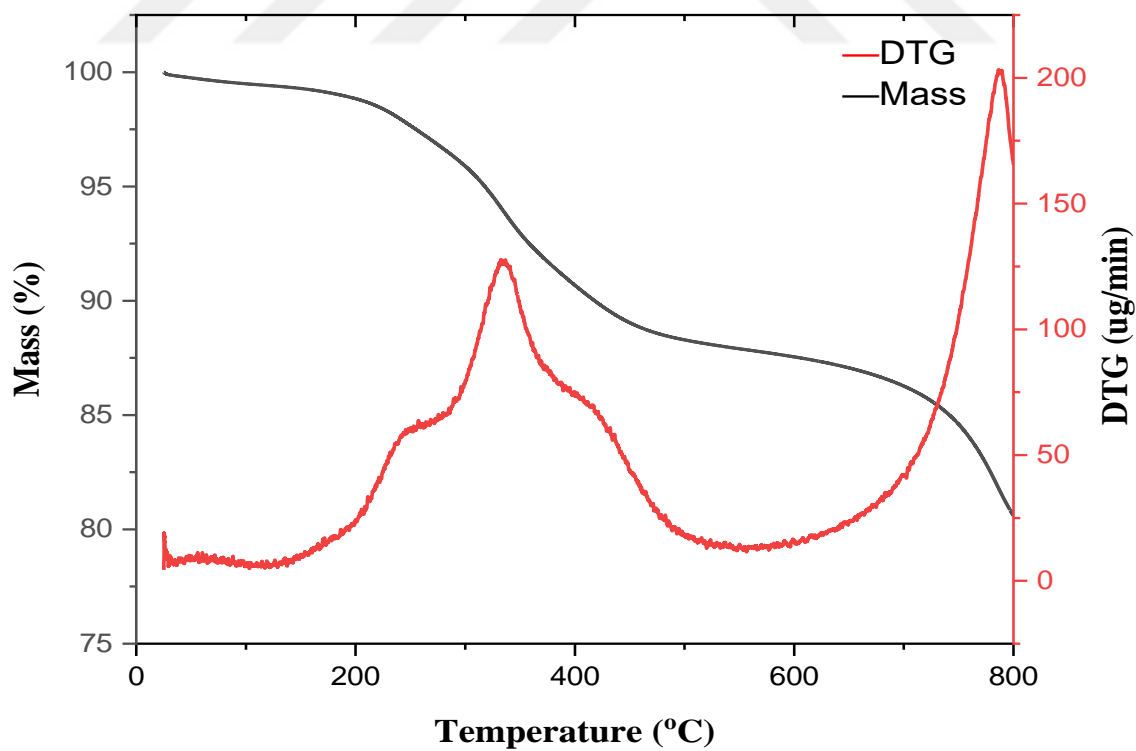


Figure 3.40. TGA and DTG curve of PVC-g-poly(POHMAC-co-VTM)-g-Fe₃O₄

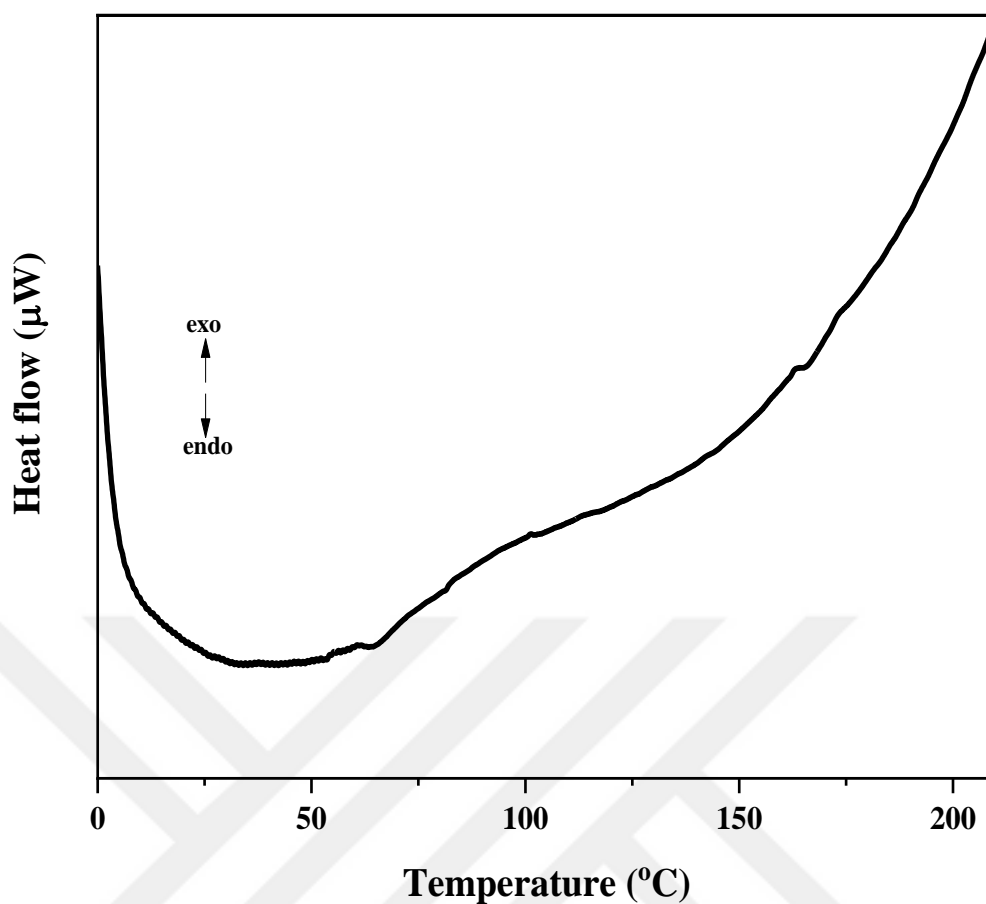


Figure 3.41. DSC curve of PVC-g-poly(POHMAC-co-VTM)-g-Fe₃O₄

Table 3.15. TGA, DTG and DSC evaluation of PVC-g-poly(POHMAC-co-VTM)-g-Fe₃O₄

Polymer	T_g (°C)	T_i (°C)	%		Stage number (DTG)	T_{max} (°C) DTG
			Mass loss at 400 °C	Residue at 800 °C		
Poly(POHMAC-co-VTM)	57	265	41.3	20.8	2	227,423
Poly(POHMAC-co-VTM)-g-Fe ₃ O ₄	85	282	11.3	22.7	3	257,333,413
PVC-g-Poly(POHMAC-co-VTM)-g-Fe ₃ O ₄	63	277	9.3	19.4	2	332,786

3.3.3. Magnetic property

Figure 3.42 shows the magnetization curve obtained from the VSM of PVC-g-poly(POHMAC-co-VTM)-g-Fe₃O₄.

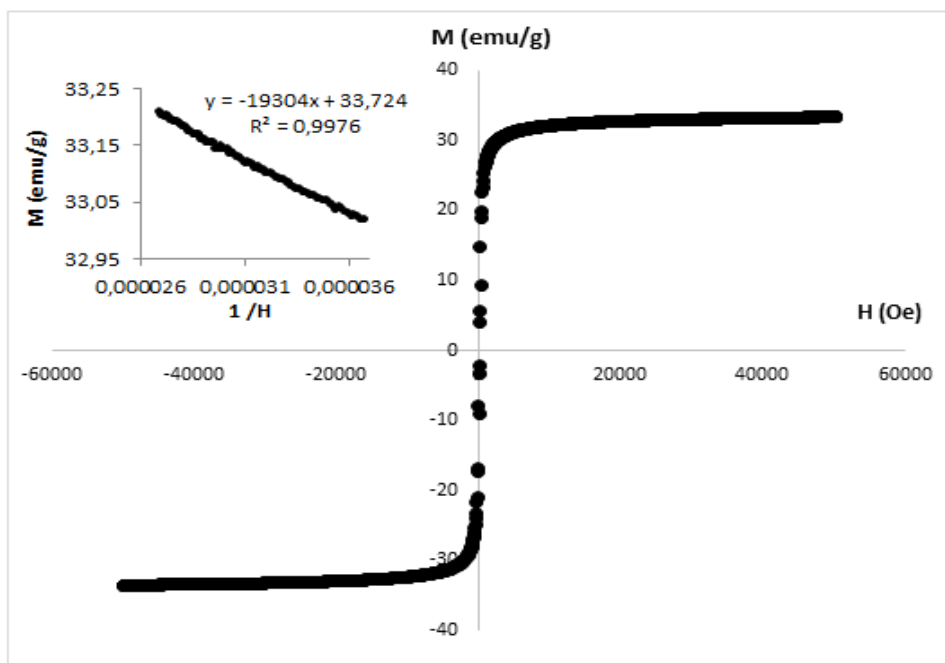


Figure 3.42. VSM plot of PVC-g-poly(POHMAC-co-VTM)-g-Fe₃O₄

3.3.4. Electrical investigation

Variation of dielectric constant, dielectric loss factor, and conductivity of poly(POHMAC-co-VTM), poly(POHMAC-co-VTM)-g-Fe₃O₄ and PVC-g-poly(POHMAC-co-VTM)-g-Fe₃O₄ with frequency at room temperature are shown in Figures 3.43 – 3.51 respectively.

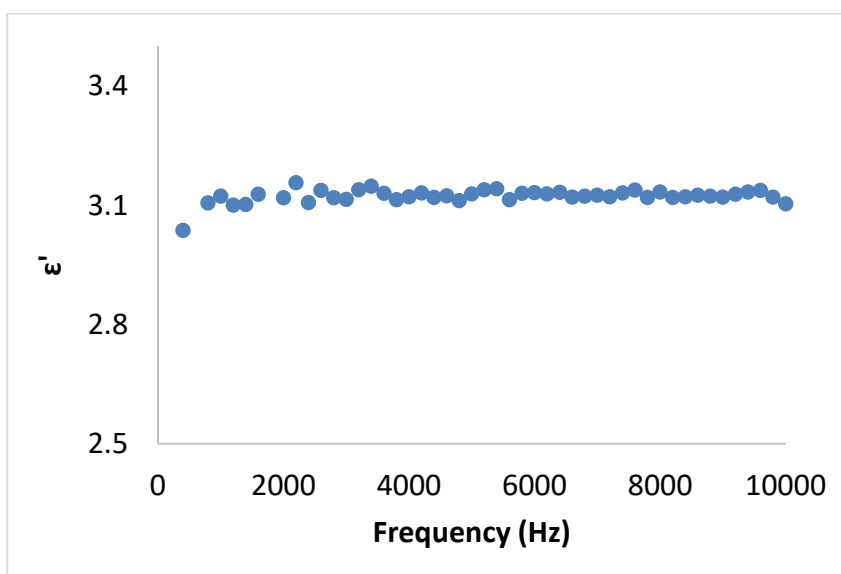


Figure 3.43. Variation of dielectric constant of poly(POHMAC-co-VTM) with frequency at room temperature

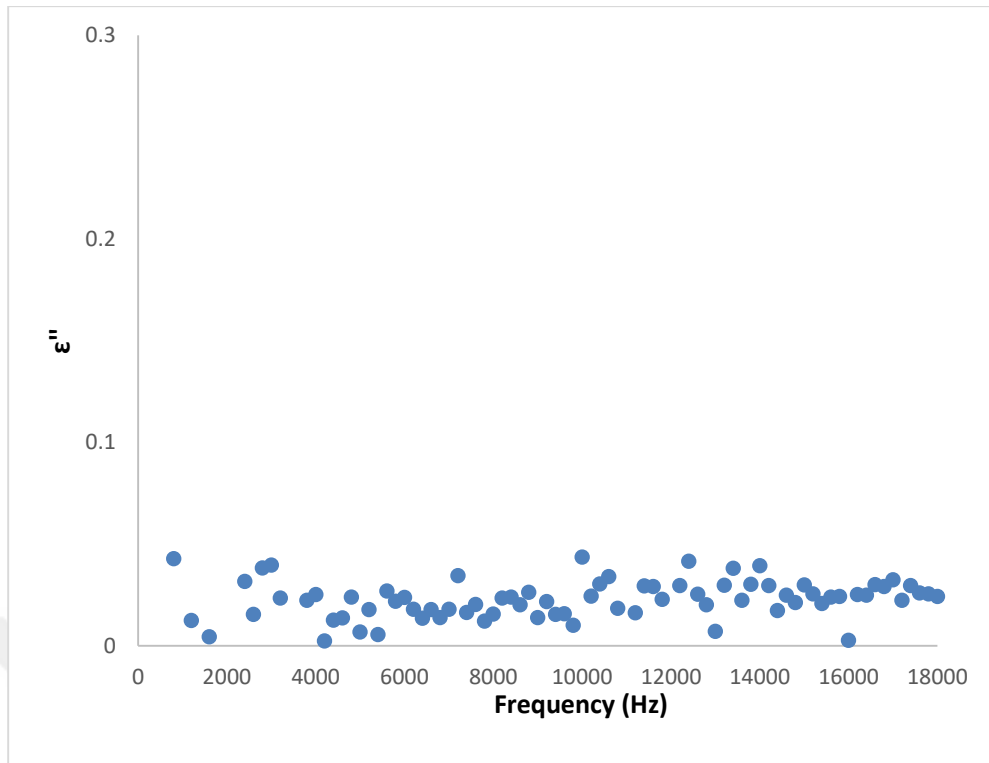


Figure 3.44. Variation of dielectric loss factor of poly(POHMAC-co-VTM) with frequency at room temperature

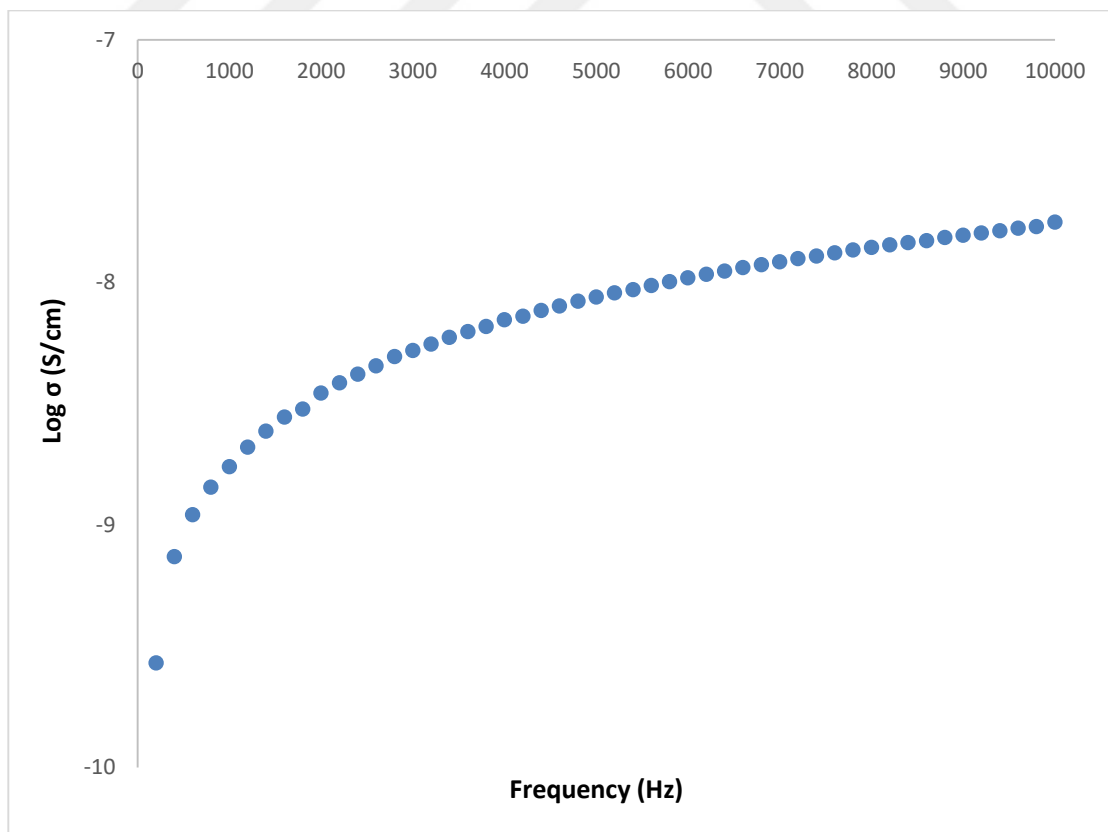


Figure 3.45. Variation of conductivity of poly(POHMAC-co-VTM) with frequency at room temperature

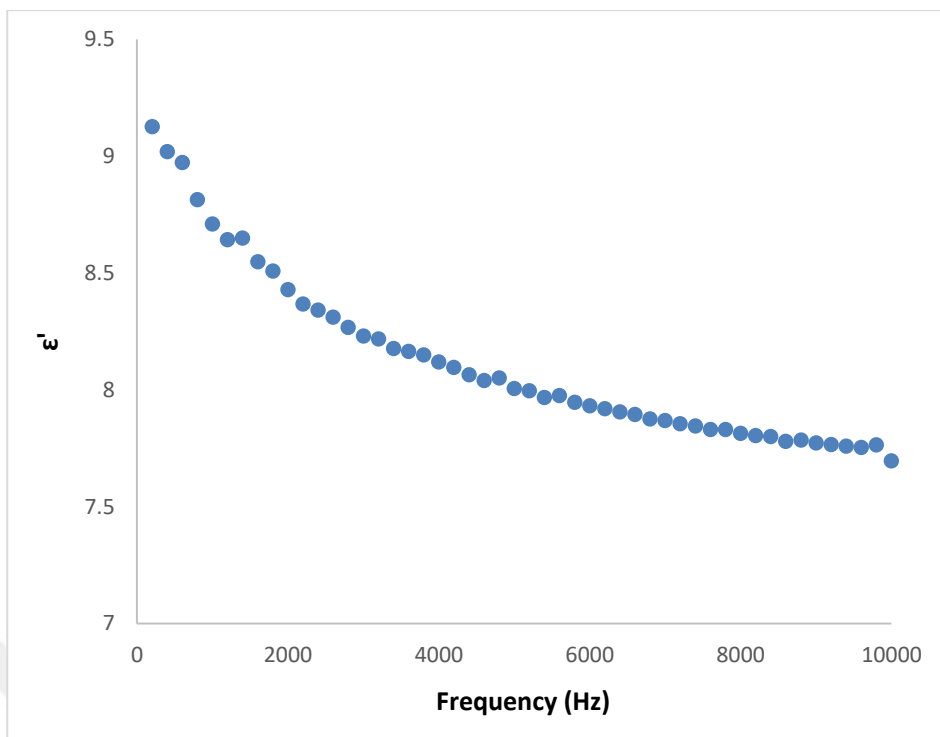


Figure 3.46. Variation of dielectric constant of poly(POHMAC-*co*-VTM)-*g*-Fe₃O₄ with frequency at room temperature

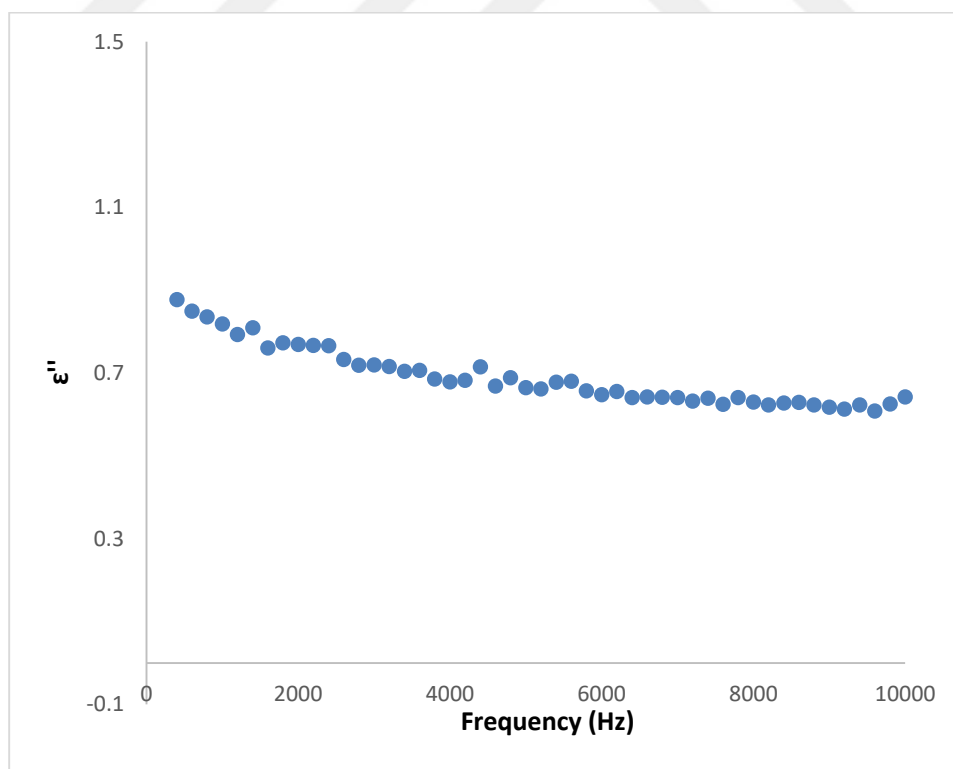


Figure 3.47. Variation of dielectric loss factor of poly(POHMAC-*co*-VTM)-*g*-Fe₃O₄ with frequency at room temperature

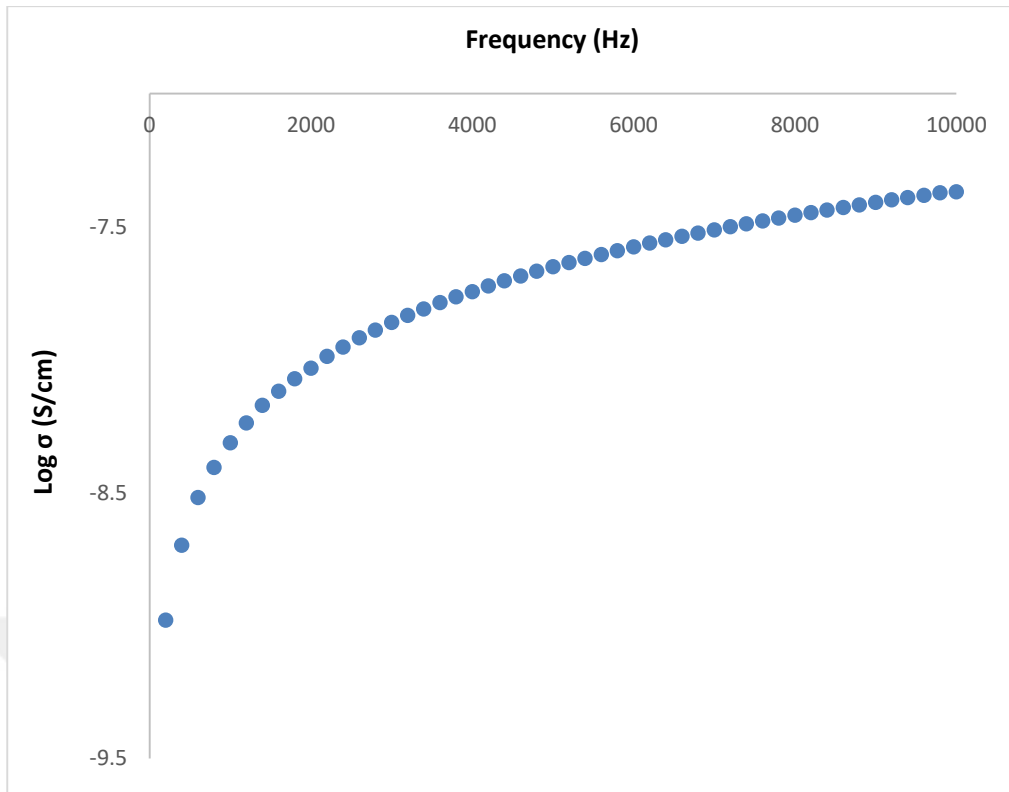


Figure 3.48. Variation of conductivity of poly(POHMAC-co-VTM)-g-Fe₃O₄ with frequency at room temperature

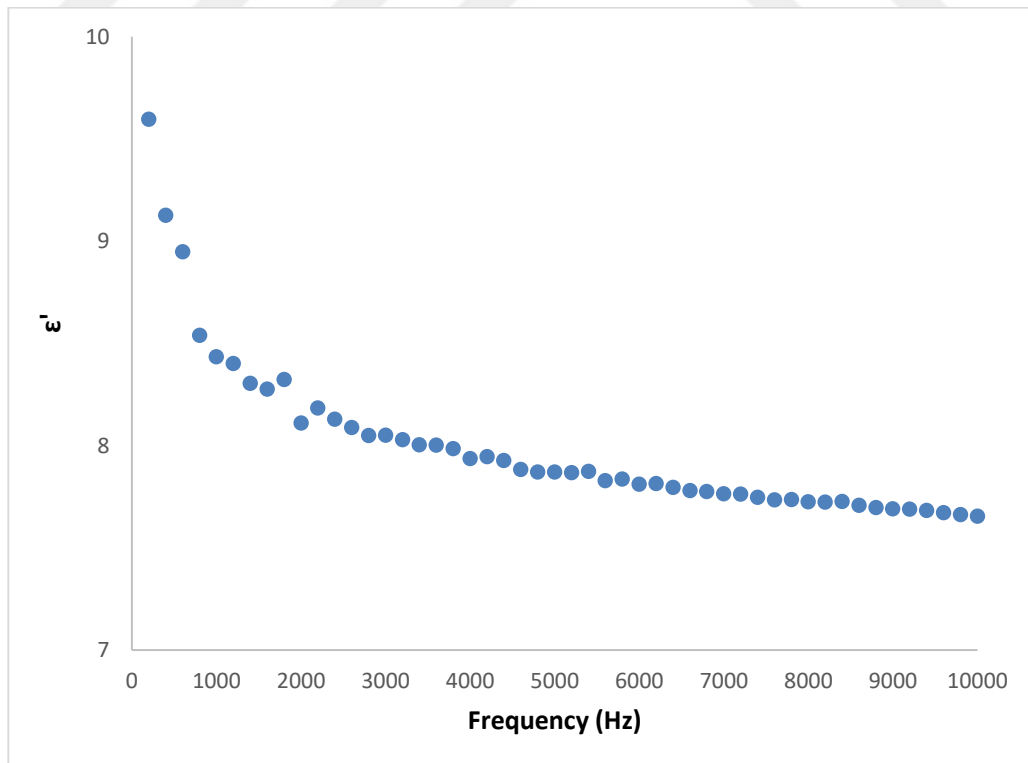


Figure 3.49. Variation of dielectric constant of PVC-g-poly(POHMAC-co-VTM)-g-Fe₃O₄ with frequency at room temperature

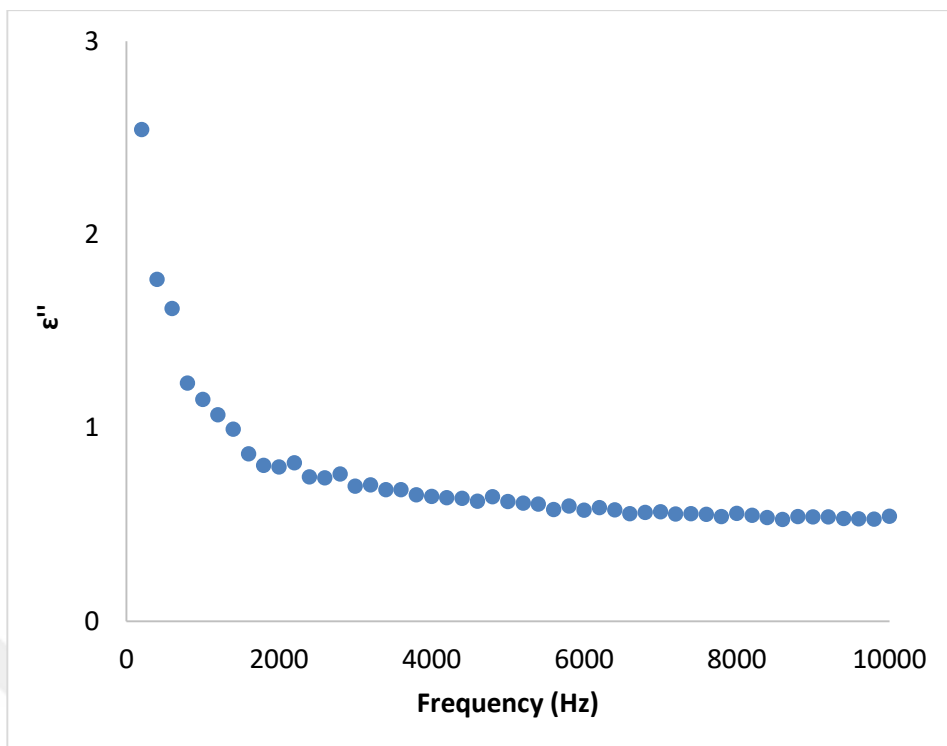


Figure 3.50. Variation of dielectric loss factor of PVC-g-poly(POHMAC-co-VTM)-g-Fe₃O₄ with frequency at room temperature

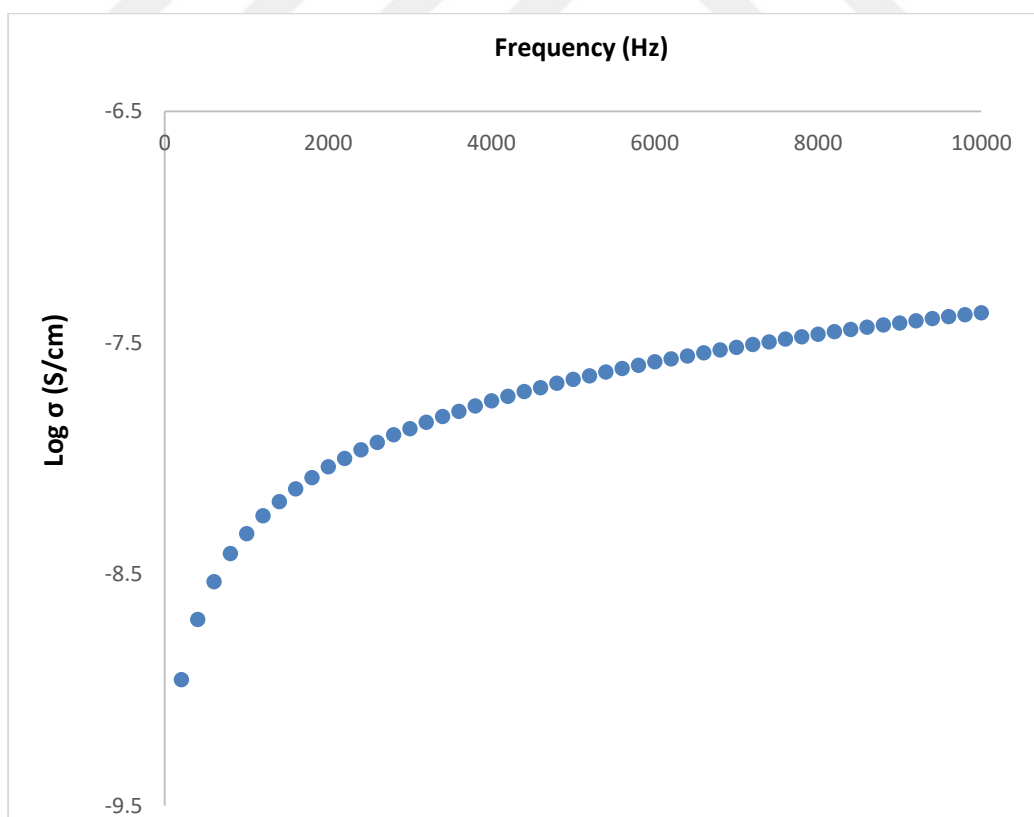


Figure 3.51. Variation of conductivity of PVC-g-poly(POHMAC-co-VTM)-g-Fe₃O₄ with frequency at room temperature

3.4. Composite of PVC with POH-N₃PTMS-g-Fe₃O₄

3.4.1. Characterization

The FT-IR spectrum of N₃PTMS is given in Figure 3.52 and evaluated in Table 3.16.

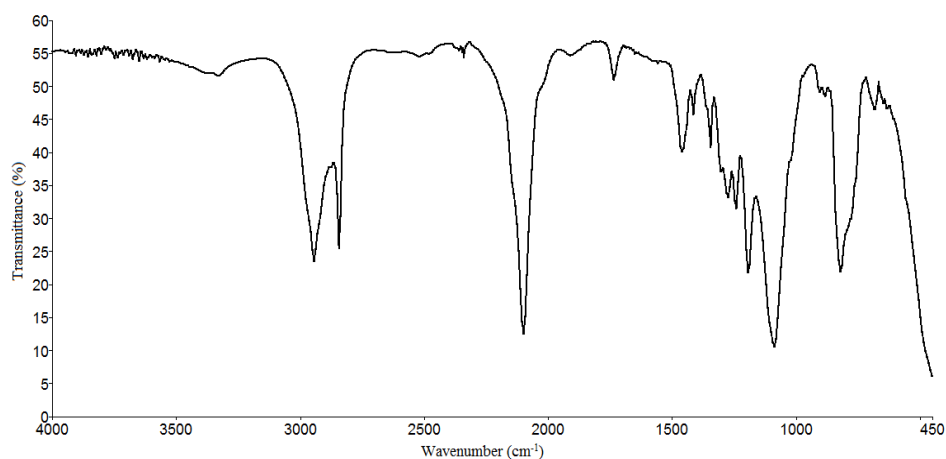


Figure 3.52. FT-IR spectrum of N₃PTMS

Table 3.16. FT-IR spectrum evaluation of N₃PTMS

Wavelength (cm-1)	Vibration Type
2843; 2944	C-H stretching from aliphatic -CH ₂
2102	N ⁻ =N ⁺ =N ⁻ stretching
1087	Si-O

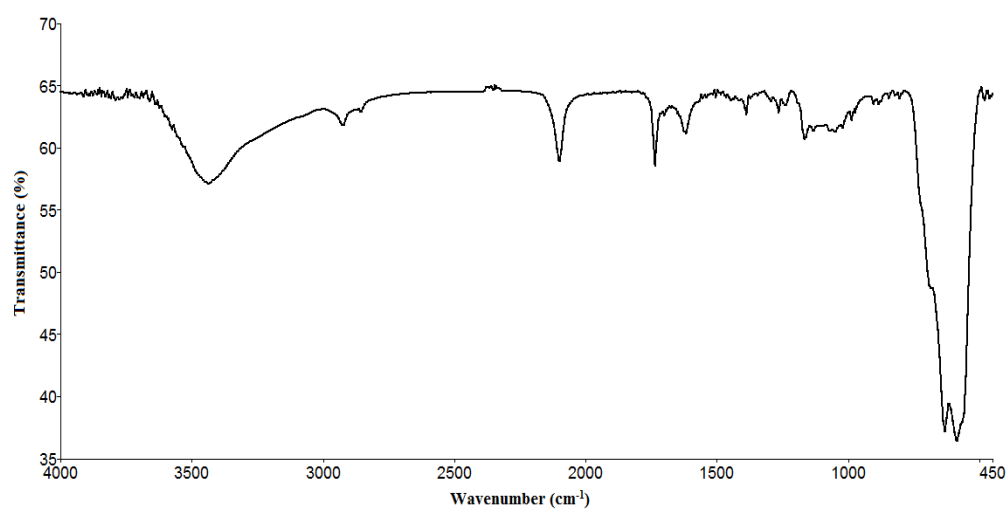


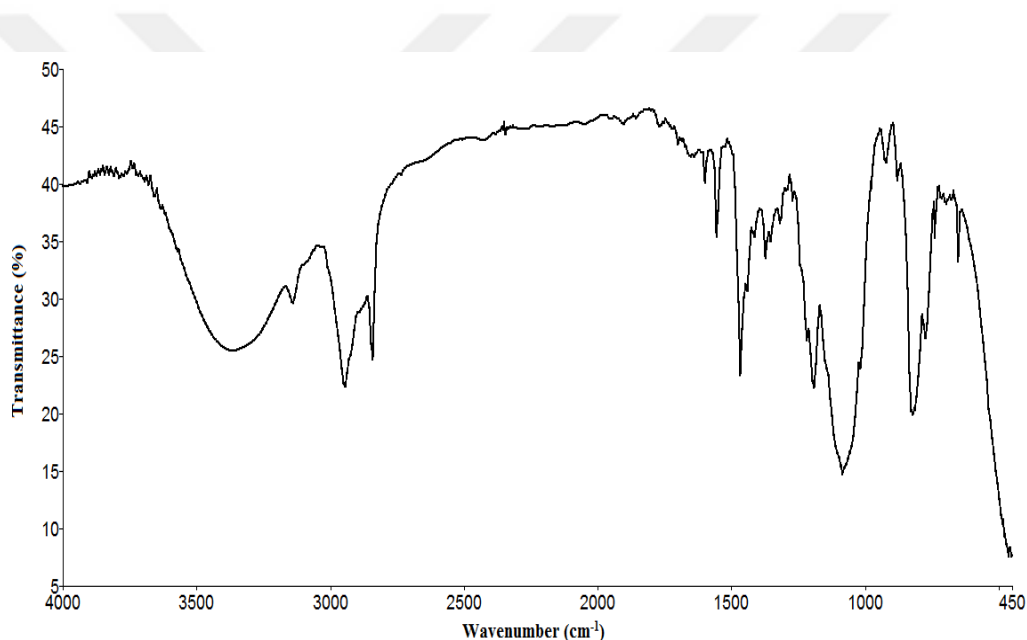
Figure 3.53. FT-IR spectrum of N₃PTMS-g-Fe₃O₄

Table 3.17. FT-IR spectrum evaluation of N₃PTMS-g-Fe₃O₄

Wavelength (cm ⁻¹)	Vibration Type
3435	O-H stretch
2923	aliphatic C-H stretching
2099	N ⁻ =N ⁺ =N ⁻ stretching
586	Fe-O

The FT-IR spectrum of N₃PTMS-g-Fe₃O₄ is given in Figure 3.53 and evaluated in Table 3.17.

The FT-IR spectrum of POH-N₃PTMS-g-Fe₃O₄ is given in Figure 3.54 and evaluated in Table 3.18.

**Figure 3.54.** FT-IR spectrum of POH-N₃PTMS-g-Fe₃O₄**Table 3.18.** FT-IR spectrum evaluation of POH-N₃PTMS-g-Fe₃O₄

Wavelength (cm ⁻¹)	Vibration Type
3364	O-H stretch
2945	aliphatic -C-H stretch
1598	C=C stretch
1467	C-N stretch
652	Fe-O

3.4.2. Thermal properties

The TGA and DTG, DSC curves of $N_3TMS-g-Fe_3O_4$, and $POH-N_3PTMS-g-Fe_3O_4$ are shown in Figures 3.55 – 3.58 respectively and evaluated in Table 3.19.

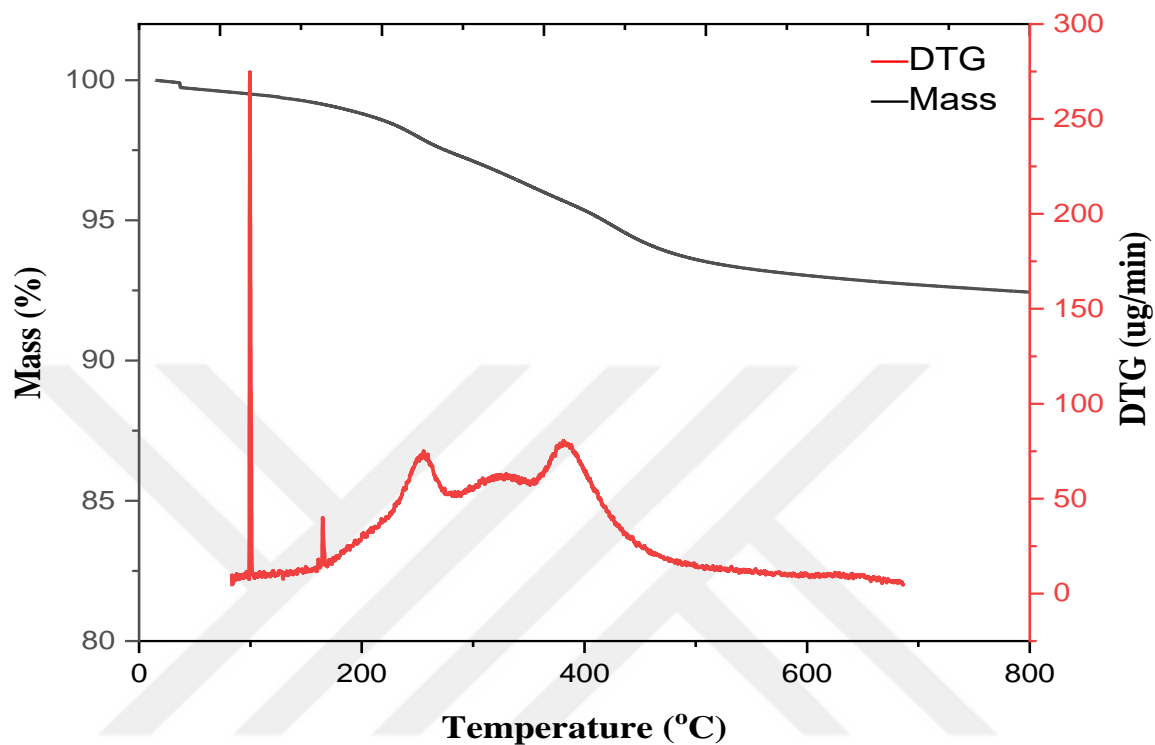


Figure 3.55. TGA and DTG curve of $N_3PTMS-g-Fe_3O_4$

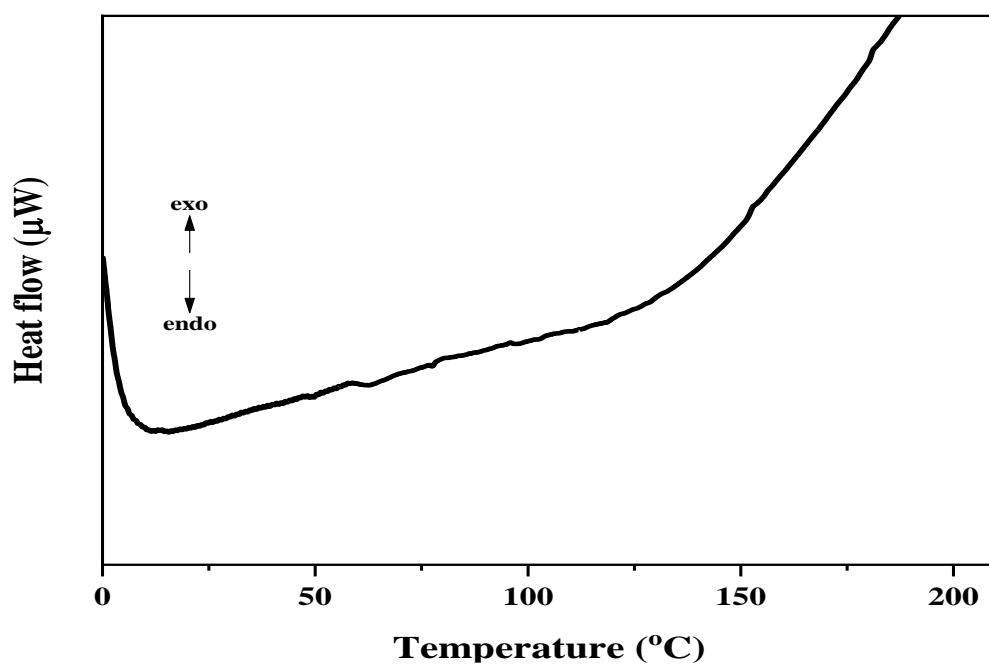


Figure 3.56. DSC curve of $N_3PTMS-g-Fe_3O_4$

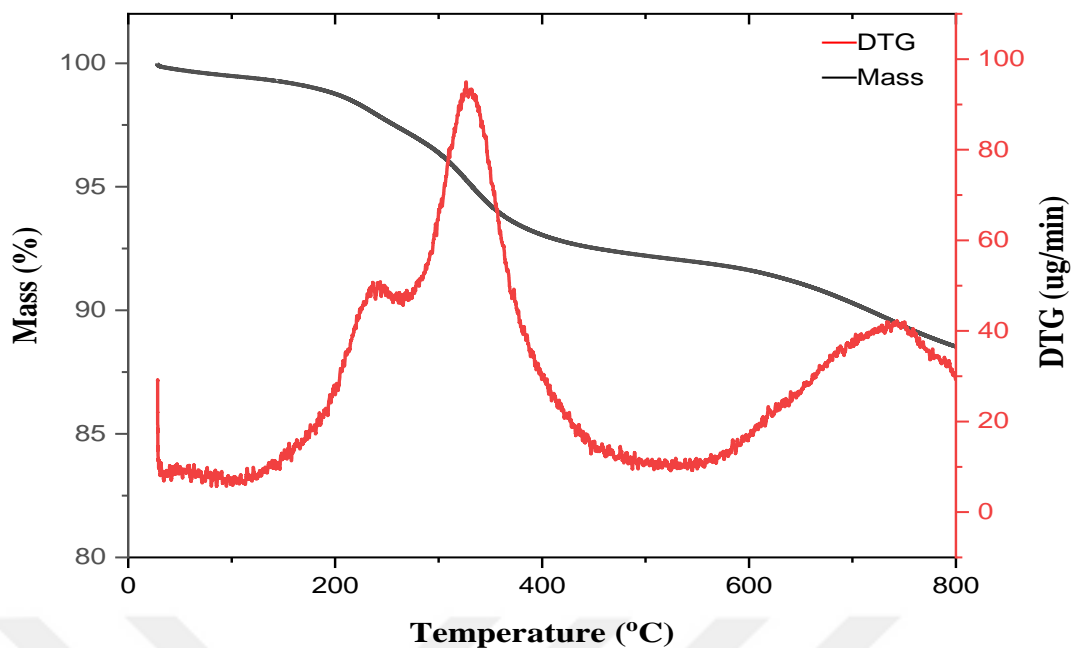


Figure 3.57. TGA and DTG curve of POH-N₃PTMS-g-Fe₃O₄

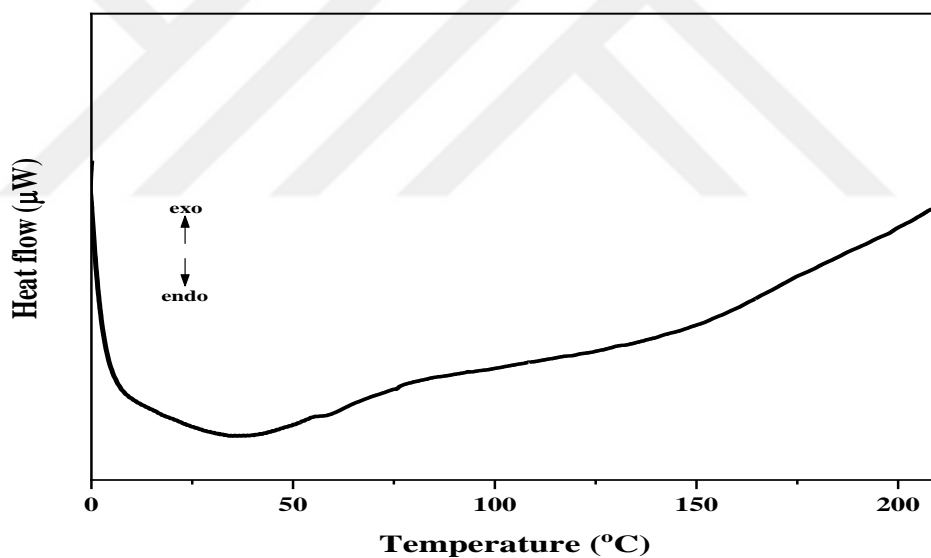


Figure 3.58. DSC curve of POH-N₃PTMS-g-Fe₃O₄

Table 3.19. TGA, DTG and DSC evaluation of POH-N₃PTMS-g-Fe₃O₄

Polymer	T_g (°C)	T_i (°C)	% Mass loss at 400 °C	% Residue at 800 °C	Stage number (DTG)	T_{max} (°C) DTG
N ₃ PTMS-g-Fe ₃ O ₄	61	226	4.6	92.4	3	251,347,424
POH-N ₃ PTMS-g- Fe ₃ O ₄	57	217	7.0	88.5	3	240,327,740

Figures 3.59 – 3.64 show the TGA and DTG, DSC curves of PVC / POH-N₃PTMS-g-Fe₃O₄ of 5%, 10%, and 20% (by wt) composites and evaluated in Table 3.20.

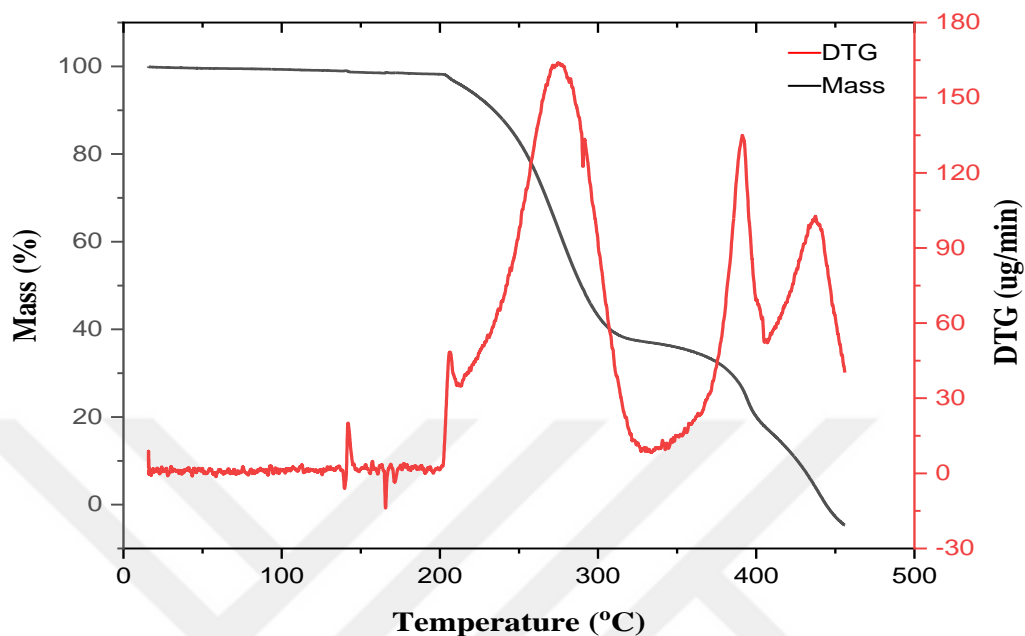


Figure 3.59. TGA and DTG curve of PVC / 5% (by wt) POH-N₃PTMS-g-Fe₃O₄ composite

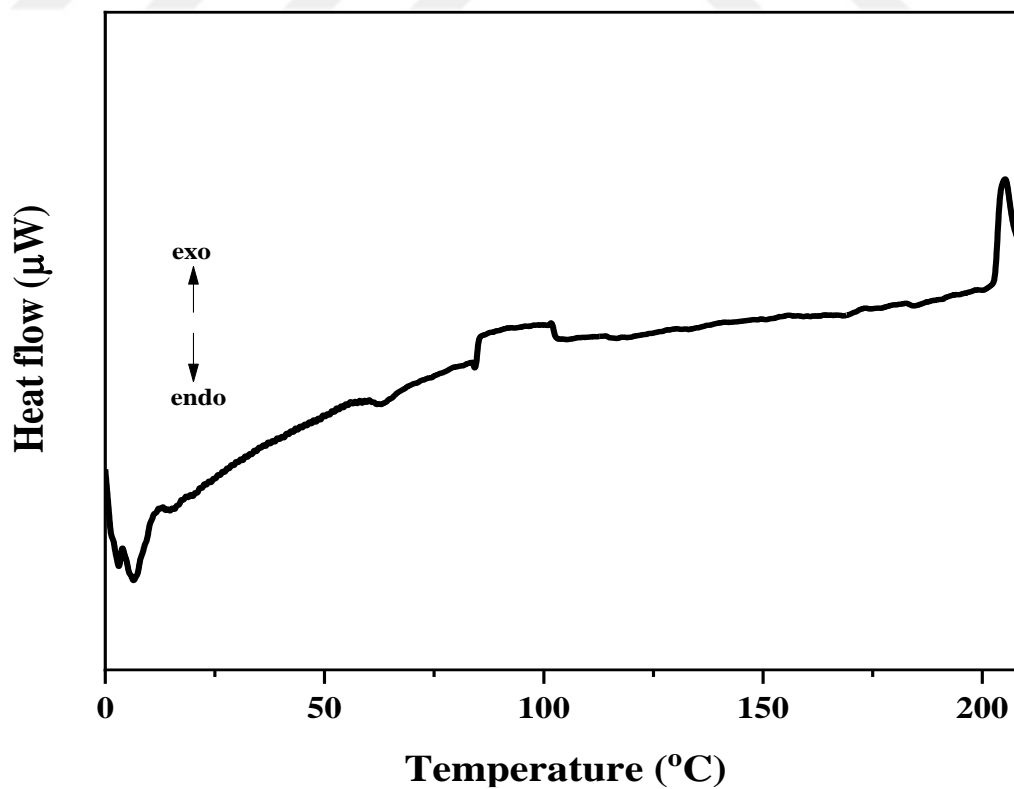


Figure 3.60. DSC curve of PVC / 5% (by wt) POH-N₃PTMS-g-Fe₃O₄ composite

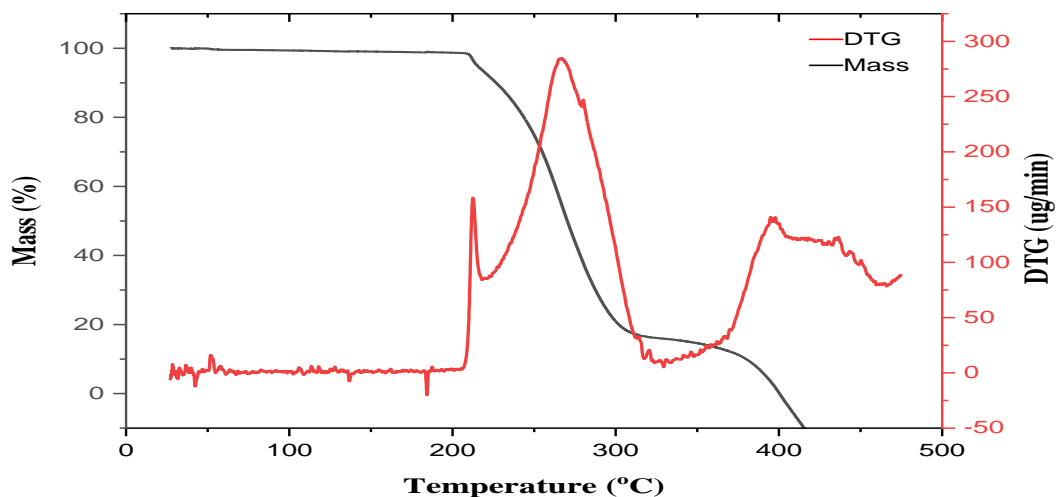


Figure 3.61. TGA and DTG curve of PVC / 10% POH-N₃PTMS-g-Fe₃O₄ composite

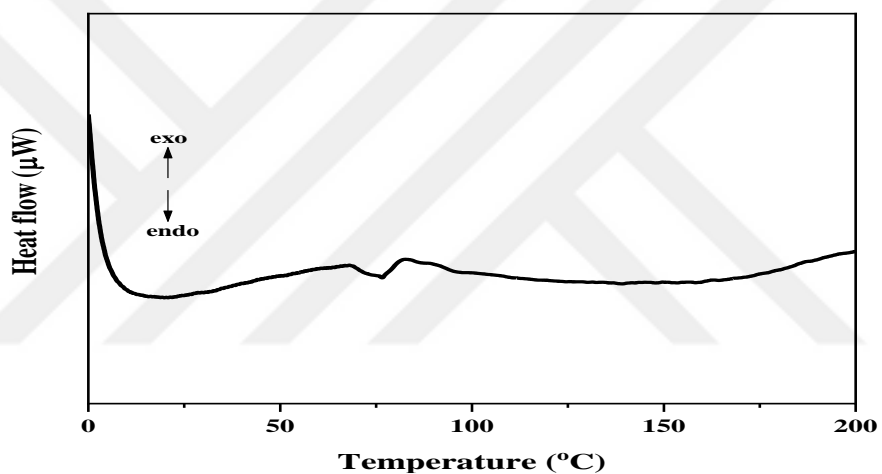


Figure 3.62. DSC curve of PVC / 10% POH-N₃PTMS-g-Fe₃O₄ composite

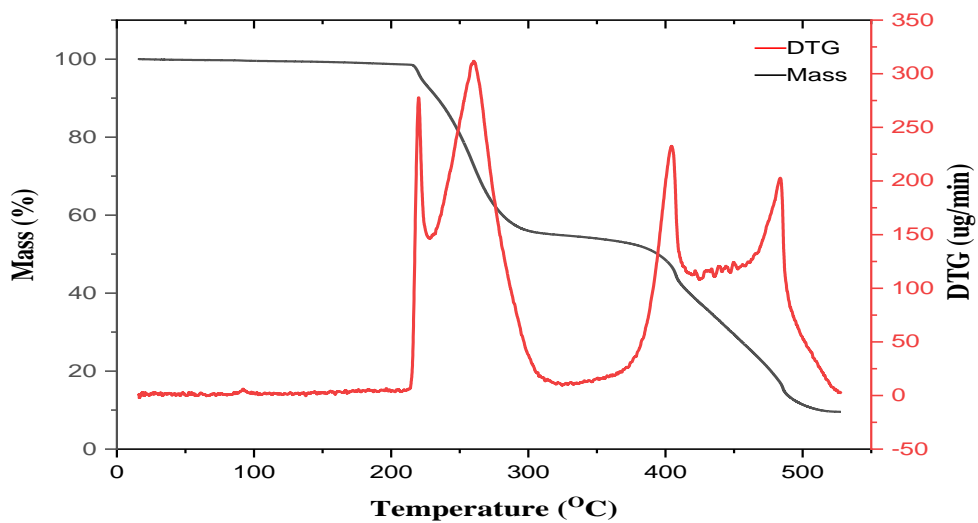


Figure 3.63. TGA and DTG curve of PVC / 20% (by wt) POH-N₃PTMS-g-Fe₃O₄ composite

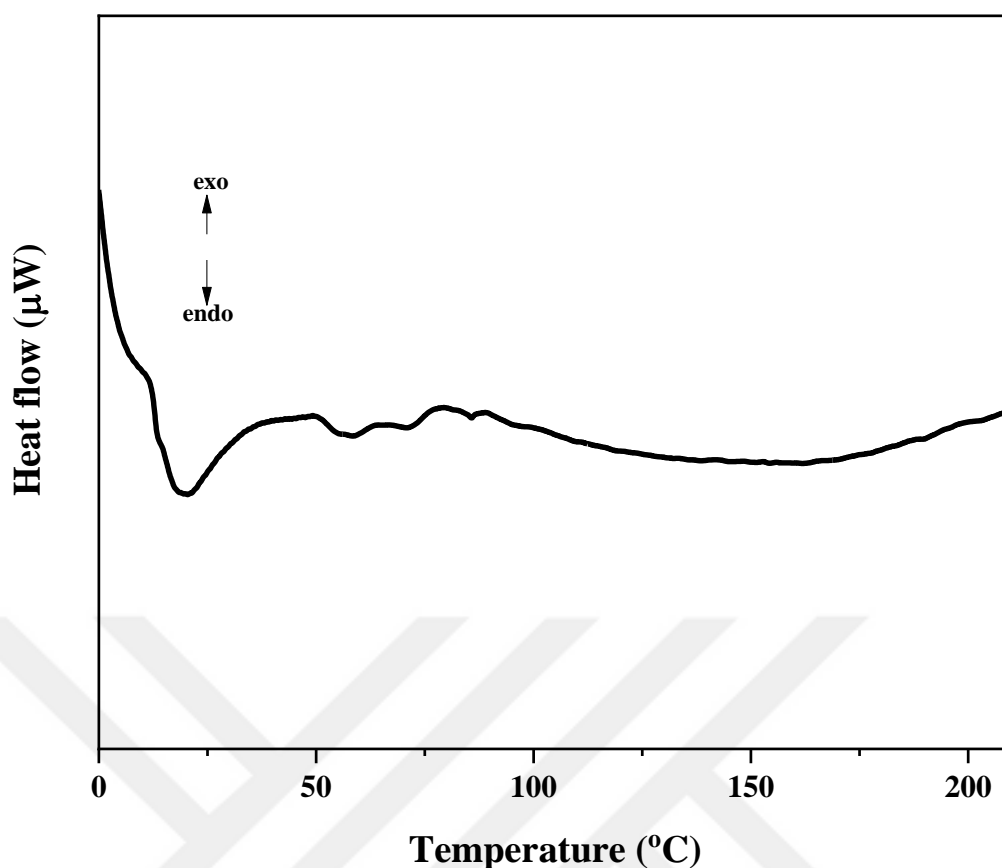


Figure 3.64. DSC curve of PVC / 20% (by wt) POH-N₃PTMS-g-Fe₃O₄ composite

Table 3.20. TGA, DTG and DSC evaluation of PVC / POH-N₃PTMS-g-Fe₃O₄ composites

Composite	T_g	T_i	% Mass loss at 300 °C	% Residue at 500 °C	Stage number (DTG)	T_{max} (°C)
	(°C)	(°C)				DTG
%5 composite	60	212	57	-	3	275,391,437
%10 composite	72	220	79	-	2	266,395
%20 composite	73	228	44	11.4	3	260,404,483

3.4.3. Morphological structures

Figures 3.65 – 3.72 show the SEM image and EDX analysis evaluation of N₃TMS-g-Fe₃O₄, POH-N₃PTMS-g-Fe₃O₄, PVC / 5% (by wt) POH-N₃PTMS-g-Fe₃O₄ composite and PVC / 20% (by wt) POH-N₃PTMS-g-Fe₃O₄ composite respectively.

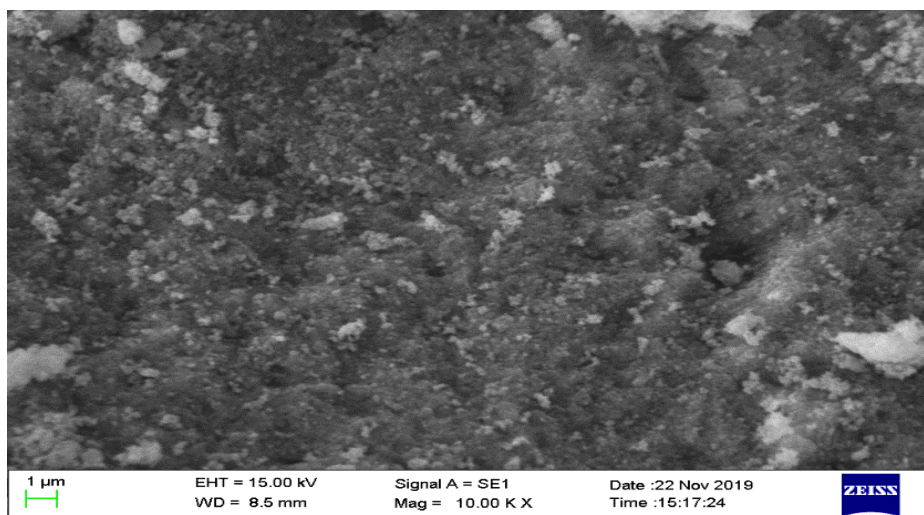


Figure 3.65. SEM image of $N_3PTMS-g-Fe_3O_4$

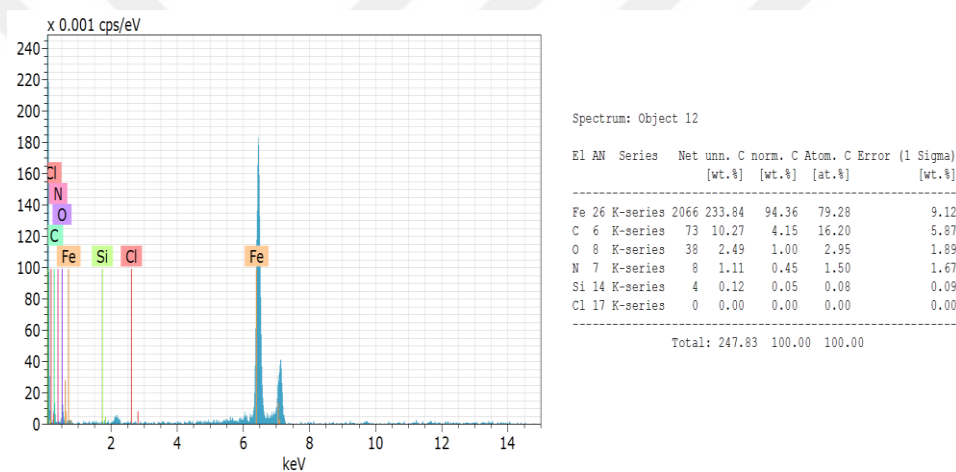


Figure 3.66. EDX image of $N_3PTMS-g-Fe_3O_4$

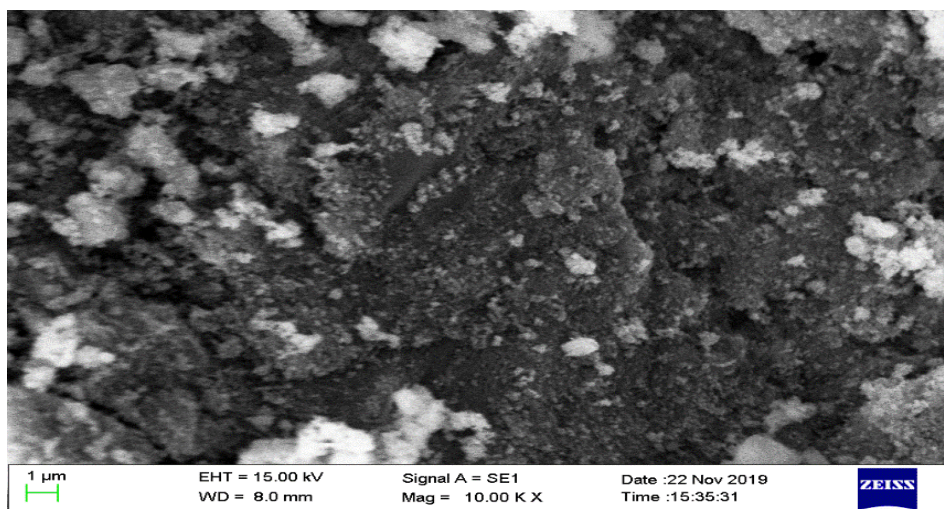


Figure 3.67. SEM image of $POH-N_3PTMS-g-Fe_3O_4$

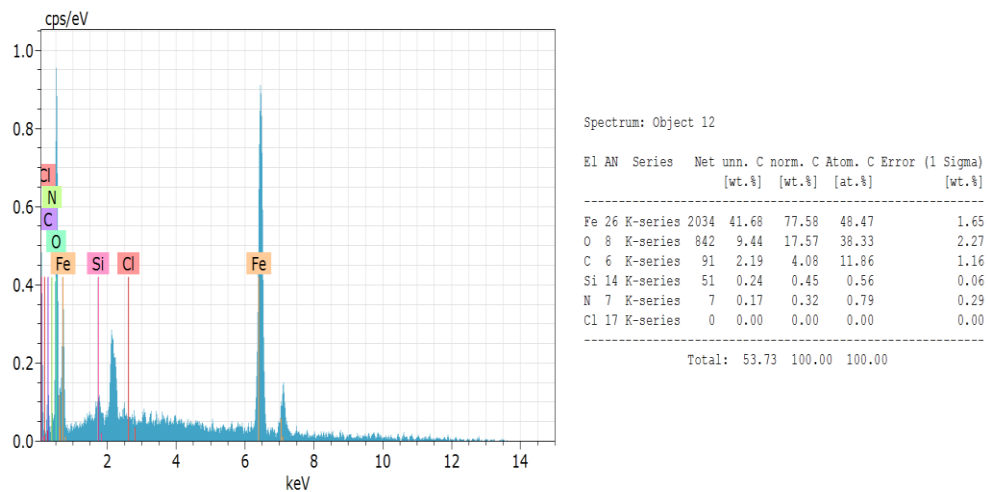


Figure 3.68. EDX image of POH-N₃PTMS-g-Fe₃O₄

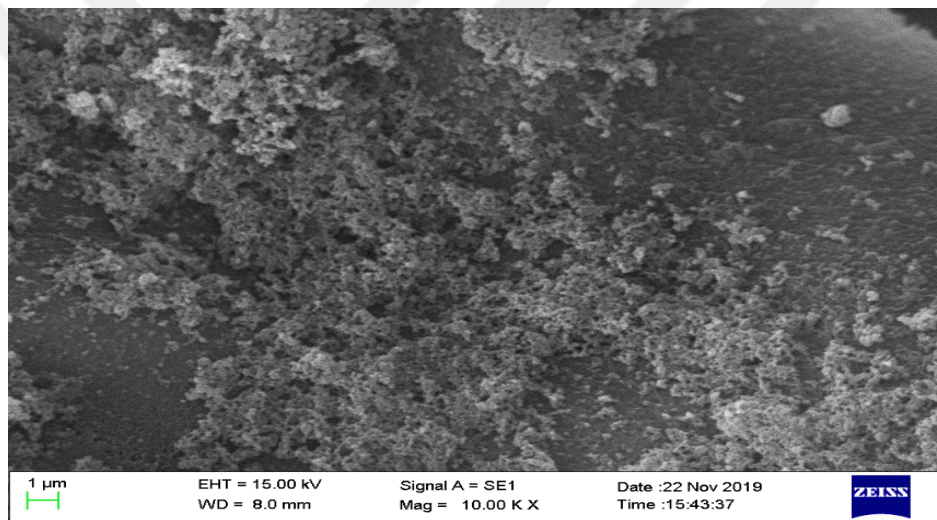


Figure 3.69. SEM image of PVC / 5% (by wt) POH-N₃PTMS-g-Fe₃O₄ composite

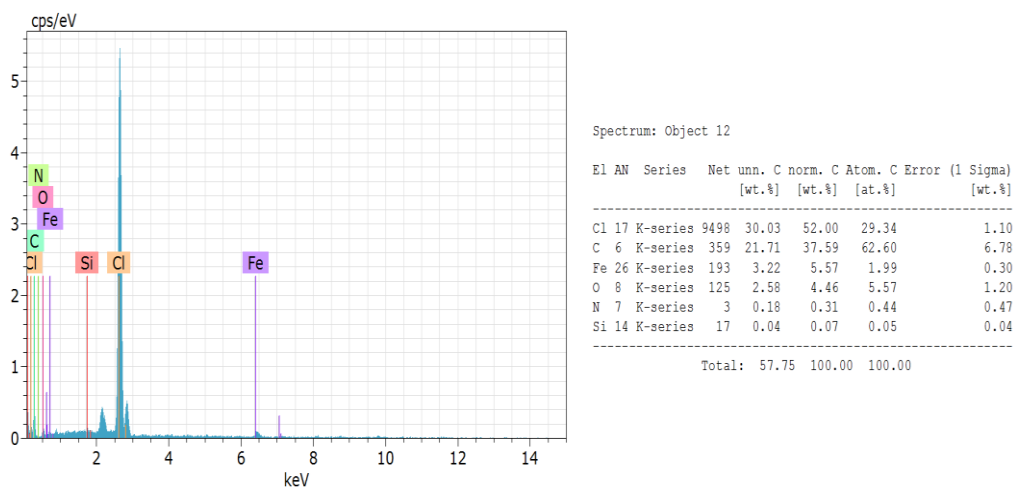


Figure 3.70. EDX image of PVC / 5% (by wt) POH-N₃PTMS-g-Fe₃O₄ composite

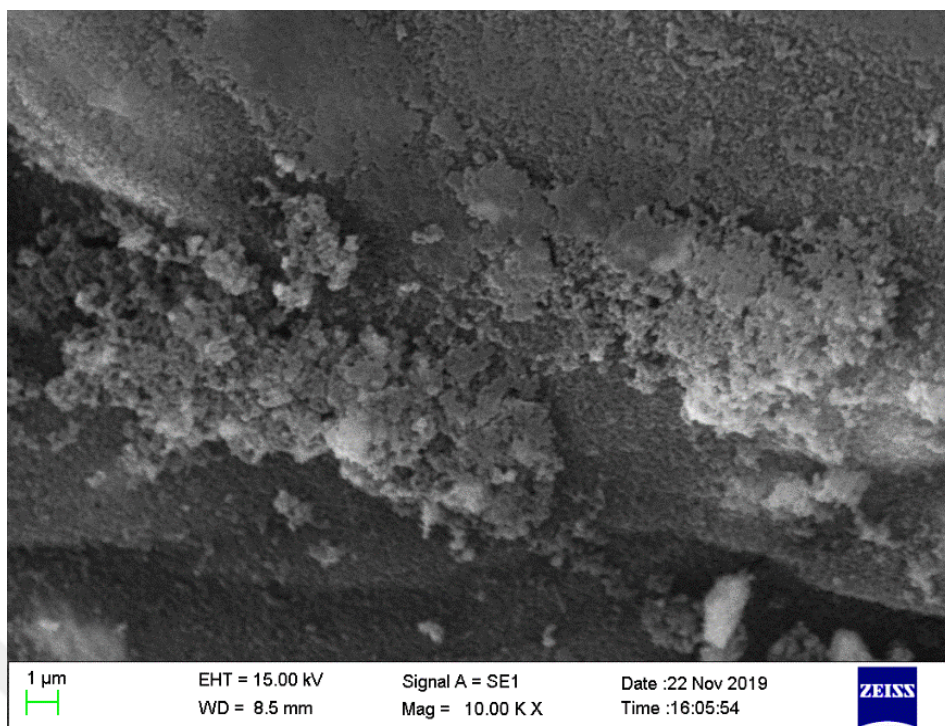


Figure 3.71. SEM image of PVC / 20% (by wt) POH-N₃PTMS-g-Fe₃O₄ composite

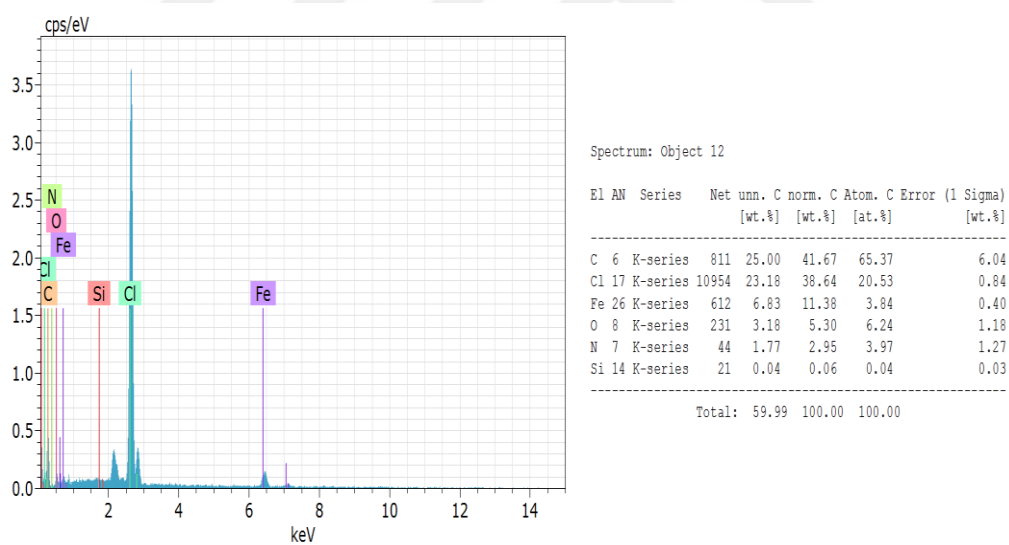


Figure 3.72. EDX image of PVC / 20% (by wt) POH-N₃PTMS-g-Fe₃O₄ composite

3.4.4. . Magnetic property

Of the composites prepared with PVC, the 10% (by wt) POH-N₃PTMS-g-Fe₃O₄ composite was characterized using VSM at a temperature of 300k as shown in Figure 3.73.

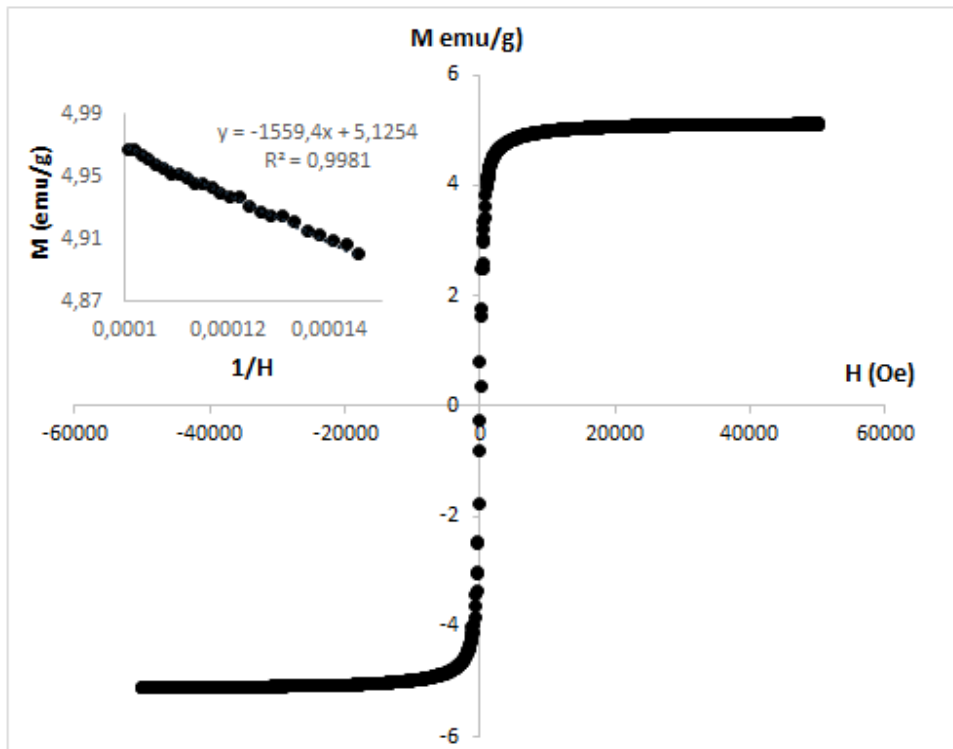


Figure 3.73. VSM plot of PVC / 10% (by wt) POH-N₃PTMS-g-Fe₃O₄ composite

3.4.5. Electrical Investigation

The variation of dielectric constant, dielectric loss, and conductivity of pure samples and composites with frequency are given in Figures 3.74 – 3.88.

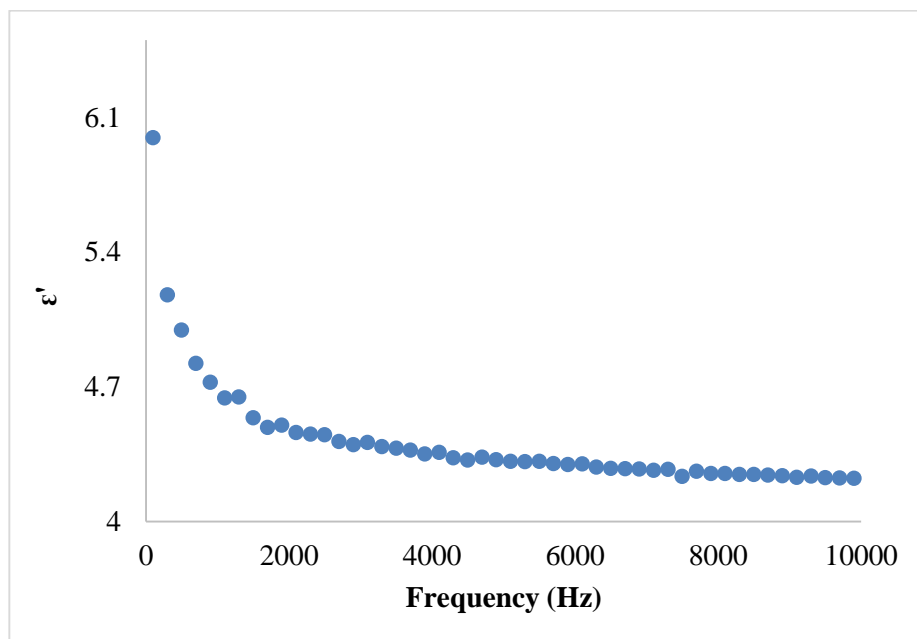


Figure 3.74. Variation of dielectric constant of POH-N₃PTMS-g-Fe₃O₄ with frequency

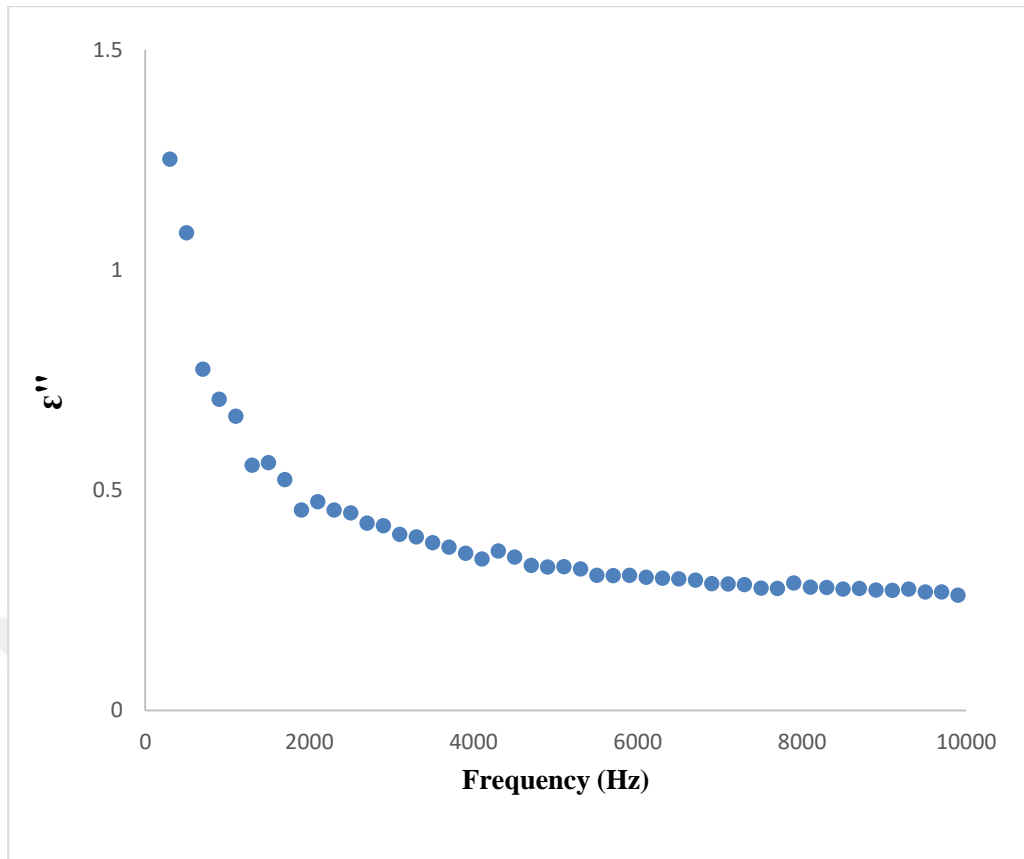


Figure 3.75. Variation of dielectric loss of POH-N₃PTMS-g-Fe₃O₄ with frequency

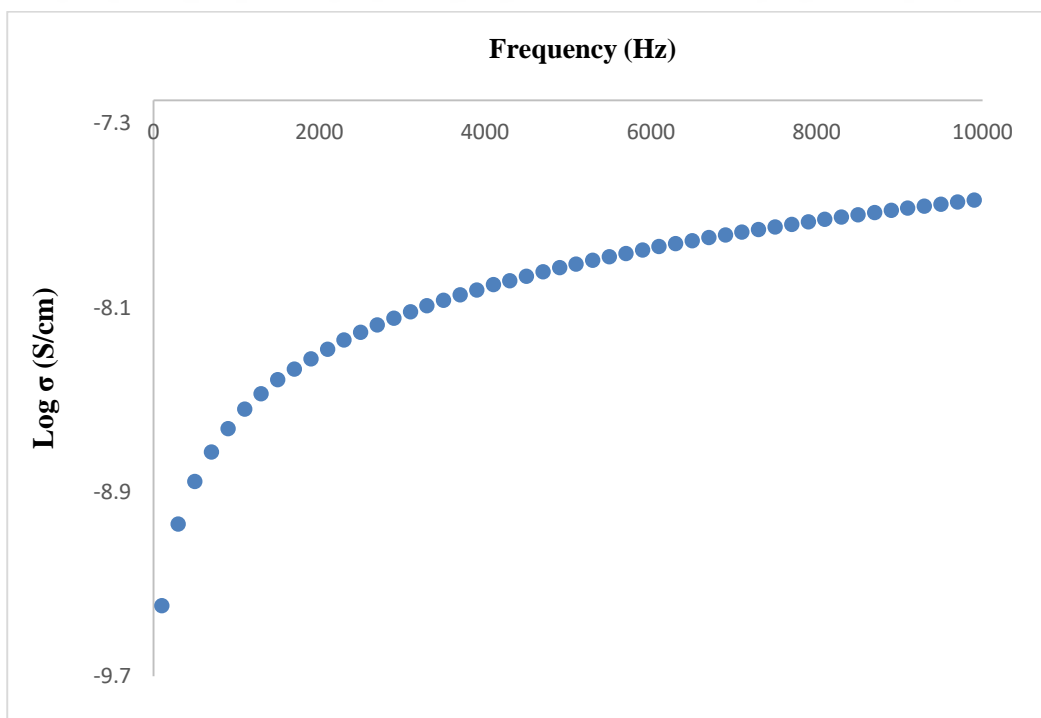


Figure 3.76. Variation of conductivity of POH-N₃PTMS-g-Fe₃O₄ with frequency

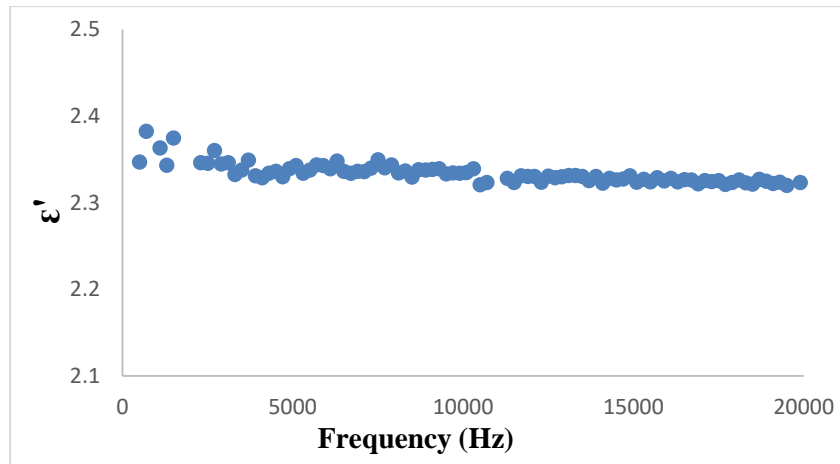


Figure 3.77. Variation of dielectric constant of PVC / 5% (by wt) POH-N₃PTMS-g-Fe₃O₄ composite with frequency

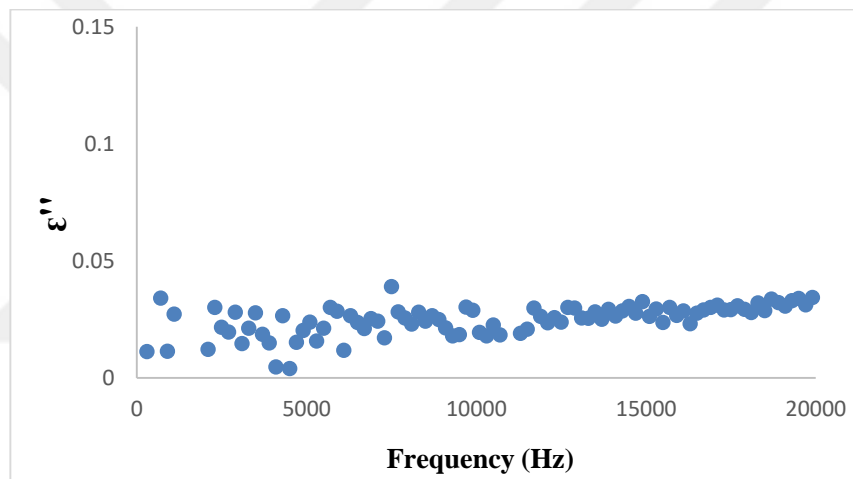


Figure 3.78. Variation of dielectric loss of PVC / 5% (by wt) POH-N₃PTMS-g-Fe₃O₄ composite with frequency

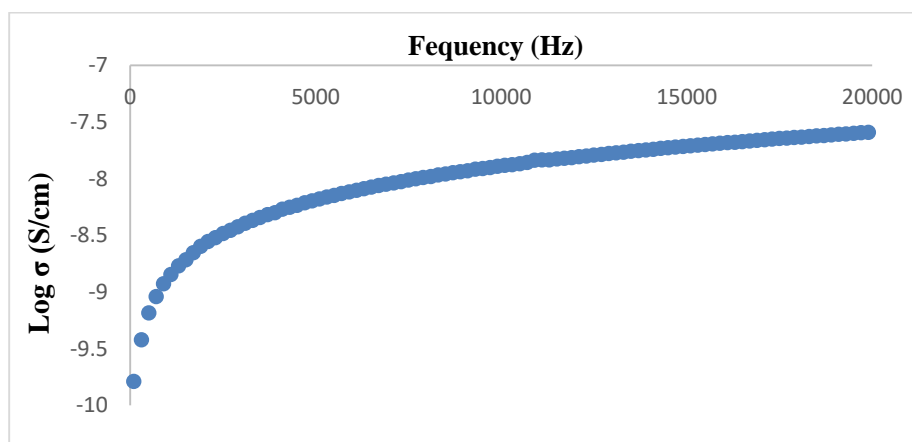


Figure 3.79. Variation of conductivity of PVC / 5% (by wt) POH-N₃PTMS-g-Fe₃O₄ composite with frequency

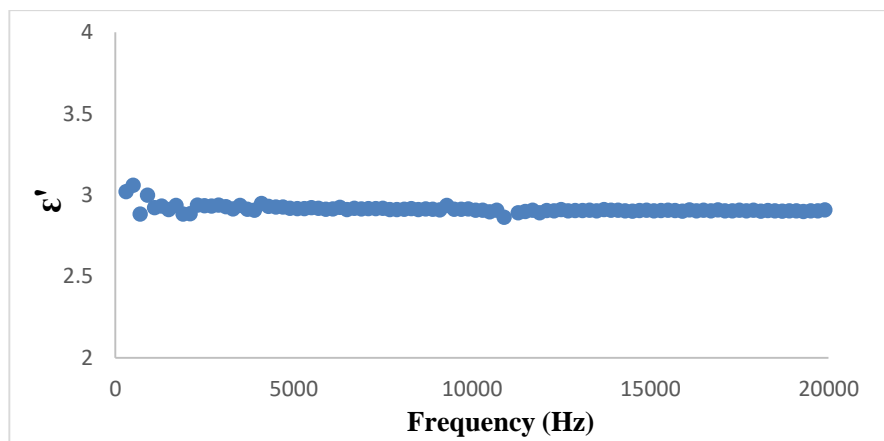


Figure 3.80. Variation of dielectric constant of PVC / 10% (by wt) POH-N₃PTMS-g-Fe₃O₄ composite with frequency

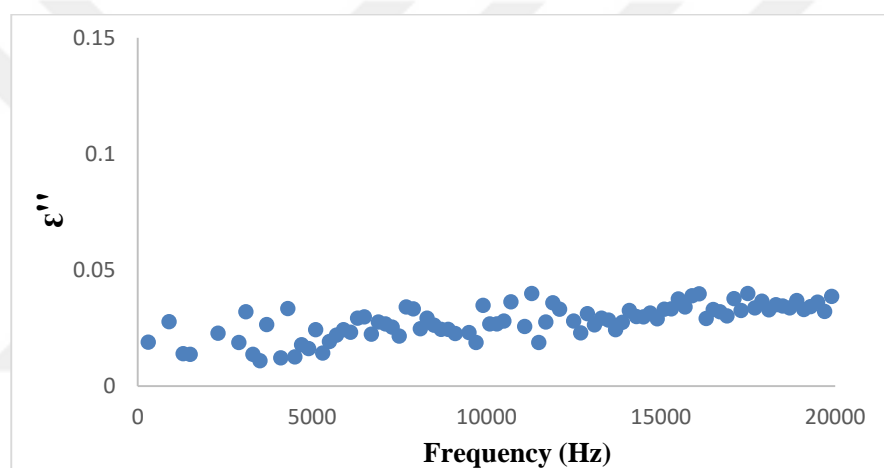


Figure 3.81. Variation of dielectric loss of PVC / 10% (by wt) POH-N₃PTMS-g-Fe₃O₄ composite with frequency

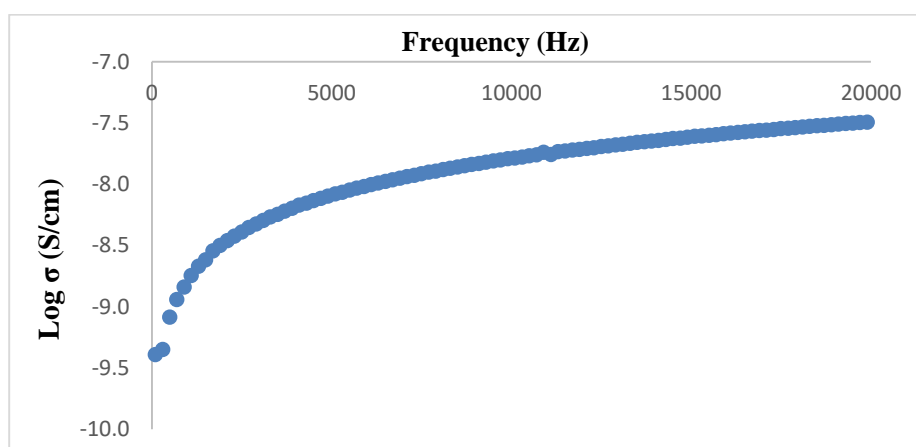


Figure 3.82. Variation of conductivity of PVC / 10% (by wt) POH-N₃PTMS-g-Fe₃O₄ composite with frequency

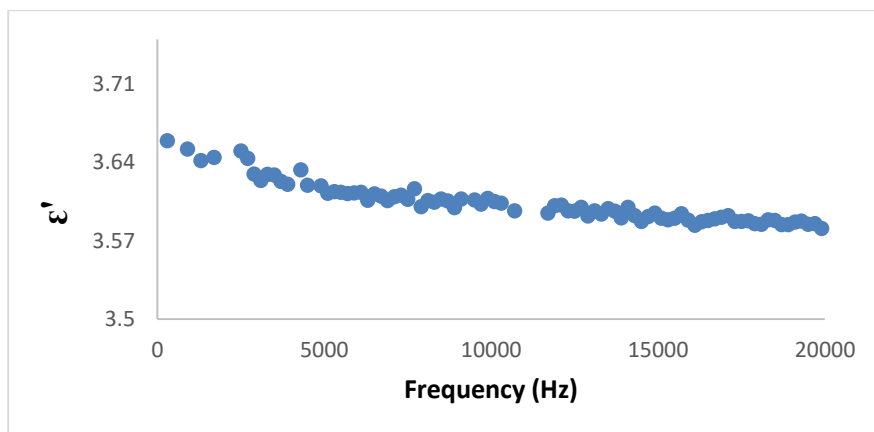


Figure 3.83. Variation of dielectric constant of PVC / 20% (by wt) POH-N₃PTMS-g-Fe₃O₄ composite with frequency

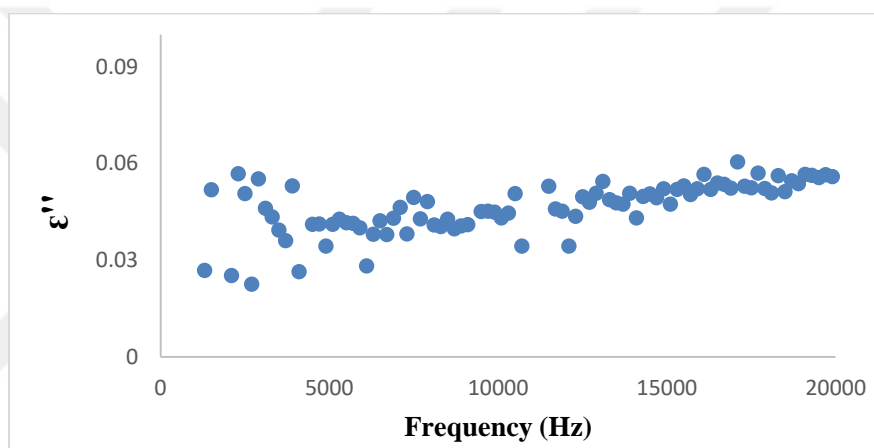


Figure 3.84. Variation of dielectric loss of PVC / 20% (by wt) POH-N₃PTMS-g-Fe₃O₄ composite with frequency

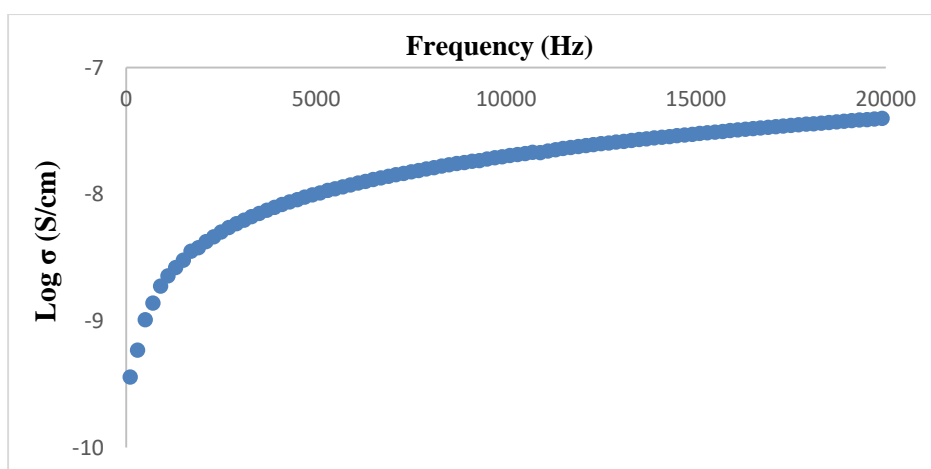


Figure 3.85. Variation of conductivity of PVC / 20% (by wt) POH-N₃PTMS-g-Fe₃O₄ composite with frequency

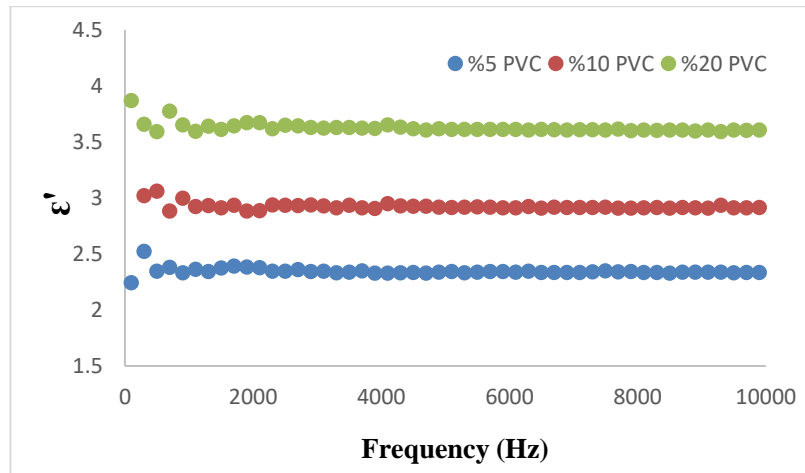


Figure 3.86. Variation of dielectric constant of PVC / POH-N₃PTMS-g-Fe₃O₄ composites with frequency

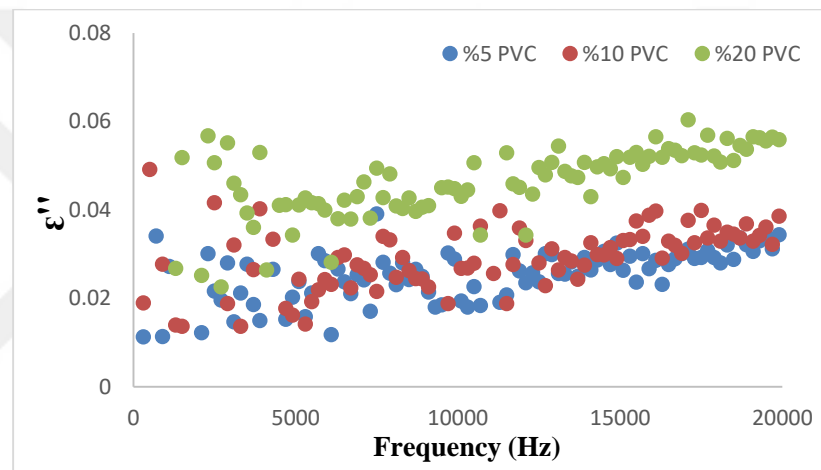


Figure 3.87. Variation of dielectric loss of PVC / POH-N₃PTMS-g-Fe₃O₄ composites with frequency

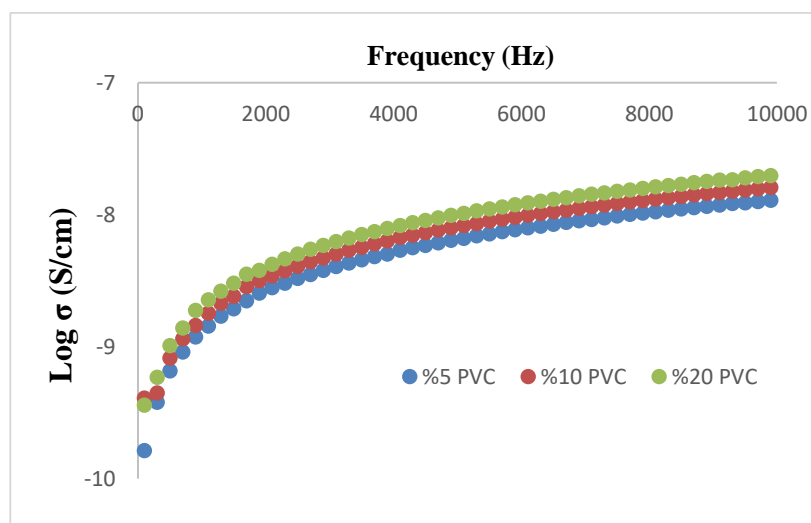


Figure 3.88. Variation of conductivity of PVC / POH-N₃PTMS-g-Fe₃O₄ composites with frequency

4. DISCUSSION

This research is primarily concerned with the modification of magnetic nanoparticle (Fe_3O_4) with polyvinyl chloride (PVC) via click reaction to produce magnetic PVC. Azide PVC was synthesized by a nucleophilic substitution reaction of PVC with sodium azide (Figure 2.1.).

The FT-IR spectrum of PVC (Figure 3.1) showed characteristics absorption peaks that are similar to that of PVC- N_3 (Figure 3.2) except 2115 cm^{-1} peak which is distinctive and unique for $\text{N}^-=\text{N}^+=\text{N}^-$ group. $2969\text{-}2911\text{ cm}^{-1}$ signal belongs to C-H stretching in the aliphatic CH_2 and CH groups and 615 cm^{-1} signals for C-Cl stretching. The $^1\text{H-NMR}$ spectrum OF PVC- N_3 in Figure 3.3 shows $3.85\text{-}4.3\text{ ppm}$ for $-\text{CHN}_3-$ protons, $4.3\text{-}4.8\text{ ppm}$ for $-\text{CHCl}-$ protons, and $2.0\text{-}2.9\text{ ppm}$ for $-\text{CH}_2-$ protons. In the $^1\text{H-NMR}$ spectrum, the displacement percentage calculated was approximately 7% from the comparison of CH- N_3 and CH-Cl protons signal integral height. The $^{13}\text{C-APT}$ spectrum of PVC and PVC- N_3 (Figure 3.4) was anticipated as 55.60 ppm for $-\text{CHN}_3-$ carbons, which is not present in PVC. From the spectrum, $44.03\text{-}42.19\text{ ppm}$ for $-\text{CH}_2-$ carbons on the left and right of the $-\text{CHN}_3-$ group was observed, and 58.10 ppm for CH(Cl) carbons in $-\text{CH}(\text{Cl})\text{-CH}_2\text{-CH}(\text{N}_3)-$ structures.

Figure 3.5-3.8 respectively showed the TGA and DSC curves of PVC and PVC- N_3 . As seen in Table 3.5, the initial decomposition temperature (T_i) was $238\text{ }^\circ\text{C}$ for PVC and $180\text{ }^\circ\text{C}$ for PVC- N_3 . The attachment of the azide group to PVC reduces the thermal stability which leads to the rapid degradation of the polymer. The % weight loss at $350\text{ }^\circ\text{C}$ for PVC was 61.7 and 56.7 for PVC- N_3 while the residue at $500\text{ }^\circ\text{C}$ is 18.3 and 35.0 respectively. DSC result showed that azidation reaction of PVC decreased its glass transition temperature (T_g) from 84.2 to $75.8\text{ }^\circ\text{C}$. This implies that the azide group to some extent increases the PVC interchain space leading to an increase in the free volume which subsequently leads to decrease T_g of the polymer.

The FT-IR spectrum characteristics vibration peaks of propargyl α -bromoisobutyrate (Figure 3.9) are; $\equiv\text{C-H}$ stretching (3294 cm^{-1}), C-H stretching in aliphatic $-\text{CH}_2-$ and $-\text{CH}_3$ groups ($2928\text{-}3006\text{ cm}^{-1}$), $\text{C}\equiv\text{C}$ stretching (2129 cm^{-1}), $-\text{C}=\text{O}$ (1730 cm^{-1}), geminal methyl (1372 and 1388 cm^{-1}), $\text{C}(=\text{O})\text{-O-}$ symmetric and asymmetric stretching (1107 and 1155 cm^{-1}) and C-Br stretching (641 cm^{-1}). For the $^1\text{H-NMR}$ spectrum (Figure 3.10), the integral height of the peaks is proportional to the numbers of H. the signals are 4.6 , 2.5 , 1.8 , and 5.3 ppm for $-\text{CH}_2\text{-O-}$, $\equiv\text{C-H}$, geminal methyl and CH_2Cl_2 protons respectively.

Poly(MMA-*co*-VTM) with propargyl terminal end was synthesized by ATRP using propargyl α -bromoisobutyrate as initiator and Cu(I)Br , and bipyridine as catalyst complex (Figure 2.3.). The Fe_3O_4 nanoparticles were bonded to the trimethoxysilane group of the

copolymer by the “grafting to” approach (Figure 2.4). The copolymer bearing Fe₃O₄ was bonded to PVC-N₃ via Click reaction (Figure 2.5).

TGA and DSC curves of poly(MMA-*co*-VTM), poly(MMA-*co*-VTM)-*g*-Fe₃O₄ and PVC-*g*-poly(MMA-*co*-VTM)-*g*-Fe₃O₄ (Table 3.10) showed the initial decomposition temperature of the copolymers respectively as 192, 265 and 265 °C which implies that addition of Fe₃O₄ and click reaction of PVC to the copolymer increases the thermal stability significantly. Both Poly(MMA-*co*-VTM)-*g*-Fe₃O₄ and PVC-*g*-poly(MMA-*co*-VTM)-*g*-Fe₃O₄ shows 15% weight loss at 350 °C but at 400 °C, the % weight loss varies and 50.8% was observed for poly(MMA-*co*-VTM) at 350 °C which also depicted multiple stages of decomposition (Figure 3.13). The % residue at 500 °C for PVC-*g*-poly(MMA-*co*-VTM)-*g*-Fe₃O₄ is 58.3 which is lower than 65.8 of poly(MMA-*co*-VTM)-*g*-Fe₃O₄, which was probably as a result of the click reaction. Poly(MMA-*co*-VTM) showed a T_g value of 48.0 which was much lower than that of poly(MMA-*co*-VTM)-*g*-Fe₃O₄ which is 94.0. This implies the bonding of the Fe₃O₄ nanoparticles to the copolymer increases the thermal stability of the copolymer. PVC-*g*-poly(MMA-*co*-VTM)-*g*-Fe₃O₄ shows no T_g value.

SEM and SEM-EDX images of PVC-*g*-poly(MMA-*co*-VTM)-*g*-Fe₃O₄ are given respectively in Figure 3.21 and 3.22. The magnetic nanoparticles are undoubtedly observable on the SEM image and the SEM-EDX result shows clearly in the structure the presence of Fe, C, Cl, Si, N, and O which were the atomic constituents of the PVC-*g*-poly(MMA-*co*-VTM)-*g*-Fe₃O₄. A vibrating sample magnetometer (VSM) (Figure 3.23) was used to investigate the magnetic property of PVC-*g*-poly(MMA-*co*-VTM)-*g*-Fe₃O₄ at 300K. The VSM plot is the essential proof of the bonding of copolymer carrying magnetic nanoparticles to the PVC. In the plot, the PVC-*g*-poly(MMA-*co*-VTM)-*g*-Fe₃O₄ shows a saturation magnetization of 41.5 emu/g. This value was lower than the saturation magnetization (M_s) values reported by different literature of pure Fe₃O₄ nanoparticles. Some of the works of literature are 70 emu/g [30] and 67.7 emu/g [65]. The lower value obtained compared to the given literature was purely due to the bonding of the polymer to the Fe₃O₄. The initial magnetic susceptibility (χ_i) value of 0.034 emu/g.Oe was calculated for the PVC-*g*-poly(MMA-*co*-VTM)-*g*-Fe₃O₄. The VSM plot also shows no hysteresis loop.

Figure 3.24 and 3.28 depict respectively the dielectric constant (ϵ') variation as a function of the applied frequency at room temperature of Poly(MMA-*co*-VTM)-*g*-Fe₃O₄ and PVC-*g*-poly(MMA-*co*-VTM)-*g*-Fe₃O₄. As can be observed in figures, the dielectric constant decreased sharply to a frequency of approximately 500 Hz, decreased very slowly from 500 Hz to 2000 Hz after which they continue more or less constant. For pure PVC, the ϵ' was around 3-4 [66]. The copolymer bonded with Fe₃O₄ nanoparticles was 13-14. The grafting of the copolymer carrying Fe₃O₄ nanoparticles to azide PVC by click reaction increased the ϵ' to 18-20. The increase was the result of the high polar nature of PVC. As depicted in Figure 3.25 and 3.29, the dielectric loss

factor (ϵ'') decreases sharply to approximately 2000 Hz, slowly in the region of 2000-4000 Hz, and then continues almost constant for both poly(MMA-*co*-VTM)-*g*-Fe₃O₄ and PVC-*g*-poly(MMA-*co*-VTM)-*g*-Fe₃O₄.

The following equation is used to measure Ac conductivity $\sigma_{ac}(\omega)$ [67].

$$\sigma_{total} = \sigma_{dc(\omega)}(\omega \rightarrow 0) + \sigma_{ac(\omega)}$$

where

ω = angular frequency

σ_{total} = measured total electrical conductivity, $\sigma_{ac(\omega)}$ is alternating electrical conductivity

$\sigma_{dc(\omega)}$ = contribution of direct electrical conductivity.

Figure 3.26 and 3.27 depict the variation of AC conductivity of poly(MMA-*co*-VTM)-*g*-Fe₃O₄ with frequency and the angular frequency at room temperature whilst Figure 3.30 and 3.31 depict those of PVC-*g*-poly(MMA-*co*-VTM)-*g*-Fe₃O₄ respectively. It was observed that AC conductivity increased from 100 Hz which was equivalent to ω value of 628 Hz to 10000 Hz which was equivalent to the ω value of 62800 Hz. The $\sigma_{dc(\omega)}(\omega \rightarrow 0)$ values for poly(MMA-*co*-VTM)-*g*-Fe₃O₄ and PVC-*g*-poly(MMA-*co*-VTM)-*g*-Fe₃O₄ at room temperature are found to be 2.66×10^{-9} S/cm and 2.20×10^{-9} S/cm respectively.

Propargyl methacrylate was synthesized from propargyl alcohol and methacryloyl chloride (Figure 2.6). The FT-IR spectrum (Figure 3.32) of propargyl methacrylate depicts an absorption peak at 2130 cm⁻¹ which is characteristic of C≡C stretching, 3293 cm⁻¹ for ≡C-H stretching, 1740 cm⁻¹ for C=O stretching and 1107; 1155 cm⁻¹ for C(=O)-O- symmetric and asymmetric stretching. Next, free radical copolymerization of propargyl methacrylate and vinyltrimethoxysilane in the presence of AIBN (Figure 2.7). FT-IR spectrum in Figure 3.33 shows an absorption band of Si-O at 1138 cm⁻¹ which indicates that the copolymer formed has a vinyltrimethoxysilane unit. The Fe₃O₄ was bonded to the vinyltrimethoxysilane unit of the copolymer (figure 2.8). Figure 3.34 shows the most important signal, Fe-O stretch at 583 cm⁻¹ indicating the presence of Fe₃O₄ nanoparticle in the sample. Finally, click reaction with azide PVC in which the C≡C stretch disappeared from the spectrum due to formation of 1,2,3-triazole ring (Figure 3.35).

From Table 3.15, the initial decomposition temperatures (T_i) of poly(POHMAC-*co*-VTM), poly(POHMAC-*co*-VTM)-*g*-Fe₃O₄ and PVC-*g*-poly(POHMAC-*co*-VTM)-*g*-Fe₃O₄ are 265, 282 and 277 °C respectively which implies that addition of Fe₃O₄ to the copolymer increases the thermal stability of the copolymer significantly. After the click reaction of PVC with the copolymer carrying Fe₃O₄, there was a minute decrease in thermal stability which was anticipated to be a result of the formation of 1,2,3-triazole ring. At 400 °C, the poly(POHMAC-*co*-VTM) showed a high % mass loss compared to poly(POHMAC-*co*-VTM)-*g*-Fe₃O₄ and PVC-*g*-

Poly(POHMAC-*co*-VTM)-*g*-Fe₃O₄. The % mass losses observed were 41.3, 11.3, and 9.3 respectively. The low % mass loss was the result of the presence of Fe₃O₄ grafted to the copolymer. The % residue at 800 °C for poly(POHMAC-*co*-VTM) was 20.8 which was lower than 22.7 for poly(POHMAC-*co*-VTM)-*g*-Fe₃O₄. The 19.4 for PVC-*g*-poly(POHMAC-*co*-VTM)-*g*-Fe₃O₄ was probably as a result of click reaction with PVC. Poly(POHMAC-*co*-VTM) showed a T_g value of 57 which was much lower than 85 for poly(POHMAC-*co*-VTM)-*g*-Fe₃O₄. This implied that the bonding of Fe₃O₄ to poly(POHMAC-*co*-VTM) increased thermal stability. For PVC-*g*-poly(POHMAC-*co*-VTM)-*g*-Fe₃O₄, the T_g value of 63 is recorded which was lower compared to poly(POHMAC-*co*-VTM)-*g*-Fe₃O₄. This simply implied that the formation of the 1,2,3-triazole ring decreased the interchain attractive forces leading to an increase in chain flexibility which increases the free volume of the copolymer and subsequently, decreases the T_g value. The poly(POHMAC-*co*-VTM) and PVC-*g*-poly(POHMAC-*co*-VTM)-*g*-Fe₃O₄ shows two stage decomposition as compared to poly(POHMAC-*co*-VTM)-*g*-Fe₃O₄ which shows three stage decomposition. The samples T_{max} values are seen Table 3.15.

A vibrating sample magnetometer (VSM) was used to investigate the magnetic property of PVC-*g*-poly(POHMAC-*co*-VTM)-*g*-Fe₃O₄ at 300K (Figure 3.42). The VSM plot is the essential proof of the bonding of poly(POHMAC-*co*-VTM)-*g*-Fe₃O₄ with the PVC-N₃. From the plot, the PVC-*g*-poly(POHMAC-*co*-VTM)-*g*-Fe₃O₄ showed a saturation magnetization (M_s) of 33.7 emu/g which was lower than saturation magnetization (M_s) values reported by different literature of pure Fe₃O₄ nanoparticle. Some of the works of literature were 53.81 emu/g [32] and 65 emu/g [68]. The lower value obtained for PVC-*g*-poly(POHMAC-*co*-VTM)-*g*-Fe₃O₄ than the given literature was purely due to the bonding of the PVC to the copolymer bearing Fe₃O₄.

The inset graphs in Figure 3.43 and 3.44 showed an abnormal behavior of dielectric constant and dielectric loss of Poly(POHMAC-*co*-VTM) with a change in frequency at room temperature. The ϵ' value was 3.0 from the graph. For AC conductivity (Figure 3.43), it was observed that it increased rapidly to a certain frequency of 1000 Hz and then slowly increased continuously. The ϵ' , ϵ'' and σ_{ac} depicted in Figure 3.46-3.48 respectively of poly(POHMAC-*co*-VTM)-*g*-Fe₃O₄ showed that, both the ϵ' and ϵ'' decreased rapidly to a frequency of 1000 Hz, very slowly to a frequency of 6000 Hz and then becomes more or less constant. The ϵ' and ϵ'' values respectively observed were 9.1 and 0.9. The σ_{ac} increased rapidly to a frequency of 1000 Hz, then it decreased slowly to 6000 Hz and then remained more or less constant continuously. The ϵ' , ϵ'' and σ_{ac} of PVC-*g*-poly(POHMAC-*co*-VTM)-*g*-Fe₃O₄ were shown in Figure 3.49-3.51 respectively. The ϵ' and ϵ'' followed the same pattern in which a rapid increase was observed up to a frequency of 800 Hz, then slowly decrease to 5000 Hz and then become more or less constant. The respective values of ϵ' and ϵ'' were 9.6 and 2.5. And for σ_{ac} , it increases rapidly to a certain

frequency of 800 Hz, then increases continuously slowly up to 5000 Hz and remain more or less constant. The ϵ' of poly(POHMAC-*co*-VTM) increases from 3.0 to 9.1 following grafting with Fe₃O₄ nanoparticles. After click reaction with azide PVC, the ϵ' also increases to 9.6 which is as a result of the polar nature of PVC.

3-azidopropyltrimethoxysilane was synthesized through a nucleophilic substitution reaction of 3-chloropropyltrimethoxysilane with sodium azide (Figure 2.10). The FT-IR spectrum of 3-azidopropyltrimethoxysilane (Figure 3.52) showed an absorption peak at 2101 cm⁻¹ which was distinctive and characteristic stretching vibration for N⁻=N⁺=N⁻ group. The signal confirms the occurrence of the reaction. Others of importance were 2843-2944 cm⁻¹ (C-H stretching from aliphatic -CH₂) and 1087 cm⁻¹ (Si-O). The FT-IR spectrum of N₃PTMS-*g*-Fe₃O₄ (Figure 3.53) formed by grafting of Fe₃O₄ to 3-azidopropyltrimethoxysilane shows the characteristic signal at 586 cm⁻¹ (Fe-O which indicates the presence of Fe₃O₄) and 3435 cm⁻¹ (O-H stretch from Fe₃O₄ particle surface). 2923 and 2099 cm⁻¹ for aliphatic C-H and N⁻=N⁺=N⁻ stretching vibrations respectively. The N₃PTMS-*g*-Fe₃O₄ undergoes click reaction with propargyl alcohol (Figure 2.12). The FT-IR spectrum (Figure 3.54) shows the signals formed as a result of the click reaction i.e 1598 and 1467 cm⁻¹ for C=C and C-N stretching vibrations respectively. 5, 10, and 20 % by weight composites of PVC were prepared using the modified Fe₃O₄.

The initial decomposition temperatures (T_i) of N₃PTMS-*g*-Fe₃O₄ and POH-N₃PTMS-*g*-Fe₃O₄ (Table 3.19) are 226 and 217 °C respectively. The decrease in thermal stability of POH-N₃PTMS-*g*-Fe₃O₄ compared to N₃PTMS-*g*-Fe₃O₄ was the result of the formation of the 1,2,3-triazole ring. At 400 °C, N₃PTMS-*g*-Fe₃O₄ % mass loss is 4.6 which was lower than 7.0 for POH-N₃PTMS-*g*-Fe₃O₄. The % residues at 800 °C were 92.4 and 88.5 respectively. The reason for the higher % mass loss at 400 °C and a lower % residue for POH-N₃PTMS-*g*-Fe₃O₄ at 800 °C was probably the click reaction. The glass transition temperature (T_g) of N₃PTMS-*g*-Fe₃O₄ is 61 which was slightly higher than that of POH-N₃PTMS-*g*-Fe₃O₄ which is 57. The decreased in the T_g is due to the increase in chain flexibility of the compound as a result of click reaction with propargyl alcohol. As seen in Table 3.19, Both N₃PTMS-*g*-Fe₃O₄ and POH-N₃PTMS-*g*-Fe₃O₄ shows three stage decomposition though of different T_{max} . From Table 3.20, the T_i for the 5, 10, and 20 % PVC composites of POH-N₃PTMS-*g*-Fe₃O₄ were 212, 220, and 228 °C respectively. An increase in thermal stability was observed due to an increase in % POH-N₃PTMS-*g*-Fe₃O₄ in the composites. At 300 °C, % mass loss were 57, 79, and 44. For the % residue, 5 and 10 % composites undergo complete decomposition at 500 °C while for the 20 % composite, the residue was 11.4. This was the result of the higher % POH-N₃PTMS-*g*-Fe₃O₄ in the composite. The T_g value is 60 for 5% which was lower than 72 for 10%. This implied that 10% is more stable than 5% composite. The T_g value for 20% is 73 which was very close to 10% even though the 20% has

twice the % POH-N₃PTMS-g-Fe₃O₄ than that of 10% composite. As seen in Table 3.20, the 5 and 20% composite shows three stage decomposition whereas the 10% composite shows two stages.

SEM images of N₃PTMS-g-Fe₃O₄ (Figure 3.65) and POH-N₃PTMS-g-Fe₃O₄ (3.67) were both taken at 10,000 magnification. It can be seen that qualitatively the Fe₃O₄ domination reduced after click reaction with propargyl alcohol. EDX results allowed the determination of the elemental composition of the samples. Fe, C, O, N, Si, and Cl were present in both samples. Figure 3.69 and 3.71 respectively displayed the SEM images of 5 and 20% PVC/POH-N₃PTMS-g-Fe₃O₄ composite. Both composites show that most of the POH-N₃PTMS-g-Fe₃O₄ were dispersed well within the PVC matrix with minor irregularities which were more visible on 20% SEM image. This was probably because of the higher % POH-N₃PTMS-g-Fe₃O₄ in the composite. EDX analysis result from Figure 3.70 and 3.72 showed the presence of Fe, C, Cl, O, N, and Si in both the composites.

In Figure 3.73, VSM was used to investigate the magnetic property of PVC / 10% (by wt) POH-N₃TMS-g-Fe₃O₄ composite at 300K. From the plot, the PVC / 10% (by wt) POH-N₃TMS-g-Fe₃O₄ composite showed saturation magnetization (M_s) of 5.12 emu/g which was much lower compared to the saturation magnetization (M_s) values reported by different literature of pure Fe₃O₄ nanoparticle. The M_s value from the VSM plot was the essential proof of the presence of Fe₃O₄ within the composite.

A well-known method used to characterize the dielectric properties of the pure sample and its composite was the use of an impedance analyzer. The inset graphs in Figure 3.74 and 3.75, showed the ϵ' and ϵ'' of POH-N₃PTMS-g-Fe₃O₄ respectively. Both the properties follow the same pattern in which they rapidly decreased to a frequency of 900 Hz, very slowly to a frequency of 5000 Hz, and then became more or less constant. The ϵ' and ϵ'' values respectively were 6.0 and 1.3. For the σ_{ac} (Figure 3.76), it increased rapidly to a frequency of 900 Hz and then continuous very slowly linearly with an increase in applied frequency. The variation of ϵ' of 5,10 and 20% (by wt) composites (Figure 3.86) with frequency shows some irregularities at first but the pattern becomes almost similar in which they sharply decrease to a frequency of 900 Hz, very slowly to a frequency of 3500 Hz and then remain more or less constant continuously. The 5, 10, and 20% composites ϵ' values were 2.2, 3.0, and 3.9 respectively. The sequential increase in ϵ' was the result of % (by wt) POH-N₃PTMS-g-Fe₃O₄ within the composites. For the ϵ'' (Figure 3.87), the composites showed an irregular pattern with the change in applied frequency, and the values recorded are 0.01, 3.02, and 3.66 which were observed to also increase with the % POH-N₃PTMS-g-Fe₃O₄. And for the σ_{ac} (Figure 3.88), it increased rapidly to a frequency of 700 Hz, very slowly to a certain frequency of 400 Hz, and then continuous more or less constant.

REFERENCES

- [1] Fried, J.R. (2014). Introduction to polymer science, *Polymer Science and Technology, 3rd ed., Prentice Hall, Upper Saddle River, NJ, C*, 1-24.
- [2] Blasco, E., Sims, M.B., Goldmann, A.S., Sumerlin, B.S., and Barner-Kowollik, C. (2017). 50th anniversary perspective: Polymer functionalization, *Macromolecules*, C 50, 5215-5252.
- [3] Carey, F.A. and Sundberg, R.J., (2007). *Advanced Organic Chemistry: Part B: Reaction and Synthesis*, Springer Science & Business Media,
- [4] Hiemenz, P.C. and Lodge, T.P., (2007). *Polymer chemistry*, CRC press,
- [5] Ravve, A., *Physical properties and physical chemistry of polymers*, in *Principles of Polymer Chemistry* 2012, Springer. p. 17-67.
- [6] Moad, G., Chiefari, J., Mayadunne, R.T., Moad, C.L., Postma, A., Rizzardo, E., and Thang, S.H. *Initiating free radical polymerization*. in *Macromolecular Symposia*. 2002. Wiley Online Library.
- [7] Darling, T.R., Davis, T.P., Fryd, M., Gridnev, A.A., Haddleton, D.M., Ittel, S.D., Matheson Jr, R.R., Moad, G., and Rizzardo, E. (2000). Living polymerization: Rationale for uniform terminology, *Journal of Polymer Science Part A: Polymer Chemistry*, C 38, 1706-1708.
- [8] Mishra, V. and Kumar, R. (2012). Living radical polymerization: A review, *J. Sci. Res*, C 56, 141-176.
- [9] Matyjaszewski, K. and Xia, J. (2001). Atom transfer radical polymerization, *Chemical reviews*, C 101, 2921-2990.
- [10] Tsarevsky, N.V., Braunecker, W.A., Tang, W., Brooks, S.J., Matyjaszewski, K., Weisman, G.R., and Wong, E.H. (2006). Copper-based ATRP catalysts of very high activity derived from dimethyl cross-bridged cyclam, *Journal of Molecular Catalysis A: Chemical*, C 257, 132-140.
- [11] Herrero, M., Tiemblo, P., Reyes-Labarta, J., Mijangos, C., and Reinecke, H. (2002). PVC modification with new functional groups. Influence of hydrogen bonds on reactivity, stiffness and specific volume, *Polymer*, C 43, 2631-2636.
- [12] Kiskan, B., Demiray, G., and Yagci, Y. (2008). Thermally curable polyvinylchloride via click chemistry, *Journal of Polymer Science Part A: Polymer Chemistry*, C 46, 3512-3518.
- [13] Smith, J.G., *Organic chemistry/Janice Gorzynski Smith*, 2011.
- [14] Bicak, N., Sherrington, D., and Bulbul, H. (2001). Vinylamine polymer via chemical modification of PVC, *European Polymer Journal*, C 37, 801-805.
- [15] Pi, Z. and Kennedy, J. (2001). Cationic grafting of olefins from PVC: The effect of reaction conditions, *Journal of Polymer Science Part A: Polymer Chemistry*, C 39, 1675-1680.
- [16] Martínez, G. (2006). Synthesis of PVC-g-PS through stereoselective nucleophilic substitution on PVC, *Journal of Polymer Science Part A: Polymer Chemistry*, C 44, 2476-2486.
- [17] Millán, J., Martínez, G., and Jimeno, M. (1991). Nucleophilic Substitution in PVC. Additional NMR Proof of the conformational mechanism, *European polymer journal*, C 27, 483-486.
- [18] Navarro, R., Perrino, M., García, C., Elvira, C., Gallardo, A., and Reinecke, H. (2016). Opening new gates for the modification of PVC or other PVC derivatives: Synthetic strategies for the covalent binding of molecules to PVC, *Polymers*, C 8, 152.
- [19] Marqués, T., Navarro, R., Gallardo, A., Garcia, C., Elvira, C., and Reinecke, H. (2016). PVC bearing primary aliphatic or aromatic amine groups, *Journal of Polymer Research*, C 23, 246.
- [20] Ammari, F. and Meganem, F. (2014). Poly (vinyl chloride) functionalization by aliphatic and aromatic amines: application to the extraction of some metal cations, *Turkish Journal of Chemistry*, C 38, 638-649.
- [21] Asan, N. and Öztürk, T. (2017). Synthesis and Characterization of Poly (Vinyl Chloride-Graft-Ethylene Glycol) Graft Copolymers by " Click" Chemistry, *Hacettepe Journal of Biology and Chemistry*, C 45, 35-42.
- [22] Kolb, H.C., Finn, M., and Sharpless, K.B. (2001). Click chemistry: diverse chemical function from a few good reactions, *Angewandte Chemie International Edition*, C 40, 2004-2021.
- [23] Worrell, B., Malik, J., and Fokin, V.V. (2013). Direct evidence of a dinuclear copper intermediate in Cu (I)-catalyzed azide-alkyne cycloadditions, *science*, C 340, 457-460.
- [24] Lopes, M.M., Domingues, M., Mendes, O., and Schneider, K. (2018). An Adaptive Multiresolution Scheme with Second Order Local Time-stepping for Reaction-Diffusion Equations, *Journal of Applied Nonlinear Dynamics*, C 7, 287-295.
- [25] Lutz, J.F., Börner, H.G., and Weichenhan, K. (2005). Combining atom transfer radical polymerization and click chemistry: a versatile method for the preparation of end-functional polymers, *Macromolecular Rapid Communications*, C 26, 514-518.

- [26] Thakur, V.K. and Thakur, M.K., (2015). *Chemical functionalization of carbon nanomaterials: Chemistry and applications*, CRC Press,
- [27] Mantovani, G., Ladmiral, V., Tao, L., and Haddleton, D.M. (2005). One-pot tandem living radical polymerisation–Huisgens cycloaddition process (“click”) catalysed by N-alkyl-2-pyridylmethanimine/Cu (I) Br complexes, *Chemical Communications*, C, 2089-2091.
- [28] Fleischmann, S., Hinrichs, K., Oertel, U., Reichelt, S., Eichhorn, K.J., and Voit, B. (2008). Modification of polymer surfaces by click chemistry, *Macromolecular Rapid Communications*, C 29, 1177-1185.
- [29] Li, Y., Yang, J., and Benicewicz, B.C. (2007). Well-controlled polymerization of 2-azidoethyl methacrylate at near room temperature and click functionalization, *Journal of Polymer Science Part A: Polymer Chemistry*, C 45, 4300-4308.
- [30] Lafarge, J., Kebir, N., Schapman, D., and Burel, F. (2013). Design of self-disinfecting PVC surfaces using the click chemistry, *Reactive and Functional Polymers*, C 73, 1464-1472.
- [31] Öztürk, T., Ayyıldız, H., Meyvacı, E., and Gökteş, M. (2017). Synthesis and characterization of poly (epichlorohydrin-graft-ethylene glycol) graft copolymers by "click" chemistry, *Karaelmas Fen ve Mühendislik Dergisi*, C 7, 47-54.
- [32] Jia, P., Wang, R., Hu, L., Zhang, M., and Zhou, Y. (2017). Self-Plasticization of PVC via click reaction of a monoocetyl phthalate derivative, *Polish Journal of Chemical Technology*, C 19, 16-19.
- [33] Wiedmann, T.O., Schandl, H., Lenzen, M., Moran, D., Suh, S., West, J., and Kanemoto, K. (2015). The material footprint of nations, *Proceedings of the National Academy of Sciences*, C 112, 6271-6276.
- [34] Masala, O. and Seshadri, R. (2004). Synthesis routes for large volumes of nanoparticles, *Annu. Rev. Mater. Res.*, C 34, 41-81.
- [35] Chen, H.M. and Liu, R.-S. (2011). Architecture of metallic nanostructures: synthesis strategy and specific applications, *The Journal of Physical Chemistry C*, C 115, 3513-3527.
- [36] Hanemann, T. and Szabó, D.V. (2010). Polymer-nanoparticle composites: from synthesis to modern applications, *Materials*, C 3, 3468-3517.
- [37] Baker, C., Doyle, D., Geltenbort, P., Green, K., Van der Grinten, M., Harris, P., Iaydjiev, P., Ivanov, S., May, D., and Pendlebury, J. (2006). Improved experimental limit on the electric dipole moment of the neutron, *Physical Review Letters*, C 97, 131801.
- [38] Wu, W., He, Q., and Jiang, C. (2008). Magnetic iron oxide nanoparticles: synthesis and surface functionalization strategies, *Nanoscale research letters*, C 3, 397.
- [39] Solans, C., Izquierdo, P., Nolla, J., Azemar, N., and Garcia-Celma, M. (2005). Nano-emulsions, *Current opinion in colloid & interface science*, C 10, 102-110.
- [40] Sahoo, S., Agarwal, K., Singh, A., Polke, B., and Raha, K. (2010). Characterization of γ - and α -Fe₂O₃ nano powders synthesized by emulsion precipitation-calcination route and rheological behaviour of α -Fe₂O₃, *International Journal of Engineering, Science and Technology*, C 2.
- [41] Suslick, K.S. (1990). Sonochemistry, *science*, C 247, 1439-1445.
- [42] Bang, J.H. and Suslick, K.S. (2007). Sonochemical synthesis of nanosized hollow hematite, *Journal of the American Chemical Society*, C 129, 2242-2243.
- [43] Li, L., Jiang, W., Luo, K., Song, H., Lan, F., Wu, Y., and Gu, Z. (2013). Superparamagnetic iron oxide nanoparticles as MRI contrast agents for non-invasive stem cell labeling and tracking, *Theranostics*, C 3, 595.
- [44] Akbarzadeh, A., Samiei, M., and Davaran, S. (2012). Magnetic nanoparticles: preparation, physical properties, and applications in biomedicine, *Nanoscale research letters*, C 7, 144.
- [45] Ninjbadgar, T., Yamamoto, S., and Fukuda, T. (2004). Synthesis and magnetic properties of the γ -Fe₂O₃/poly-(methyl methacrylate)-core/shell nanoparticles, *Solid State Sciences*, C 6, 879-885.
- [46] Marutani, E., Yamamoto, S., Ninjbadgar, T., Tsujii, Y., Fukuda, T., and Takano, M. (2004). Surface-initiated atom transfer radical polymerization of methyl methacrylate on magnetite nanoparticles, *Polymer*, C 45, 2231-2235.
- [47] Zhou, Y., Wang, S., Ding, B., and Yang, Z. (2008). Modification of magnetite nanoparticles via surface-initiated atom transfer radical polymerization (ATRP), *Chemical Engineering Journal*, C 138, 578-585.
- [48] Schick, C., Lexa, D., and Leibowitz, L. (2002). Differential scanning calorimetry and differential thermal analysis, *Characterization of materials*, C, 1-13.
- [49] Nair, M.R., Thomas, G.V., and Nair, M.G. (2007). Thermogravimetric analysis of PVC/ELNR blends, *Polymer Degradation and Stability*, C 92, 189-196.
- [50] Swapp, S., *Scanning Electron Microscopy (SEM): University of Wyoming*, 2017.

- [51] Sarecka-Hujar, B., Balwierz, R., Ostrozka-Cieslik, A., Dyja, R., Lukowiec, D., and Jankowski, A. *Scanning electron microscopy and X-ray energy dispersive spectroscopy-useful tools in the analysis of pharmaceutical products*. in *Journal of Physics Conference Series*. 2017.
- [52] Williams, D.B. and Carter, C.B., (1996). *Transmission Electron Microscopy: Spectrometry*. IV, Plenum Press New York,
- [53] Kameda, T., Ono, M., Grause, G., Mizoguchi, T., and Yoshioka, T. (2009). Chemical modification of poly (vinyl chloride) by nucleophilic substitution, *Polymer Degradation and Stability*, C 94, 107-112.
- [54] Reinecke, H. and Mijangos, C. (1996). PVC modification with bifunctional thiol compounds, *Polymer Bulletin*, C 36, 13-18.
- [55] Nagasaki, Y., Hashimoto, G., Grase, G., Kameda, T., and Yoshioka, T. *Modification of PVC with long alkyl chains by nucleophilic substitution*. in *7th international Symposium on Feedstock Recycling of Polymeric Materials, New Delhi, India*. 2013.
- [56] Salavagione, H.J., Martínez, G., and Ballesteros, C. (2010). Functionalization of multi-walled carbon nanotubes by stereoselective nucleophilic substitution on PVC, *Macromolecules*, C 43, 9754-9760.
- [57] Harth, E., Horn, B.V., Lee, V.Y., Germack, D.S., Gonzales, C.P., Miller, R.D., and Hawker, C.J. (2002). A facile approach to architecturally defined nanoparticles via intramolecular chain collapse, *Journal of the American Chemical Society*, C 124, 8653-8660.
- [58] Jia, P., Hu, L., Feng, G., Bo, C., Zhang, M., and Zhou, Y. (2017). PVC materials without migration obtained by chemical modification of azide-functionalized PVC and triethyl citrate plasticizer, *Materials Chemistry and Physics*, C 190, 25-30.
- [59] Akat, H. and Ozkan, M. (2011). Synthesis and characterization of poly (vinylchloride) type macrophotoinitiator comprising side-chain thioxanthone via click chemistry, *Express Polymer Letters*, C 5.
- [60] Jia, P., Hu, L., Yang, X., Zhang, M., Shang, Q., and Zhou, Y. (2017). Internally plasticized PVC materials via covalent attachment of aminated tung oil methyl ester, *RSC Advances*, C 7, 30101-30108.
- [61] Jia, P., Zhang, M., Hu, L., Wang, R., Sun, C., and Zhou, Y. (2017). Cardanol groups grafted on poly (vinyl chloride)—synthesis, performance and plasticization mechanism, *Polymers*, C 9, 621.
- [62] Asan, N. and Öztürk, T., *Synthesis and characterization of poly (vinyl chloride-graft-ethylene glycol) graft copolymers by "click" chemistry*. *Hacet J Biol Chem* 45: 35–42, 2017.
- [63] Zhu, D.Y., Cao, G.S., Qiu, W.L., Rong, M.Z., and Zhang, M.Q. (2015). Self-healing polyvinyl chloride (PVC) based on microencapsulated nucleophilic thiol-click chemistry, *Polymer*, C 69, 1-9.
- [64] Arslan, M. and Tasdelen, M. (2017). Polymer nanocomposites via click chemistry reactions, *Polymers*, C 9, 499.
- [65] ve Karakterizasyonu, K.S. Synthesis and Characterization of Poly (vinyl chloride-graft-ethylene glycol) Graft Copolymers by "Click" Chemistry.
- [66] Tukur, A., Pekdemir, M.E., Haruna, H., and Coşkun, M. (2020). Magnetic nanoparticle bonding to PVC with the help of click reaction: characterization, thermal and electrical investigation, *Journal of Polymer Research*, C 27, 161.
- [67] Harun, M.H., Saion, E., Kassim, A., Hussain, M.Y., Mustafa, I.S., and Omer, M.A.A. (2008). Temperature dependence of AC electrical conductivity of PVA-PPy-FeCl₃ composite polymer films, Iskandar Shahrin Mustafa² and Muhd Ahmad Ali Omer², *Malaysian Polymer Journal*, C 3, 24-31.
- [68] Öztürk, T., Ayyıldız, H., Meyvacı, E., and Gökteş, M. (2017). Synthesis and characterization of poly (epichlorohydrin-graft-ethylene glycol) graft copolymers by "click" chemistry, *Karaelmas Science and Engineering Journal*, C 7, 47-54.

CURRICULUM VITAE

Abdulrahman TUKUR

PERSONAL INFORMATION

Date of Birth: 11-July-1986

Place of Birth: Sokoto

Nationality: Nigeria

Email: tukurabdurrahman@fud.edu.ng

EDUCATION

- ✓ Usman Danfodiyo University Sokoto, Faculty of Science, Department of Pure and Applied Chemistry, 2012
- ✓ Sultan Bello Secondary School Sokoto, 2003

WORK EXPERIENCE

Federal University Dutse, Graduate Assistant. 2015-Date

ACADEMIC ACTIVITIES

Tukur, A., Pekdemir, M.E., Haruna, H., and Coşkun, M. (2020). Magnetic nanoparticle bonding to PVC with the help of click reaction: characterization, thermal and electrical investigation, *Journal of Polymer Research*, C 27, 161.

Haruna H., Pekdemir M.E., **Tukur, A.**, and Coşkun, M (2020). Characterization, thermal and electrical properties of Aminated PVC/oxidized MWCNT composites doped with nanographite, *Journal of Thermal Analysis and Calorimetry*, C, 1-9.

Abdulrahman Tukur, Mustafa Ersin Pekdemir, Hassan Haruna, Mehmet Coşkun, Magnetic nanoparticle bonding to PVC with the help of click reaction: Characterization, thermal and electrical investigation, Oral presentation, International Conference on Physical Chemistry and Functional Materials (PCFM'19), 2019.

Hassan Haruna, Mustafa Ersin Pekdemir, **Abdulrahman Tukur**, Mehmet Coşkun, Characterization, thermal and electrical properties of Aminated PVC/oxidized MWCNT composites doped with nanographite, Oral presentation, International Conference on Physical Chemistry and Functional Materials (PCFM'19), 2019.